NASA/TM-2000-210315

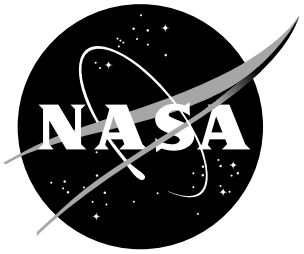

Forced Boundary-Layer Transition on X-43 (Hyper-X) in NASA LaRC 31-Inch Mach 10 Air Tunnel

Scott A. Berry, Michael DiFulvio, and Matthew K. Kowalkowski
Langley Research Center, Hampton, Virginia

August 2000

The NASA STI Program Office ... in Profile

Since its founding, NASA has been dedicated to the advancement of aeronautics and space science. The NASA Scientific and Technical Information (STI) Program Office plays a key part in helping NASA maintain this important role.

The NASA STI Program Office is operated by Langley Research Center, the lead center for NASA's scientific and technical information. The NASA STI Program Office provides access to the NASA STI Database, the largest collection of aeronautical and space science STI in the world. The Program Office is also NASA's institutional mechanism for disseminating the results of its research and development activities. These results are published by NASA in the NASA STI Report Series, which includes the following report types:

- TECHNICAL PUBLICATION. Reports of completed research or a major significant phase of research that present the results of NASA programs and include extensive data or theoretical analysis. Includes compilations of significant scientific and technical data and information deemed to be of continuing reference value. NASA counterpart of peer-reviewed formal professional papers, but having less stringent limitations on manuscript length and extent of graphic presentations.

- TECHNICAL MEMORANDUM. Scientific and technical findings that are preliminary or of specialized interest, e.g., quick release reports, working papers, and bibliographies that contain minimal annotation. Does not contain extensive analysis.

- CONTRACTOR REPORT. Scientific and technical findings by NASA-sponsored contractors and grantees.

- CONFERENCE PUBLICATION. Collected papers from scientific and technical conferences, symposia, seminars, or other meetings sponsored or co-sponsored by NASA.

- SPECIAL PUBLICATION. Scientific, technical, or historical information from NASA programs, projects, and missions, often concerned with subjects having substantial public interest.

- TECHNICAL TRANSLATION. English-language translations of foreign scientific and technical material pertinent to NASA's mission.

Specialized services that complement the STI Program Office's diverse offerings include creating custom thesauri, building customized databases, organizing and publishing research results ... even providing videos.

For more information about the NASA STI Program Office, see the following:

- Access the NASA STI Program Home Page at ***http://www.sti.nasa.gov***

- E-mail your question via the Internet to help@sti.nasa.gov

- Fax your question to the NASA STI Help Desk at (301) 621-0134

- Phone the NASA STI Help Desk at (301) 621-0390

- Write to:
  NASA STI Help Desk
  NASA Center for AeroSpace Information
  7121 Standard Drive
  Hanover, MD 21076-1320

NASA/TM-2000-210315

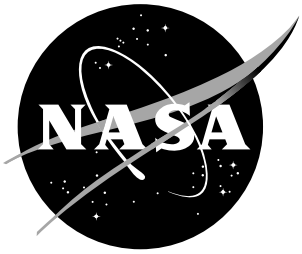

Forced Boundary-Layer Transition on X-43 (Hyper-X) in NASA LaRC 31-Inch Mach 10 Air Tunnel

Scott A. Berry, Michael DiFulvio, and Matthew K. Kowalkowski
Langley Research Center, Hampton, Virginia

National Aeronautics and
Space Administration

Langley Research Center
Hampton, Virginia 23681-2199

August 2000

Available from:

NASA Center for AeroSpace Information (CASI)
7121 Standard Drive
Hanover, MD 21076-1320
(301) 621-0390

National Technical Information Service (NTIS)
5285 Port Royal Road
Springfield, VA 22161-2171
(703) 605-6000

Contents

Abstract

Aeroheating and boundary layer transition characteristics for the X-43 (Hyper-X) configuration have been experimentally examined in the Langley 31-Inch Mach 10 Air Tunnel. Global surface heat transfer distributions, and surface streamline patterns were measured on a 0.333-scale model of the Hyper-X forebody. Parametric variations include angles-of-attack of 0-deg, 2-deg, 3-deg, and 4-deg; Reynolds numbers based on model length of 1.2 to 5.1 million; and inlet cowl door both open and closed. The effects of discrete roughness elements on the forebody boundary layer, which included variations in trip configuration and height, were investigated. This document is intended to serve as a release of preliminary data to the Hyper-X program; analysis is limited to observations of the experimental trends in order to expedite dissemination.

Introduction

NASA's X-43 (Hyper-X) program will culminate in flight tests of an operational airframe-integrated scramjet propulsion system at hypersonic conditions, which includes two flights at Mach 7 and one at Mach 10. Details about the flight and wind tunnel test program can be found in Rausch, et al. (1997a, 1997b) and McClinton, et al. (1998). A simulated launch sequence is shown in Fig. 1, while Fig. 2 shows the sequence of events during the nominal Mach-7 flight trajectory. This program will provide the first opportunity to obtain flight data on a hypersonic airbreathing propulsion system that is fully integrated with the vehicle airframe, and will validate/calibrate the experimental, numerical, and analytical methods used in the design and for prediction of flight performance of these vehicles. In an effort to reduce the uncertainties associated with this cutting-edge technology maturation program prior to the first flight, a systematic and combined experimental and numerical approach has been utilized. This includes (but is not limited to) development of aerodynamic performance and aeroheating databases, verification of performance and operability of the propulsion-airframe integration, and establishment of a method for boundary layer control. For instance, in order to provide the most robust scramjet propulsion system, a turbulent boundary layer within the engine is required. Ingestion of a turbulent boundary layer into the engine enhances the performance and operability of the scramjet through improved fuel mixing and reduced susceptibility to internal flow separations that might unstart the engine. Based on the current knowledge of boundary layer transition at hypersonic flight conditions, an estimation of the location of natural transition on the Hyper-X forebody suggests that boundary layer trip devices are necessary to ensure a turbulent boundary layer at the inlet for both Mach 7 and 10 flight conditions. Figure 3 shows a sketch of the full-scale flight vehicle, which has a forebody length of approximately 6-ft. An estimate (based on a boundary-layer transition criteria developed during the National Aero-Space program) of the distance required for natural transition to occur at these hypersonic slender-body conditions is, at best, over 50% beyond this forebody length. A wind tunnel test program has been initiated to develop potential boundary layer trip configurations for the Hyper-X flight vehicle, and has resulted in a selection of a baseline trip configuration. The testing sequence that has been completed to date is listed in Table 1.

This report presents the preliminary results of the wind tunnel tests conducted in the NASA Langley Research Center (LaRC) 31-Inch Mach 10 Air Tunnel. The purpose of these tests was to investigate the aeroheating characteristics of the Hyper-X forebody and to examine the effect of discrete roughness elements on the windward surface boundary layer. Based on preliminary trajectory information, the flight length Reynolds number (Re_L), based on a forebody length of 6-ft, is approximately 4 million at a freestream Mach number of 10. These conditions can be simulated in the LaRC 31-Inch Mach 10 Air Tunnel, which has a Re_L range of 1.2 to 5.1 million for a model length of 28-in (2.3-ft). Test techniques that were utilized during these tests include thermographic phosphors which provide global surface heating images and oil-flow which provide surface streamline information. Parametrics included in these tests, on both inlet cowl door open and closed, were the effect of angle of attack (α of 0-deg, 2-deg, 3-deg, and 4-deg), unit Reynolds number (Re between 0.5 and 2.2 million per foot), and discrete roughness elements (which included configuration and

height). The discrete roughness parametrics were included in these tests to provide information to develop an efficient trip device for the Hyper-X flight vehicle. Similar preliminary results from the LaRC 20-Inch Mach 6 Tunnel has been presented in Berry, et al. (2000).

Nomenclature

M	Mach number
Re	unit Reynolds number (1/ft.)
Re_L	Reynolds number based on a reference length
α	model angle of attack (deg)
β	model sideslip angle (deg)
p	pressure (psi)
T	temperature (deg-R)
x	longitudinal distance from the nose (in)
y	lateral distance from the centerline (in)
z	height above the waterline (in)
L	reference length of vehicle at the model scale (48.00 in)
h	heat transfer coefficient (lbm/ft^2-sec), =q/(H_{aw} - H_w) where $H_{aw} = H_{t2}$
h_{ref}	reference coefficient using Fay-Ridell calculation to stagnation point of a sphere
q	heat transfer rate (BTU/ft^2-sec)
H	enthalpy (BTU/lbm)
k	roughness element height (in)
Subscripts	
∞	freestream static conditions
t1	reservoir conditions
t2	stagnation conditions behind normal shock
aw	adiabatic wall
e	conditions at edge of the boundary layer
w	model surface
θ	momentum thickness

Test Facility

The Hyper-X forebody model has been tested in both the 20-Inch Mach 6 Air and the 31-Inch Mach 10 Air Tunnels of the LaRC Aerothermodynamic Facilities Complex (see Fig. 4). Miller (1990) and Micol (1998) provide detailed descriptions of these facilities and related instrumentation. Both are blowdown facilities that utilize dried, heated, and filtered air as the test gas.

The present tests were conducted in the LaRC 31-Inch Mach 10 Air Tunnel. Typical operating conditions for the 31-Inch Mach 10 are stagnation pressures ranging from 350 to 1450 psia and a stagnation temperature on the order of 1350-degF, which yields freestream unit Reynolds numbers of 0.5×10^6/ft to 2.2×10^6/ft. The tunnel has a closed 31- by 31-in. test section with a contoured three-dimensional water-cooled nozzle to provide a Mach number of 10. A hydraulically operated side-mounted model injection mechanism can inject the model into the flow in 0.6 seconds. The maximum run time for this facility is approximately 2 minutes; however, only approximately 5 seconds of this time is required for transient heat transfer tests. Optical access to the model is viewed through a high-quality window on the side opposite the injection mechanism.

Test Techniques

Surface Heating

The rapid advances in image processing technology which have occurred in recent years have made digital optical measurement techniques practical in the wind tunnel. One such optical acquisition method is two-color relative-intensity phosphor thermography (a diagram is shown in Fig. 5), which is currently being applied to aeroheating tests in the hypersonic wind tunnels of NASA Langley Research Center. Buck (1989, 1991) and Merski (1998) provide details about the phosphor thermography technique and Horvath (1990), Berry, et al. (1997, 1998a, 1998b) and Thompson, et al. (1998) provide additional recent examples of the application of this technique. With this technique, ceramic wind tunnel models are fabricated and coated with phosphors that fluoresce in two regions of the visible spectrum when illuminated with ultraviolet light. The fluorescence intensity is dependent upon the amount of incident ultraviolet light and the local surface temperature of the phosphors. By acquiring fluorescence intensity images with a color video camera of an illuminated phosphor model exposed to flow in a wind tunnel, surface temperature mappings can be calculated on the portions of the model that are in the field of view of the camera. A temperature calibration of the system conducted prior to the study provides the look-up tables that are used to convert the ratio of the green and red intensity images to global temperature mappings. With temperature images acquired at different times in a wind tunnel run, global heat transfer images are computed assuming one-dimensional heat conduction. The primary advantage of this technique is the global resolution of the quantitative heat transfer data. Such data can be used to identify the heating footprint of complex, three-dimensional flow phenomena (e.g., transition fronts, turbulent wedges, boundary layer vortices, etc.) that are extremely difficult to resolve by discrete measurement techniques. Phosphor thermography is routinely used in Langley's hypersonic facilities because models can be fabricated more quickly and economically than other more “conventional” techniques and the method provides quantitative global information. Comparisons of heat transfer measurements obtained from phosphor thermography to conventional thin-film resistance gauges measurements (Micol 1995) and to CFD predictions (Thompson, et al. 1998, Berry, et al. 1998b, Loomis, et al. 1997, Hamilton, et al. 1998) have shown good agreement.

Flow Visualization

The oil-flow technique, which provides visualization of the surface streamline patterns, was used to complement the surface heating tests. The model with metal inserts was spray-painted black to enhance contrast with the white pigmented oils used to trace streamline movement. A thin basecoat of clear silicon oil was first applied to the surface, and then a mist of small pigmented-oil droplets was applied to the surface. After the model surface was prepared, the model was injected into the airstream and the development of the surface streamlines was recorded with a conventional video camera. The model was retracted immediately following flow establishment and formation of streamline patterns, and post-run digital photographs were recorded with a high-resolution digital camera.

Model Description

A sketch of the 33% scale Hyper-X forebody model is shown in Fig. 6. This slender-body configuration is characterized by a thin leading edge and 3 flat ramps that provide discrete compression and processing of the flow prior to the scramjet inlet. Outboard of the flat ramps are the chines, which are designed to minimize three-dimensional effects and flow spillage. The chines of the forebody model were laterally truncated aft of the first ramp-corner, as shown in Fig. 6, in order to minimize tunnel blockage and to isolate the model within the tunnel test core. A numerically controlled milling machine was used to build the forebody model with a detachable stainless-steel leading edge and interchangeable measurement surface inserts as well as various stainless-steel trip and inlet configurations. Although a majority of the forebody (the strongback) was constructed from aluminum to save weight, the leading edge (detachable to allow replacement if damaged) was machined from stainless steel with a nose radius of 0.010-in. In order to provide for adequate thickness at the attachment point, the length of the detachable leading edge section was selected to be 5-in. The location of

the trips was placed another 2.418-in aft of the leading edge attachment point (for a total length from the model leading edge of 7.418-in). For the flight vehicle, this location represents a compromise between increasing the running length behind the trips and reducing the thermal environment around the trip. The interchangeable trip configurations were consequently designed and sized based on the local flow properties at this forebody station. The remaining flat ramp sections were designed to accommodate both a Macor and aluminum set of inserts. Macor is a machinable glass ceramic and is a registered trademark of Corning Incorporated. The engine inlet sidewalls were made of stainless steel and were designed to accommodate both open and closed engine cowl door configurations. The open configuration represents the forebody at test point with the engine cowl door in the operating position, although for the model the cowl is removed to provide optical access to the internal flat ramp surface. The closed configuration represents the forebody prior to test point with the engine cowl door down in the blocked inlet position and was tested in order to determine the impact of the trips on the closed cowl. Figure 7 is a photograph of the Hyper-X forebody model with the Macor inserts for the phosphor thermography testing in the open-cowl configuration. Figure 8 is a photograph of the Hyper-X forebody model with the aluminum inserts for flow visualization testing in the closed-cowl configuration.

In order to obtain accurate heat transfer data using the one-dimensional heat conduction equation, models need to be made of a material with low thermal diffusivity and well-defined, uniform, isotropic thermal properties. Also, the models must be durable for repeated use in the wind tunnel and not deform when thermally cycled. Normally a cast ceramic process, which can provide accurate replication of complex three-dimensional configurations, is used to build phosphor thermography models. In this case the casting process could not be utilized because of the need to interchange the various complex trip configurations. As the ramp sections behind the trip location were flat across most of the span, 0.25-in thick flat sheets of Macor were used for the phosphor substrate. The Macor substrates were then coated with a mixture of phosphors suspended in a silica-based colloidal binder. This coating consisted of a 5:1 mixture of lanthanum oxysulfide (La_2O_2S) doped with trivalent europium and zinc cadmium sulfide (ZnCdS) doped with silver and nickel in a proprietary ratio. The coatings typically do not require refurbishment between runs in the wind tunnel and are approximately 0.001 inches thick. Typically, the final step in the fabrication process is to apply fiducial marks along the body to assist in determining spatial locations accurately. The fiducial marks used for the present study were the joints between the Macor inserts, which correspond to the location of the ramp angle changes shown in the sketch in Fig. 6 and listed in Table 2.

There were four trip configurations originally developed for this study, designated as Trips 1, 2a, 2b, and 3, and these are shown in Figs. 9 through 12. A fifth configuration, designated as Trip 2c (as it was a modification of Trip 2b), was added midway through testing and is shown in Fig. 13. These five configurations were sized based on flow conditions for the 31-Inch Mach 10 Air Tunnel with the trip height (k) as the primary variable. Trip 1 (Fig. 9), referred to as the diamond configuration, is based on prior experience (Berry, et al. 1998a) and is a row of squares rotated 45-deg to the flow with spacing roughly equal to the width of each trip. As shown in Fig. 9a, this configuration was designed in two pieces with the trips protruding through holes in the base plate. Various thickness spacers between the parts provided the required variability in trip height. Figure 9b is a photograph of Trip 1 shown with the tallest height (k = 0.120-in) obtained by leaving out all of the spacers. This trip concept had been extensively tested during the NASP, Hyflite, and HySTP programs and was found to be a highly efficient vortex generator and trip. Unfortunately for the Hyper-X program, the diamond configuration had two potentially significant drawbacks. First, the diamond trips generate strong vortices that have a tendency to persist into the turbulent region thus providing a non-uniform flowfield for the inlet. The second is concern over whether this configuration, with sharp edges along the blunt face, could be structurally designed for Mach 7 and 10 flight conditions. The purpose of this experimental program, therefore, was to determine if Trip 1 could be redesigned to remedy these concerns. The remaining configurations, thus, were selected as modifications to this original trip design with the intent of providing a vortex-generating trip as efficient as Trip 1, but without the flow non-uniformity and structural concerns. Trip 2a (Fig. 10) and Trip 2b (Fig. 11) are similar in concept, both ramped tetrahedrons with the sharp apex pointing aft. For these configurations the number of vortices generated per trip was thought to be half that of Trip 1, thus the spacing between the trips was removed, which doubled the number of trips. The Trip 2a design held the length and width of each trip constrained, so the ramp angle of the trips changed in order to provide the required variability in trip height. The Trip 2b design held the width and ramp angle of each trip constrained, so the length of the trips changed in order to provide the required variability in trip

height. Trip 2c is identical to Trip 2b with the exception of a truncated base (Fig. 13), which is hoped to provide a local low-pressure region behind each trip that would enhance vortex generation. Trip 3 is also a ramped tetrahedron with the length and width constrained, but with the flared blunt base facing aft. Because of the blunt base, the spacing for Trip 3 was the same as Trip 1. A two piece tongue-in-groove construction was used for Trips 2a, 2b, 2c and 3 to provide 6 fixed-height trips for each configuration. Also, the tongue-in-groove construction required, for Trips 2a, 2b, and 2c, an extra 0.010-in spacing between trips to accommodate the tool path. Consequently, in order to maintain the same number of vortices across the span of the model the spacing between trip centers for Trips 1 and 3 was increased to 0.260-in.

The model was supported in the tunnel with the use of two struts made available from a previous study. The struts were attached to the model leeward side (vehicle upper surface) and allowed placement of the model at different positions within the tunnel test core. Figure 14 provides a sketch of the model installed in the 31-Inch Mach 10 Air Tunnel with the shorter strut, while Fig. 15 shows the longer strut. Note that the longer strut places the nose of the model at nearly the centerline of the tunnel.

Test Conditions

Nominal reservoir stagnation and corresponding freestream flow conditions for the present tests are presented in Table 3. Flow conditions for the 31-Inch Mach 10 Air Tunnel were based on measured reservoir pressures and temperatures and recent unpublished calibrations of the facility. The flow conditions shown are based on a statistical mean of all the runs at each condition and the run-to-run repeatability reflects a 95% uncertainty interval.

Data Reduction

Heating rates were calculated from the global surface temperature measurements using the one-dimensional semi-infinite solid heat-conduction equations, as discussed in detail in Buck (1991) and Merski (1998). Based on Merski (1998), phosphor system measurement error is typically quoted as ±7 to 10% for the 31-Inch Mach 10 Air Tunnel, with overall experimental uncertainty of ±15%. Global heating images are presented in terms of the ratio of heat-transfer coefficients h/h_{ref}, where h_{ref} corresponds to the Fay and Ridell (1958) stagnation-point heating to a sphere with radius 4.0-in (a 1-ft radius sphere scaled to the model size). Repeatability of centerline heat transfer distributions was generally found to be better than ±4%.

Results

Surface Heating

The phosphor thermography data was acquired in August and October of 1997, during Test 338 and in September of 1998 during Tests 349 and 351. The earlier test compared the original 4 trip configurations, while the later tests investigated the proposed modification to Trip 2b and the effect of the trips on the closed cowl. The run logs, which lists the parametrics that were investigated during 194 aeroheating runs, is presented in Table 4 for Test 338, Table 5 for Test 349, and Table 6 for Test 351, and the resulting global heating images are shown in chronological order by run number in Appendices A, B, and C, respectively. All the images were acquired with the camera approximately perpendicular to the model windward surface. The primary purpose of these wind tunnel entries was to acquire roughness transition data and to compare tripping efficiency. Therefore, most of the run matrix was set-up to investigate the effect of different trip configurations and height for a range of angles of attack and Reynolds numbers. A few baseline (no trip) cases were run and repeated to provide data for comparison to predictions in order to check data quality. The trip effectiveness run matrix for the open-cowl data is shown in Table 7 and provides a handy cross-reference of the run numbers that provide trends and repeatability. General observations based on the baseline-heating images are provided and followed by a discussion of roughness trends. Note that the images shown in Appendices A, B, and C represent the heating on the three ramped Macor surfaces directly behind the trip strip location only, as shown in the sketch of Fig. 16, and not the entire Hyper-X windward surface. The h/h_{ref}

color-bar scale of 0 to 1.0 was selected for most the heating images as this scale provided the best sensitivity to observe the trip effectiveness. A few closed-cowl images were presented using the color bar scale of 0 to 2.5 in order to highlight the high heating on the cowl (without going off-scale). For the sake of discussion in the following sections, the location of the onset of transition on the images in Appendix A, B, and C is qualitatively identified by the change in color from blue to green (based on the 0 to 1.0 scale). Ideally the onset of transition would be identified by comparison of the heating profiles extracted from the images for a series of runs to computational predictions, which is beyond the scope of this data-release document. In the discussions that follow, the heating images that are referred to by run number will be from Appendix A unless specifically identified otherwise.

The baseline (no trip) data includes the effect of Reynolds number, angle of attack, yaw, model position within the test core, and engine cowl door open and closed. Also, note that the baseline data includes cases where Trip 1 was used with k = 0.000-in (by using the maximum spacer thickness of 0.120-in). The baseline cases using Trip 1 matched the results of the baseline cases using the blank trip (Trip 0) insert (compare Runs 1 through 5 to Runs 21 and 22). For Reynolds number effects in the Mach 10 tunnel, as the unit Reynolds number is increased to 2.2 million per foot for the baseline angle of attack of 2-deg, the onset of transition is established just inside the inlet. This is illustrated by comparing Run 3 ($Re = 0.5x10^6$/ft) to Run 1 ($Re = 1.1x10^6$/ft) and Run 2 ($Re = 2.2x10^6$/ft). For the flight vehicle, the ideal location for the onset of transition would be just slightly ahead of the inlet. Thus, even in the noisy environment of a conventional-type hypersonic wind tunnel, enhancement to the location of transition by a tripping device would be required for α = 2-deg to provide the desired level of inlet efficiency. However, a slight increase in the angle of attack would have a beneficial effect on the location of transition. For instance, for a freestream unit Reynolds number of 2.2 million per foot, Runs 79, 30, and 47 (α = 2, 3, and 4-deg, respectively) show a steady forward movement of transition on the last ramp as the angle of attack is increased. Conversely, Run 64 shows that the flow remains laminar on the windward surface for α = 0-deg. Although the majority of testing was completed with zero sideslip (β = 0-deg), the few runs completed with β = 2-deg provide an indication of the increasingly complex three-dimensional flow field that would result. This is illustrated by comparing Run 141 (β = 2-deg) to Run 79 (β = 0-deg). A 2-deg sideslip to port provided a localized forward movement of transition along the starboard edge (the side turned into the flow) of the last flat ramp. The repeat runs that were completed with the two different length struts showed no effect of model placement at different locations within the tunnel test core. For example, Run 40 with the long strut placing the model nearest to tunnel centerline and Run 22 with the short strut provide nearly identical images. During the initial tunnel entries (Tests 338 and 349) only a limited number of runs were completed with the inlet door in the closed position, which provided a qualitative sense of the extreme heating environment that the closed door would encounter. For these runs, the heating was severe enough to both crack several closed-door Macor inserts and exceed the temperature limit of the phosphor thermography system (typical temperature range is 50 to 350-degF) within the first couple of data frames. New closed-door inserts had to be re-designed and manufactured for a subsequent test entry (Test 351) before quantitative heating data could be obtained.

For Trip 1 at the baseline condition (α = 2-deg and $Re = 2.2x10^6$/ft) the effect of varying the trip height (k) provides a steady forward movement of the onset of transition from just inside the inlet to the beginning of Ramp 2. The first trip height that just begins to affect the location of transition, the so-called *incipient*[1] trip height is k = 0.030-in. For example, compare Run 10 (k = 0.030-in) to Run 7 (k = 0.015-in) and Run 22 (no trip baseline). Also, the faint lines of increased heating behind each trip, which are a result of the vortices that are generated by the trips scrubbing on the surface, begin to appear by the k = 0.030-in trip height. By k = 0.060-in, a significant forward movement of the transition front (the *critical* value) on ramp 3 is evident in the image of Run 14 and the vortices behind each trip have become more pronounced. Increasing the trip height further, the vortices begin to appear on Ramp 2 and by the largest trip height, k = 0.120-in (Run 18), transition onset is at the beginning of Ramp 2. Note in Run 18 the relative consistency of the vortices across

[1] Note that the terminology used here is similar to the definitions of Bertin, et al. (1982). *Incipient* identifies the maximum roughness height that has no effect on the onset of transition. *Critical* identifies the roughness height that first begins to move transition rapidly towards the nose. *Effective* identifies the minimum roughness height that establishes transition onset just downstream of the roughness element.

the span of Ramp 2 and that the streaks persist through the turbulent regions of Ramp 3 and into the inlet. Because the largest trip height did not provide transition onset directly behind the trip elements (the start of the image), the *effective* trip height was not reached.

For Trips 2a, 2b, 2c, and 3, the effect of varying k provided similar results as with Trip 1 but with some subtle differences. Trips 2a, 2b, and 2c provided roughly the same *incipient* and *critical* values of k as Trip 1, but without evidence of strong vortices in either the laminar or turbulent regions. However, as the maximum trip height is reached, the onset of transition for Trips 2a, 2b, and 2c is slightly behind the results shown for Trip 1. On the other hand, the results from Trip 3 most closely resembled Trip 1 in both effectiveness and strength of vortices. As the largest trip height is reached, transition onset is just slightly behind the results from Trip 1. By comparing Run 94 (Trip 1) and Run 98 (Trip 3) to Run 90 (Trip 2a) and Run 95 (Trip 2b), the greater effectiveness of the blunt configurations (at the largest trip height) is evident, however with the caveat of strong vortices persisting through the onset of transition. In terms of a trip configuration that provides adequate transition enhancement without persistent vortices, Trip 2c was the best performer.

Finally, in an exploratory fashion, the effect of mass addition or blowing as a trip mechanism was investigated to determine if reasonably small amounts of mass injection could provide the vortices that would induce transition. Conceptually, blowing has the advantage of being an active type of transition control that can be turned on and off as needed. For instance, for Hyper-X the blowing would be turned on just prior to the inlet door being opened, which could potentially remove the vortex-induced heating augmentation of the trips to the closed cowl door. During Test 349, two runs were conducted with a trip insert which had 3 small bleed holes hooked into a common manifold that was connected to the shop pressurized air system. The 0.010-in diameter holes were symmetrically distributed with the two outer holes being 1-in on either side of the hole on model centerline. The first run (Run 23 of Appendix B) with blowing utilized the shop air at full pressure (100 psi), which provided significant transition enhancement. Unfortunately, a metering or control system was not available for these runs. Thus for the second run (Run 24 of Appendix B), the only way to reduce the amount of blowing was to partially disconnect the shop air system (in effect bleeding off some fraction of the pressure that was feeding the holes), which still provided noticeable transition enhancement when compared to the no trip cases. While these blowing runs were only exploratory in nature, the results seem encouraging enough to warrant further study.

Flow Visualization

The oil-flow data was acquired in August of 1997 and April of 1998, during Tests 338 and 346, respectively. The run logs, which lists the parametrics that were investigated during the 40 flow visualization runs of Test 338 and Test 346, are presented in Table 6 and 7, respectively, and the resulting oil-flow images are shown in chronological order by test and run number in Appendix D. The digital images utilized in this report were all acquired post-test with the camera approximately perpendicular to the model windward surface. A few close-up photographs showing the details of the vortex patterns behind the trips were acquired and are included in Appendix B. All the oil-flow images were acquired with the model at zero sideslip (β = 0-deg). General observations that can be made based on the baseline oil-flow images are listed below and followed by a discussion of results with trips. The first few oil-flow runs were completed using the standard technique of a random pattern of tiny drops of white pigmented oil sprayed onto the black model surface. Unfortunately, while this approach is especially useful for tracing the surface streamline directions, it was not adequate for visualizing the vortices that were being generated by the trips. A relatively new approach was tried, where the model was essentially covered or painted with the white pigmented oil, with improved results. This form of oil-flow is similar in concept to the sublimating chemical technique. The entire model is coated with, in this case, oil and during the run the higher energy flow removes or scrubs away the oil to reveal the footprint of complex flow features. This second technique provided clear indications of the vortices, regions of separations, and lines of reattachments, and was applied for the remainder of the tests. Please note when viewing these images that oil accumulation lines identify both the lateral (vertical in the image) lines of separation at the end of the ramps and the axial (horizontal) lines between pairs of counter-rotating vortices. The paint brush marks (which tend to be small white lines running in a lateral direction) identify the regions of low shear or separated flow.

The oil-flow images of the runs without trips shows a complex three-dimensional flow pattern that is dominated by the separated regions at the end of Ramp 1 and 2. These separated regions, which appear relatively two-dimensional over the width of the flat ramps, merge with a separated or low shear area, which run the length of the chines, to generate a chine vortex emanating from the compression ramp corners. The images of Runs 163 and 165 provide the best evidence of these chine vortices. The surface streamlines, as provided by Runs 153 – 155, indicate flow spillage off the flat ramps. Perhaps as little as a third of the surface streamlines on the end of the first flat ramp appear to be captured by the inlet.

The addition of trips to the forebody provides the added complexity of streamwise vortices within the boundary layer that tend to diminish the separated regions at the end of the compression ramps. As the flow separations are removed, the surface streamlines indicate reduced spillage off the flat ramps (implying improved mass capture), as indicated by the image of Run 158. The previous observation regarding the inlet capture of only a third of the surface streamlines on the end of the first flat ramp without trips appears to be improved to about a half with trips. One must keep in mind that these streamlines only indicate the flow direction at the surface. The painted-oil images with trips clearly indicate that the inlet ingests all the vortices, with the exception of those generated by the two outboard trips (see Run 15 of Test 346). (Thus the surface streamlines as generated by the oil-flow method are not necessarily a good indication of the mass capture of the inlet.) The effect of trip height on the forward extent of separation at the compression ramp corners appears to be in agreement with the heating results. The close-up images provide additional details regarding the flow-field structure behind the trips. For instance, Trips 1 and 3 clearly appear to have double the vortices behind them than Trips 2a and 2b (thus justifying the decision to double the number of trips for the Trip 2a and 2b design). Also, the close-up images show how much influence the trips have up-stream in the form of separated or diverted flow in front of the trips.

Conclusions

An experimental investigation of the boundary layer trip effectiveness and the effect of the trips on the aeroheating characteristics for a 33% scale Hyper-X forebody model has been conducted in the LaRC 31-Inch Mach 10 Tunnel. Phosphor thermography was used to provide global heating images of a portion of the windward surface for a variety of angles-of-attack and Reynolds numbers. Additionally, the effect of discrete roughness elements was investigated, which included trip configuration and height parametrics. The aeroheating results were complemented with oil-flow images that provided surface streamline information. As this report was intended to be a data-release of the experimental results for review by the Hyper-X program, analysis was limited to observations of experimental trends.

Acknowledgment

This experimental effort was accomplished with the help of many dedicated individuals. The trip configurations were selected and designed with the assistance of Aaron Auslender of AGDD/HAPB and Doug Dilley of NYMA, Inc. William Kimmel of ETTD/MISB designed the model hardware. Kevin Meidinger of FD/ARES led a team of machinists that constructed the model hardware and helped design the trips. Greg Draughon of FD/MTSS supported the Macor machining and installation. Mike Powers and Mark Griffin of FD/CMFSB sprayed the phosphor coatings on the Macor surfaces. Jeff Werner and Paul Tucker of FSSD/ASS, and Sheila Wright of CSC provided facility support. And Glenn Bittner of CSC and Ron Merski of AGDD/AB assisted with the phosphor thermography system. The authors greatly appreciate the invaluable assistance of these individuals and the contributions of others not mentioned that assisted behind the scenes.

References

Berry SA, DiFulvio M, and Kowalkowski MK. 2000. Forced Boundary Layer Transition on X-43 (Hyper-X) in NASA LaRC 20-Inch Mach 6 Air Tunnel. *NASA TM-2000-210316*

Berry SA, Bouslog SA, Brauckmann GJ, and Caram JM. 1998a. Shuttle Orbiter Experimental Boundary-Layer Transition Results with Isolated Roughness. *J. Spacecr. Rockets 35(3): 241-248*

Berry SA, Horvath TJ, DiFulvio M, Glass C, and Merski NR. 1998b. X-34 Experimental Aeroheating at Mach 6 and 10. *AIAA Paper 98-0881*

Berry SA, Horvath TJ, Roback VE, and Williams GB. 1997. Results of Aerothermodynamic and Boundary-Layer Transition Testing of 0.0362-Scale X-38 (Rev. 3.1) Vehicle in NASA Langley 20-Inch Mach 6 Tunnel. *NASA TM-112857*

Bertin JJ, Hayden TE, and Goodrich WD. 1982. Shuttle Boundary-Layer Transition Due to Distributed Roughness and Surface Cooling *J. Spacecr. Rockets 19(5):389-396*

Buck GM. 1989. Automated Thermal Mapping Techniques Using Chromatic Image Analysis. *NASA TM 101554*

Buck GM. 1991. Surface Temperature/Heat Transfer Measurement Using A Quantitative Phosphor Thermography System. *AIAA Paper 91-0064*

Fay JA, Ridell FR. 1958. Theory of Stagnation Point Heat Transfer in Dissociated Air. *J. Aerosp. Sci.* 25(2):73-85,121

Hamilton HH, Berry SA, Horvath TJ, and Weilmuenster KJ. 1998. Computational/ Experimental Aeroheating Predictions for X-33 Phase II Vehicle. *AIAA Paper 98-0869*

Horvath TJ, Rhode MN, and Buck GM. 1990. Aerothermodynamic Measurements on a Proposed Assured Crew Return Vehicle (ACRV) Lifting Body Configuration at Mach 6 and 10 in Air. *AIAA Paper 90-1744*

Loomis MP, Venkatapathy E, Davies CB, Campbell CH, Berry SA, Horvath TJ, and Merski NR. 1997. Aerothermal CFD Validation and Prediction for the X-38 Program. *AIAA Paper 97-2484*

McClinton CR, Holland SD, Rock KE, Englund WC, Voland RT, Huebner LD, and Rogers RC. 1998. Hyper-X Wind Tunnel Program. *AIAA Paper 98-0553*

Merski NR. 1998. Reduction and Analysis of Phosphor Thermography Data with the IHEAT Software Package. *AIAA Paper 98-0712*

Micol JR. 1995. Aerothermodynamic Measurement and Prediction for a Modified Orbiter at Mach 6 and 10 in Air. *J. Spacecr. Rockets 32(5):737-748*

Micol JR. 1998. Langley Aerothermodynamic Facilities Complex: Enhancements and Testing Capabilities. *AIAA Paper 98-0147*

Miller CG. 1990. Langley Hypersonic Aerodynamic/Aerothermodynamic Testing Capabilities - Present and Future. *AIAA Paper 90-1376*

Rausch VL, McClinton CR, and Crawford JL. 1997a. Hyper-X: Flight Validation of Hypersonic Airbreathing Technology. *ISABE Paper 97-7024*

Rausch VL, McClinton CR, and Hicks JW. 1997b. NASA Scramjet flights to Breath New Life into Hypersonics. *Aerospace America 35(7): 40-46*

Thompson RA, Hamilton HH, Berry SA, and Horvath TJ. 1998. Hypersonic Boundary Layer Transition for X-33 Phase II Vehicle. *AIAA Paper 98-0867*

Table 1: Hyper-X Boundary-Layer Trip Screening Tests in NASA Tunnels

Year	Tunnel	Test	Occupancy Dates	Runs	Description
1997	**31-In M-10**	**338**	**Aug 14 – Aug 29**	**1-76**	**Phosphor**
1997	20-In M-6	6755	Sept 2 - Sept 5	1-61	Phosphor and schlieren
1997	**31-In M-10**	**338**	**Sept 30 - Oct 20**	**77-170**	**Phosphor and oil-flow**
1998	20-In M-6	6768	Mar 30 – Apr 2	22	Oil-flow
1998	**31-In M-10**	**346**	**Apr 6 - Apr 10**	**1-20**	**Oil-flow**
1998	**31-In M-10**	**349**	**Sept 3 - Sept 8**	**1-25**	**Phosphor with new trip**
1998	**31-In M-10**	**351**	**Sept 16 - Sept 18**	**1-19**	**Phosphor on closed cowl**
1999	Hypulse		Feb 23 – Mar 26	1-28	Thin-film and schlieren
1999	20-In M-6	6791	Aug 10	1-10	Phosphor with new trip
1999	20-In M-6	6793	Sept 15 - Sept 17	1-11	Phosphor w/ leading edge roughness

Table 2: Trip location and fiducial marks.

Location	x (in)	x/L
Trips	7.418	0.1545
Start of Macor	8.166	0.1701
End of 1st Ramp	12.433	0.2590
End of 2nd Ramp	17.767	0.3701
End of Model	28.000	0.5833

L = 48-in (Length of full vehicle at model scale).

Table 3: Nominal flow conditions and run-to-run repeatability for 31-Inch Mach 10 Tunnel.

$Re_\infty(x10^6/ft)$	M_∞	P_{t1} (psi)	T_{t1} (°R)	H_{t1}(BTU/lbm)	P_{t2}(psi)
0.6 ± 2.2	9.7 ± 0.1	348.1 ± 0.7	1802.3 ± 1.3	451.5 ± 1.4	1.2 ± 0.6
1.1 ± 2.5	9.8 ± 0.1	721.3 ± 0.9	1816.3 ± 1.2	455.8 ± 1.4	2.4 ± 0.8
2.2 ± 2.3	9.9 ± 0.1	1451.7 ± 0.8	1808.1 ± 1.1	454.8 ± 1.2	4.5 ± 0.7

Table 4: Run log for aeroheating portion of test T338 conducted in LaRC 31-Inch Mach 10 Tunnel.

Run Number	*Model*	*α (deg)*	*β (deg)*	*Re (x10^6/ft)*	*Trip Type*	*k (in)*	*Cowl*	*Results*
1	1-S	2	0	1.1	1	0.000	Open	
2	1-S	2	0	2.2	1	0.000	Open	
3	1-S	2	0	0.5	1	0.000	Open	
4	1-S	2	0	1.1	1	0.000	Open	
5	1-S	2	0	2.2	1	0.000	Open	
6	1-S	2	0	1.1	1	0.015	Open	
7	1-S	2	0	2.2	1	0.015	Open	
8	1-S	2	0	2.2	1	0.015	Open	
9	1-S	2	0	1.1	1	0.030	Open	
10	1-S	2	0	2.2	1	0.030	Open	
11	1-S	2	0	1.1	1	0.045	Open	
12	1-S	2	0	2.2	1	0.045	Open	
13	1-S	2	0	1.1	1	0.060	Open	
14	1-S	2	0	2.2	1	0.060	Open	
15	1-S	2	0	1.1	1	0.090	Open	
16	1-S	2	0	2.2	1	0.090	Open	
17	1-S	2	0	1.1	1	0.120	Open	
18	1-S	2	0	2.2	1	0.120	Open	
19	1-S	2	0	1.1	1	0.075	Open	
20	1-S	2	0	2.2	1	0.075	Open	
21	1-S	2	0	1.1	0	no trip	Open	new baseline
22	1-S	2	0	2.2	0	no trip	Open	new baseline
23	1-S	2	0	1.1	2b	0.060	Open	
24	1-S	2	0	2.2	2b	0.060	Open	
25	1-S	2	0	1.1	3	0.060	Open	
26	1-S	2	0	2.2	3	0.060	Open	
27	1-S	2	0	1.1	2a	0.060	Open	
28	1-S	2	0	2.2	2a	0.060	Open	
29	1-L	3	0	1.1	0	no trip	Open	
30	1-L	3	0	2.2	0	no trip	Open	
31	1-L	3	0	1.1	1	0.060	Open	
32	1-L	3	0	2.2	1	0.060	Open	
33	1-L	3	0	1.1	2a	0.060	Open	
34	1-L	3	0	2.2	2a	0.060	Open	
35	1-L	3	0	1.1	2b	0.060	Open	
36	1-L	3	0	2.2	2b	0.060	Open	
37	1-L	3	0	1.1	3	0.060	Open	
38	1-L	3	0	2.2	3	0.060	Open	
39	1-L	2	0	1.1	0	no trip	Open	
40	1-L	2	0	2.2	0	no trip	Open	
41	1-L	2	0					**Bad Run** no phosphor data
42	1-L	2	0	2.2	1	0.060	Open	
43	1-L	2	0	2.2	2a	0.060	Open	
44	1-L	2	0	2.2	2b	0.060	Open	
45	1-L	2	0	2.2	3	0.060	Open	
46	1-S	4	0	1.1	0	no trip	Open	
47	1-S	4	0	2.2	0	no trip	Open	
48	1-S	4	0	2.2	1	0.030	Open	
49	1-S	4	0	2.2	1	0.045	Open	
50	1-S	4	0	2.2	1	0.060	Open	
51	1-S	4	0	2.2	1	0.075	Open	

Run Number	*Model*	*α (deg)*	*β (deg)*	*Re (x10^6/ft)*	*Trip Type*	*k (in)*	*Cowl*	*Results*
52	1-S	4	0	2.2	1	0.090	Open	
53	1-S	4	0	2.2	1	0.120	Open	
54	1-S	4	0	2.2	2a	0.060	Open	
55	1-S	4	0	2.2	2a	0.045	Open	
56	1-S	4	0	2.2	2a	0.030	Open	
57	1-S	4	0	2.2	2b	0.060	Open	
58	1-S	4	0	2.2	3	0.060	Open	
59	1-S	4	0	2.2	2b	0.045	Open	
60	1-S	4	0	2.2	3	0.045	Open	
61	1-S	4	0	2.2	2b	0.030	Open	
62	1-S	4	0	2.2	3	0.030	Open	
63	1-S	0	0	1.1	0	no trip	Open	
64	1-S	0	0	2.2	0	no trip	Open	
65	1-S	0	0	2.2	1	0.120	Open	
66	1-S	0	0	2.2	1	0.090	Open	
67	1-S	0	0	2.2	1	0.075	Open	
68	1-S	0	0	2.2	1	0.060	Open	
69	1-S	0	0	2.2	1	0.030	Open	
70	1-S	0	0	2.2	2a	0.060	Open	
71	1-S	0	0	2.2	2b	0.060	Open	
72	1-S	0	0	2.2	3	0.060	Open	
73	2-S	2	0	1.1	0	no trip	Closed	High heating on cowl!
74	2-S	2	0	0.05	0	no trip	Closed	
75	2-S	2	0	2.2	0	no trip	Closed	Cowl overscale on 1st frame
76	2-S	2	0	1.1	1	0.060	Closed	Cracked closed-cowl corner
77	1-S	2	0	2.2	0	no trip	Open	
78	1-S	2	0	1.1	0	no trip	Open	
79	1-S	2	0	2.2	0	no trip	Open	
80	1-S	2	0	2.2	1	0.060	Open	
81	1-S	2	0	2.2	1	0.030	Open	
82	1-S	2	0	2.2	1	0.045	Open	
83	1-S	2	0	2.2	1	0.075	Open	
84	1-S	2	0	2.2	1	0.090	Open	
85	1-S	2	0				Open	**Bad Run** no phosphor data
86	1-S	2	0				Open	**Bad Run** no phosphor data
87	1-S	2	0	2.2	2a	0.090	Open	
88	1-S	2	0				Open	**Bad Run**
89	1-S	2	0	2.2	2a	0.060	Open	
90	1-S	2	0	2.2	2a	0.120	Open	
91	1-S	2	0	2.2	2b	0.060	Open	
92	1-S	2	0				Open	**Bad Run** heater tripped
93	1-S	2	0	2.2	2b	0.090	Open	
94	1-S	2	0	2.2	1	0.120	Open	
95	1-S	2	0	2.2	2b	0.120	Open	
96	1-S	2	0	2.2	3	0.060	Open	
97	1-S	2	0	2.2	3	0.090	Open	
98	1-S	2	0	2.2	3	0.120	Open	
99	1-S	0	0	2.2	0	no trip	Open	
100	1-S	0	0	1.1	0	no trip	Open	
101	1-S	0	0	2.2	1	0.030	Open	?
102	1-S	0	0	2.2	1	0.060	Open	
103	1-S	0	0	2.2	1	0.090	Open	
104	1-S	0	0	2.2	1	0.120	Open	

Run Number	*Model*	*α (deg)*	*β (deg)*	*Re (x10^6/ft)*	*Trip Type*	*k (in)*	*Cowl*	*Results*
105	1-L	0	0	2.2	2a	0.060	Open	
106	1-L	0	0	2.2	2a	0.090	Open	
107	1-L	0	0	2.2	2a	0.120	Open	
108	1-L	0	0	2.2	2b	0.060	Open	
109	1-L	0	0	2.2	2b	0.090	Open	
110	1-L	0	0	2.2	2b	0.120	Open	
111	1-L	0	0	2.2	3	0.060	Open	
112	1-L	0	0	2.2	3	0.090	Open	
113	1-L	0	0	2.2	3	0.120	Open	
114	1-L	4	0	2.2	0	no trip	Open	
115	1-L	4	0	2.2	0	no trip	Open	
116	1-L	4	0	2.2	1	0.030	Open	
117	1-L	4	0	2.2	1	0.060	Open	
118	1-L	4	0	2.2	1	0.090	Open	
119	1-L	4	0	2.2	1	0.120	Open	
120	1-L	4	0	2.2	2a	0.060	Open	
121	1-L	4	0	2.2	2a	0.090	Open	
122	1-S	4	0	2.2	2a	0.090	Open	
123	1-S	4	0	2.2	2a	0.120	Open	
124	1-S	4	0	2.2	2b	0.060	Open	
125	1-S	4	0	2.2	2b	0.090	Open	
126	1-S	4	0	2.2	2b	0.120	Open	
127	1-S	4	0	2.2	3	0.060	Open	
128	1-S	4	0	2.2	3	0.090	Open	
129	1-S	4	0	2.2	3	0.120	Open	
130	1-S	2	0	2.2	2a	0.015	Open	
131	1-S	2	0	2.2	2a	0.030	Open	
132	1-S	2	0	2.2	2b	0.045	Open	
133	1-S	2	0	2.2	2a	0.030	Open	
134	1-S	2	0	2.2	2b	0.015	Open	
135	1-S	2	0	2.2	2b	0.030	Open	
136	1-S	2	0	2.2	2a	0.045	Open	
137	1-S	2	0	2.2	3	0.015	Open	
138	1-S	2	0	2.2	3	0.030	Open	
139	1-S	2	0	2.2	3	0.045	Open	
140	1-S	2	2	1.1	0	no trip	Open	
141	1-S	2	2	2.2	0	no trip	Open	
142	1-S	2	2	2.2	1	0.120	Open	
143	1-S	2	2	2.2	1	0.015	Open	
144	1-S	2	2	2.2	1	0.030	Open	
145	1-S	2	2	2.2	1	0.045	Open	
146	1-S	2	2	2.2	1	0.060	Open	
147	1-S	2	2	2.2	1	0.075	Open	
148	1-S	2	2	2.2	1	0.090	Open	
149	2-S	2	0	1.1	0	no trip	Closed	Closed cowl
150	2-S	2	0	2.2	0	no trip	Closed	Closed cowl

Table 5: Run log for Test 349 conducted in LaRC 31-Inch Mach 10 Air Tunnel.

Run Number	*Model*	*α (deg)*	*β (deg)*	*Re (x10⁶/ft)*	*Trip Type*	*k (in)*	*Cowl*	*Results*
1	1-S	2	0	2.2	0	no trip	Closed	
2	1-S	2	0	0.5	0	no trip	Closed	
3	1-S	2	0	1.1	0	no trip	Closed	
4	1-S	2	0	2.2	1	0.030	Closed	
5	1-S	2	0	0.5	1	0.030	Closed	Cowl phosphor is slowly eroding
6	1-S	2	0	1.1	1	0.030	Closed	
7	1-S	2	0	0.5	1	0.045	Closed	
8	1-S	2	0	1.1	1	0.045	Closed	Closed cowl cracked again
9	1-S	2	0	0.5	1	0.060	Closed	
10	1-S	2	0	0.5	1	0.090	Closed	Removed damaged cowl
11	1-S	2	0	0.5	0	no trip	Open	Finish screening with open cowl
12	1-S	2	0	0.5	0	no trip	Open	
13	1-S	2	0	1.1	0	no trip	Open	
14	1-S	2	0	2.2	0	no trip	Open	
15	1-S	2	0	2.2	2c	0.120	Open	
16	1-S	2	0	2.2	2c	0.060	Open	
17	1-S	2	0	2.2	2c	0.030	Open	
18	1-S	2	0	2.2	2c	0.120	Open	
19	1-S	2	0	2.2	Cavity	0.060	Open	
20	1-S	2	0	2.2	1	0.120	Open	
21	1-S	2	0	2.2	1	0.060	Open	
22	1-S	2	0	2.2	2b	0.120	Open	
23	1-S	2	0	2.2	Blowing	-	Open	Max shop air (~100psi)
24	1-S	2	0	2.2	Blowing	-	Open	Reduced shop air
25	1-S	2	0	2.2	2c	0.120	Open	

Table 6: Run log for Test 351 conducted in LaRC 31-Inch Mach 10 Air Tunnel.

Run Number	*Model*	*α (deg)*	*β (deg)*	*Re (x10⁶/ft)*	*Trip Type*	*k (in)*	*Cowl*	*Results*
1	1-S	2	0	0.5	0	no trip	Closed	
2	1-S	2	0	0.5	1	0.120	Closed	
3	1-S	2	0	0.5	1	0.060	Closed	
4	1-S	2	0	0.5	2b	0.120	Closed	
5	1-S	2	0	0.5	2c	0.120	Closed	
6	1-S	4	0	0.5	0	no trip	Closed	**Bad run** no phosphor data
7	1-S	4	0	0.5	1	0.120	Closed	
8	1-S	4	0	0.5	0	no trip	Closed	Re-ran run 6
9	1-S	4	0	0.5	2c	0.120	Closed	
10	1-S	4	0	0.5	2b	0.120	Closed	
11	1-S	2	0	1.1	0	no trip	Closed	
12	1-S	2	0	1.1	1	0.120	Closed	
13	1-S	2	0	1.1	2b	0.120	Closed	
14	1-S	2	0	1.1	2c	0.120	Closed	
15	1-S	4	0	1.1	0	no trip	Closed	
16	1-S	4	0	1.1	1	0.120	Closed	
17	1-S	4	0	1.1	2c	0.120	Closed	
18	1-S	4	0	1.1	2b	0.120	Closed	
19	1-S	2	0	2.2	0	no trip	Closed	

Table 5: Trip screening test matrix cross-reference of open-cowl runs conducted in the LaRC 31-Inch Mach 10 Tunnel.

		Trip 1				Trip 2a				Trip 2b				Trip 2c				Trip 3				Baseline			
	α	0	2	3	4	0	2	3	4	0	2	3	4	0	2	3	4	0	2	3	4	0	2	3	4
k	Re																								
0.000	0.5		A3																				B11 B12		
	1.1		A1 A4																			A63 A100	A21 A39 A78 B13	A29	A46 A115
	2.2		A2 A5																			A64 A99	A22 A40 A70 A79 B14	A30	A47 A114
0.015	0.5																								
	1.1		A6																						
	2.2		A7 A8				A130				A134								A137						
0.030	0.5																								
	1.1		A9																						
	2.2	A14 A69	A10 A81		A48 A116		A133		A56		A135		A61		B17				A138		A62				
0.045	0.5																								
	1.1		A11																						
	2.2		A12 A82		A49		A136		A55		A132		A59						A139		A60				
0.060	0.5																								
	1.1		13	A31			A27	A33			A23	A35							A25	A37					
	2.2	A68 A102	A14 A42 A80 B21	A32	A50 A117	A70 A105	A28 A43 A89	A34	A54 A120	A71 A108	A24 A44 A91	A36	A57 A124		B16			A72 A111	A26 A45 A96	A38	A58 A127				
0.075	0.5																								
	1.1		A19																						
	2.2	A67	A20 A83		A51																				
0.090	0.5																								
	1.1		A15																						
	2.2	A66 A103	A16 A84		A52 A118	A106	A87		A121	A109	A93		A125					A112	A97		A128				
0.120	0.5																								
	1.1		A17																						
	2.2	A65 A104	A18 A94 B20		A53 A119	A107	A90		A123	A110	A95 B22		A126		B15 B18 B25			A113	A98		A129				

Note: A designates Test 338, B designates Test 349

Table 8: Run log for flow visualization portion of test T338 conducted in the LaRC 31-Inch Mach 10 Tunnel.

Run Number	*Model*	*_ (deg)*	*Re/ft (x10^6)*	*Trip Type*	*k (in)*	*Cowl*	*Oil-Flow Type*	*Oil Flow Results*
151	1-S	2	2.2	0	no trip	Open	Dots	Insufficient oil flow
152	1-S	2	2.2	0	no trip	Open	Dots	Insufficient oil flow
153	1-S	2	2.2	0	no trip	Open	Dots	OK
154	1-S	2	2.2	0	no trip	Open	Dots	OK
155	1-S	2	2.2	0	no trip	Open	Dots	OK
156	1-S	2	2.2	1	0.045	Open	Dots	OK
157	1-S	2	2.2	1	0.045	Open	Dots	OK
158	1-S	2	2.2	1	0.060	Open	Dots	OK
159	1-S	2	2.2	1	0.060	Open	Paint	OK
160	1-S	2	2.2	2a	0.060	Open	Paint	OK
161	1-S	2	2.2	3	0.060	Open	Paint	OK
162	1-S	2	2.2	2b	0.060	Open	Paint	OK
163	1-S	2	2.2	0	no trip	Open	Paint	OK
164	2-S	2	2.2	0	no trip	Open	Paint	Insufficient oil flow
165	2-S	2	2.2	0	no trip	Closed	Paint	OK
166	2-S	2	2.2	1	0.060	Closed	Paint	OK
167	1-S	2	2.2	1	0.060	Open	Paint	OK
168	1-S	0	2.2	0	no trip	Open	Paint	OK
169	1-S	4	2.2	0	no trip	Open	Paint	OK
170	1-S	2	2.2	0	no trip	Open	Paint	Insufficient oil flow

Table 9: Run log for flow visualization test T346 conducted in the LaRC 31-Inch Mach 10 Tunnel.

Run Number	*Model*	*α (deg)*	*Re/ft (x10^6)*	*Trip Type*	*k (in)*	*Cowl*	*Oil-Flow Type*	*Oil Flow Results*
1	2-S	2	2	1	0.06	Closed	Dots	OK
2	2-S	2	2	2b	0.12	Closed	Dots	OK
3	2-S	2	2	1	0.12	Closed	Dots	OK
4	2-S	2	2	3	0.12	Closed	Dots	OK
5	2-S	2	2	2a	0.12	Closed	Dots	OK
6	2-S	2	2	0	no trip	Closed	Dots	OK
7	1-S	2	2	0	no trip	Open	Dots	OK
8	1-S	2	2	3	0.12	Open	Dots	OK
9	1-S	2	2	2a	0.12	Open	Paint	Insufficient oil flow
10	1-S	2	2	2b	0.12	Open	Paint	OK
11	1-S	2	2	1	0.12	Open	Paint	OK
12	1-S	2	2	0	no trip	Open	Paint	Insufficient oil flow
13	1-S	2	2	0	no trip	Open	Paint	Insufficient oil flow
14	1-S	2	2	0	no trip	Open	Paint	OK
15	1-S	2	2	1	0.12	Open	Paint	OK
16	1-S	2	2	2b	0.12	Open	Paint	Insufficient oil flow
17	1-S	2	2	2a	0.12	Open	Paint	Insufficient oil flow
18	1-S	2	2	2b	0.12	Open	Paint	OK
19	1-S	2	2	3	0.12	Open	Paint	OK
20	1-S	2	2	2a	0.12	Open	Paint	OK

Figure 1a. Hyper-X vehicle mated to Pegasus booster awaiting drop from B-52.

Figure 1b. Hyper-X vehicle lofted to test-point by Pegasus booster.

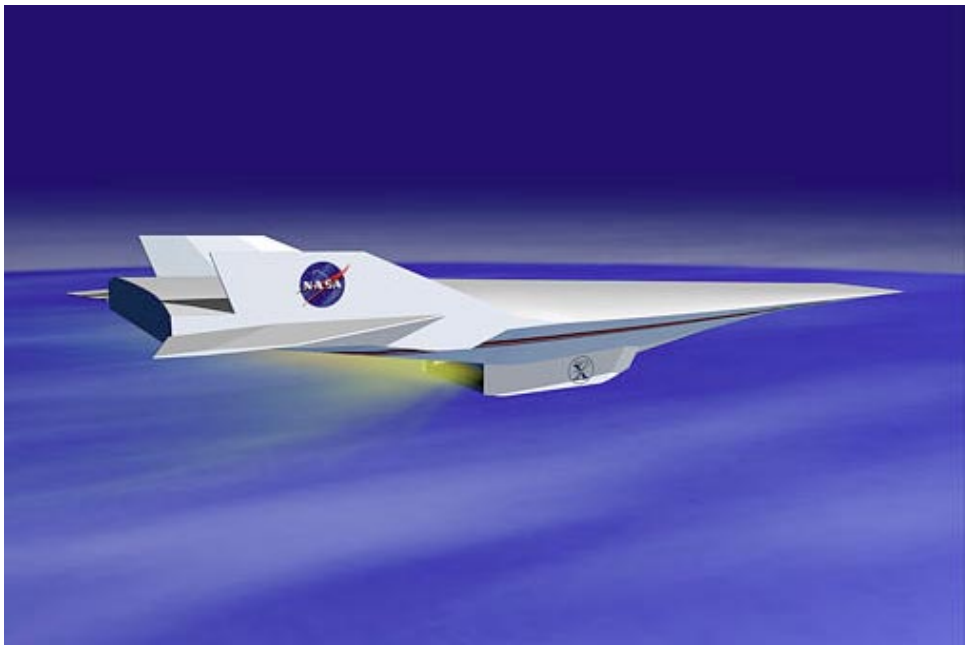

Figure 1c. Hyper-X vehicle flying at test-point.

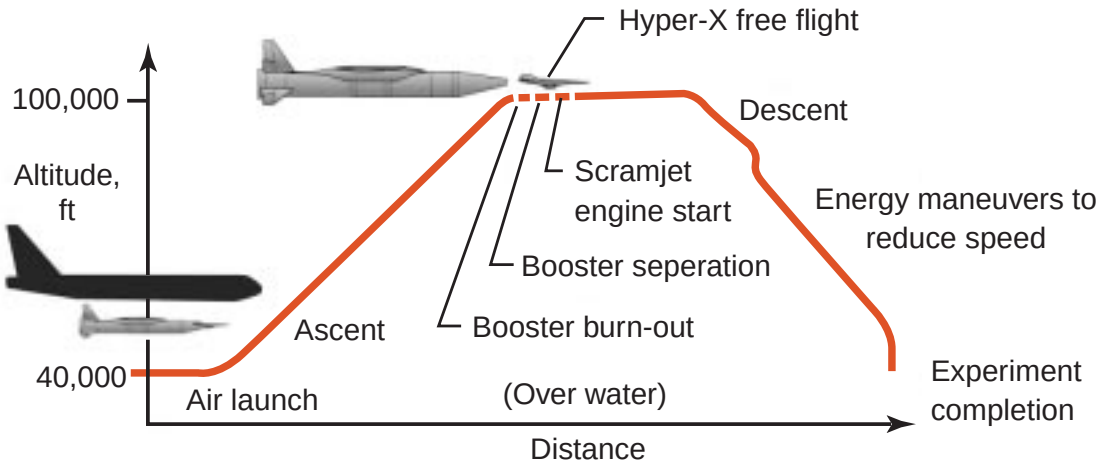

Figure 2. Preliminary Hyper-X trajectory

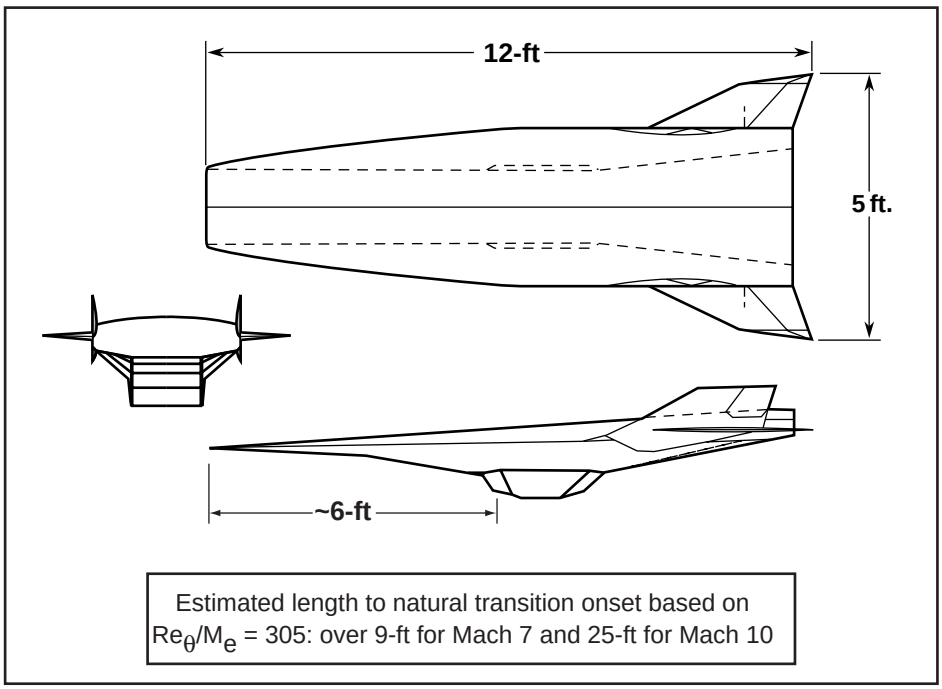

Figure 3. Hyper-X vehicle dimensions.

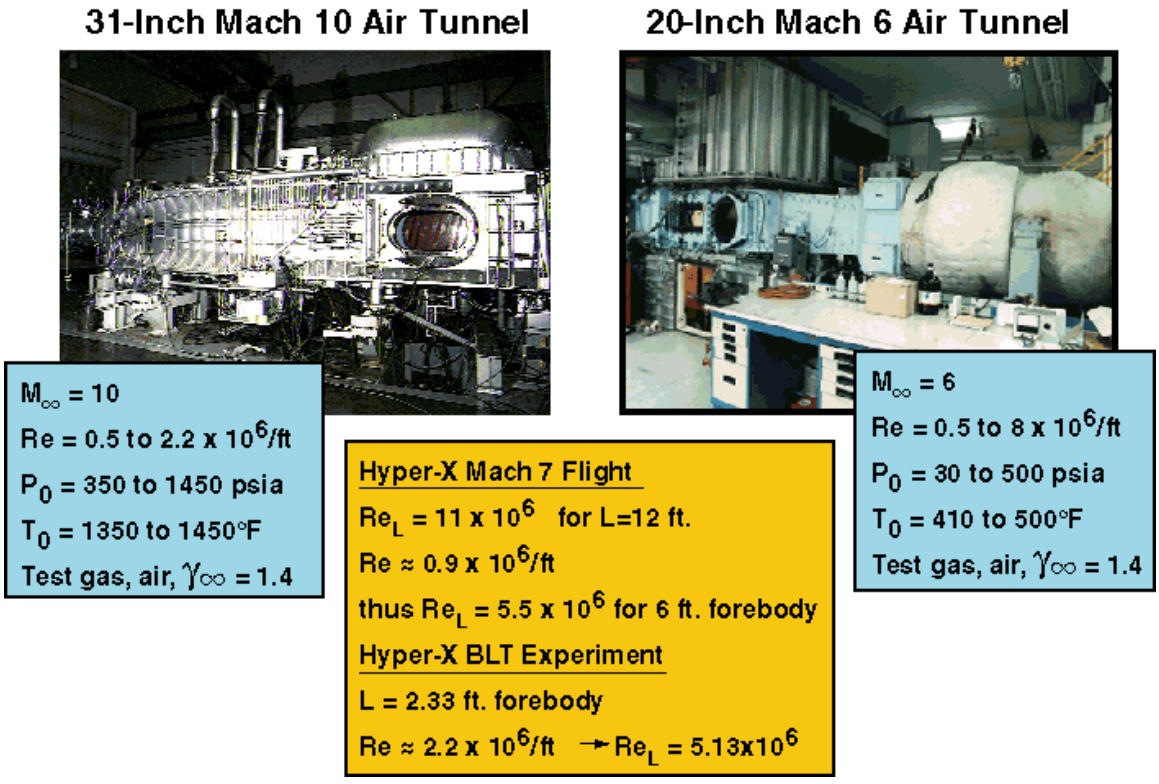

Figure 4. NASA Langley facilities utilized for Hyper-X transition tests.

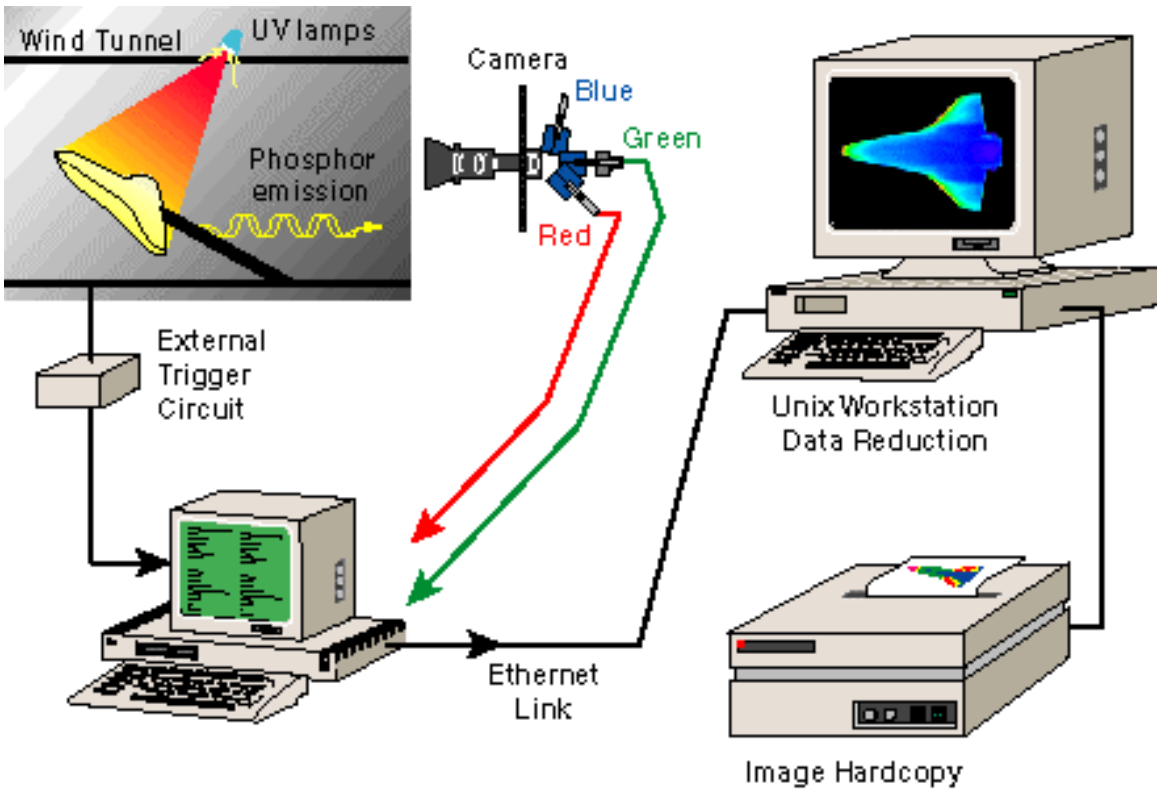

Figure 5. Schematic of phosphor thermography system.

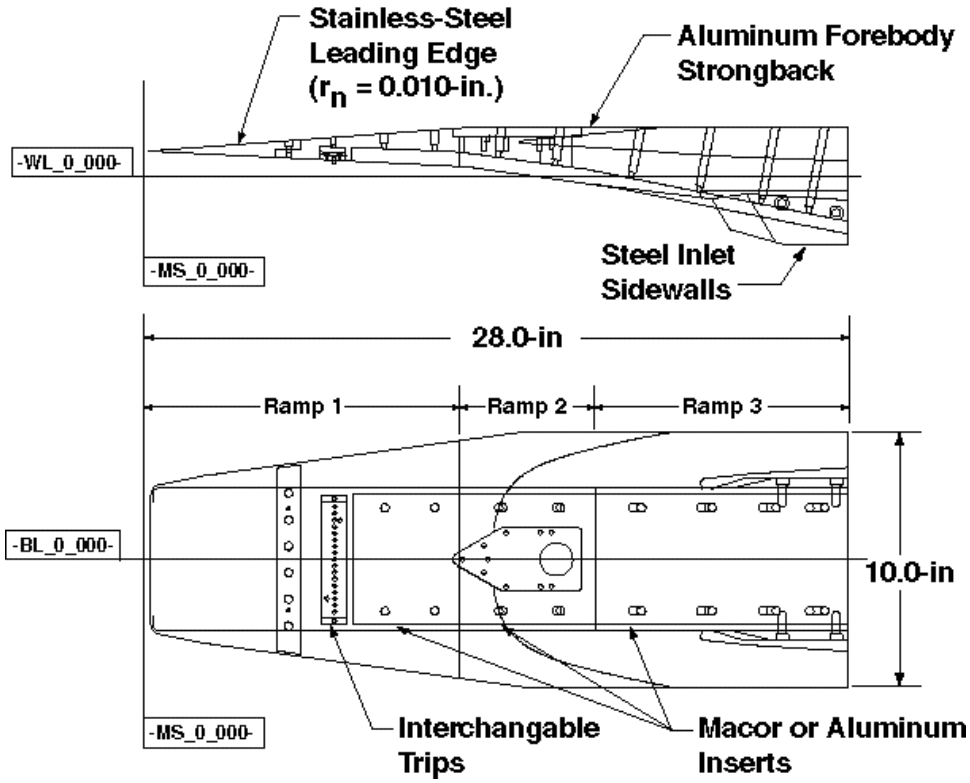

Figure 6. Hyper-X forebody model dimensions.

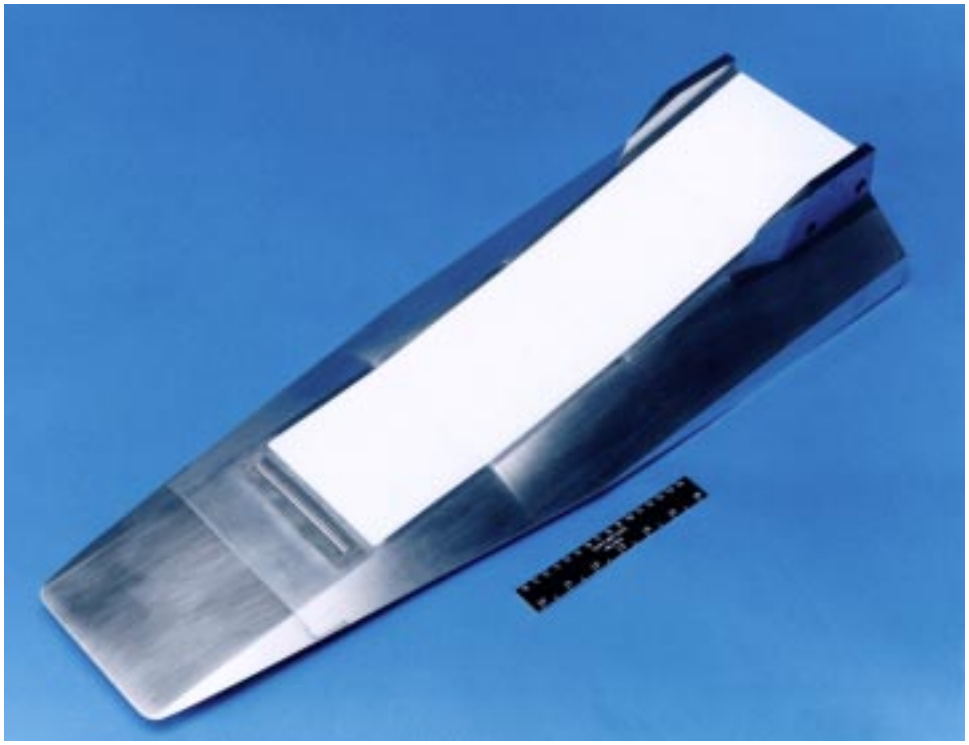

Figure 7. Photograph of 0.333-scale Hyper-X forebody model in the open-cowl configuration with Macor inserts for phosphor thermography testing.

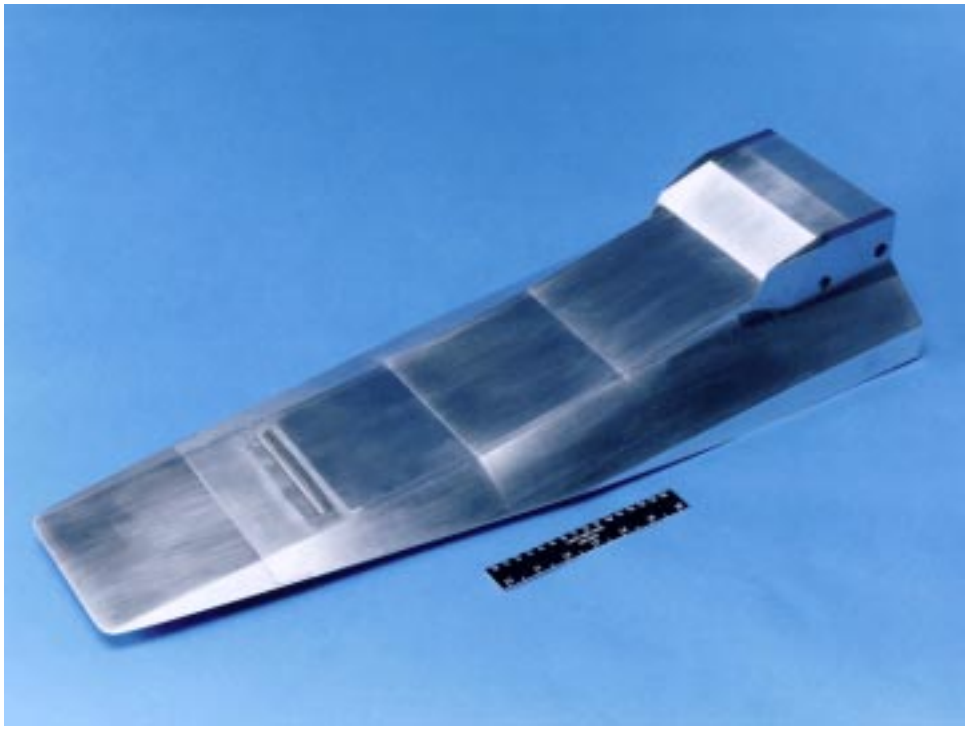

Figure 8. Photograph of 0.333-scale Hyper-X forebody model in the closed-cowl configuration with metal inserts for flow visualization testing.

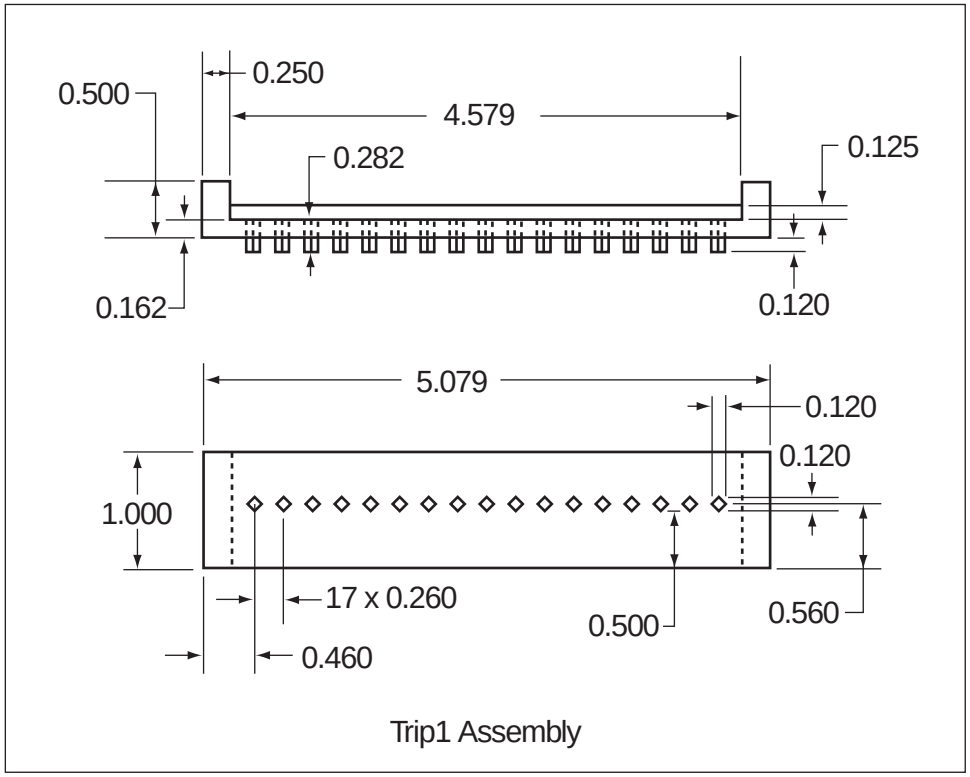

Figure 9a. Detail sketch of Trip Configuration 1.

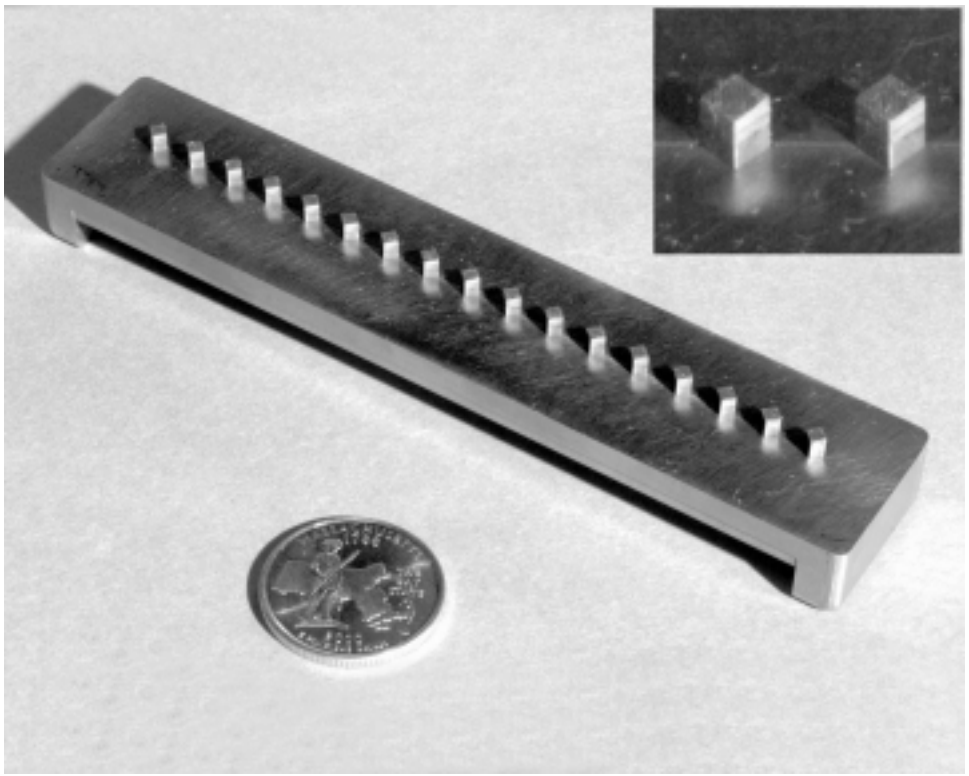

Figure 9b. Photograph of Trip Configuration 1.

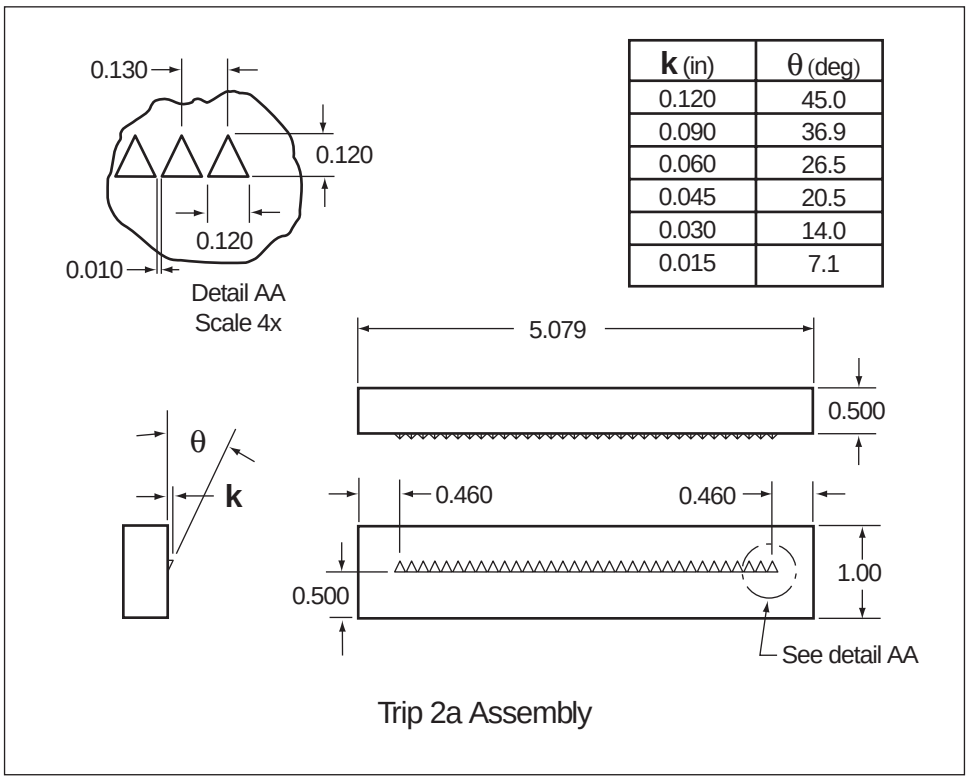

Figure 10a. Detailed sketch of Trip Configuration 2a.

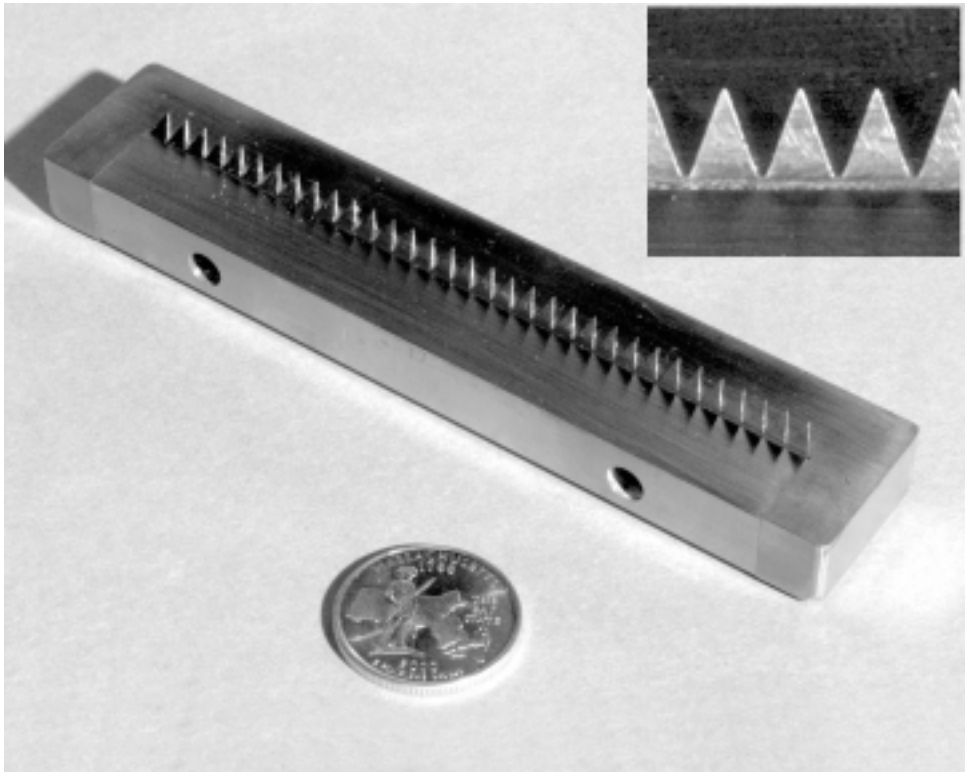

Figure 10b. Photograph of Trip Configuration 2a.

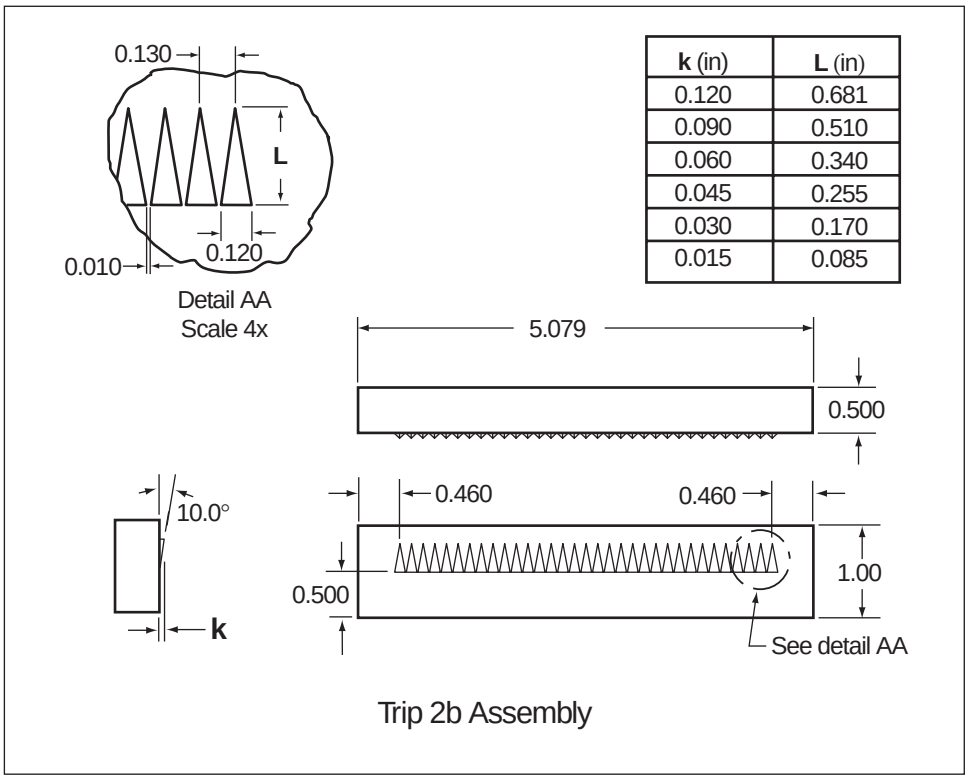

Figure 11a. Detailed sketch of Trip Configuration 2b.

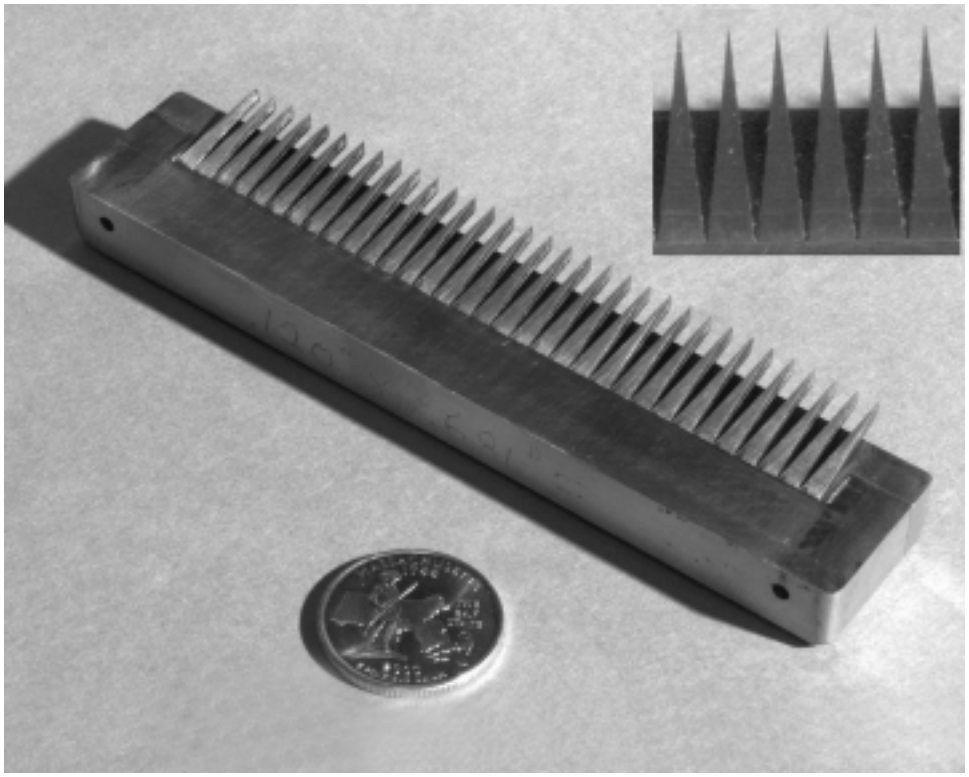

Figure 11b. Photograph of Trip Configuration 2b.

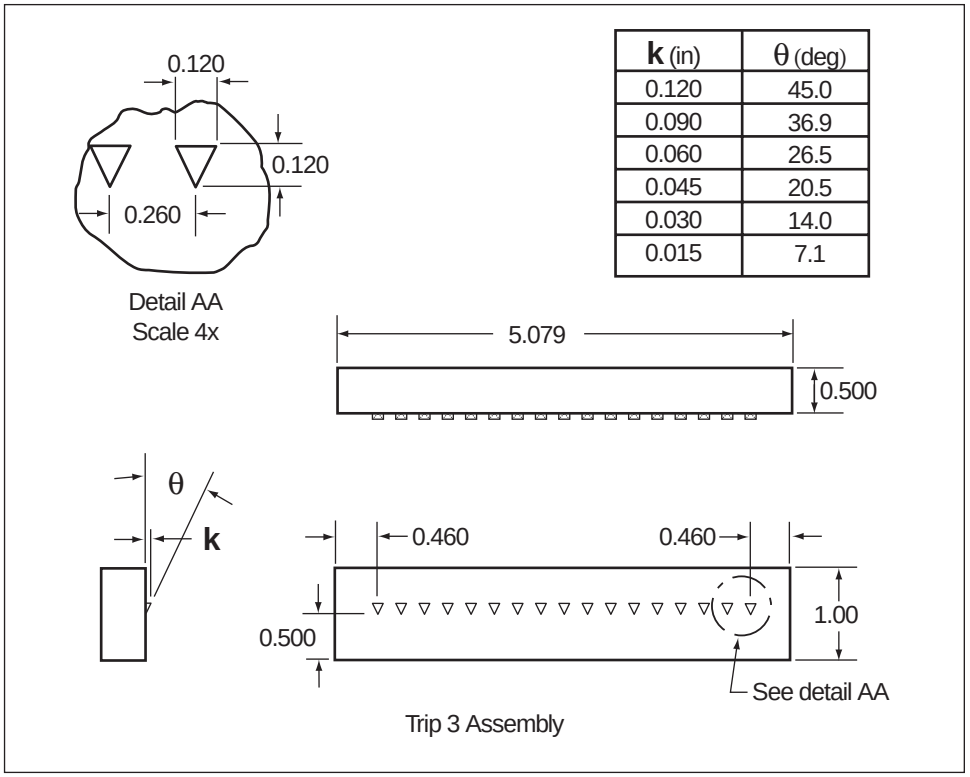

Figure 12a. Detailed sketch of Trip Configuration 3.

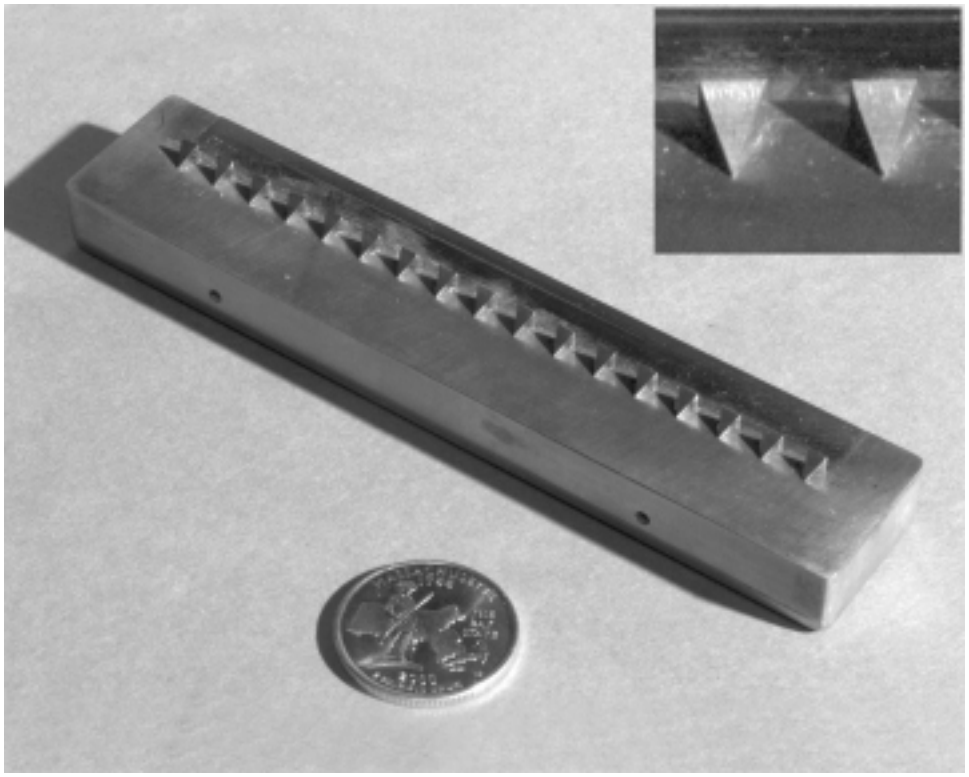

Figure 12b. Photograph of Trip Configuration 3.

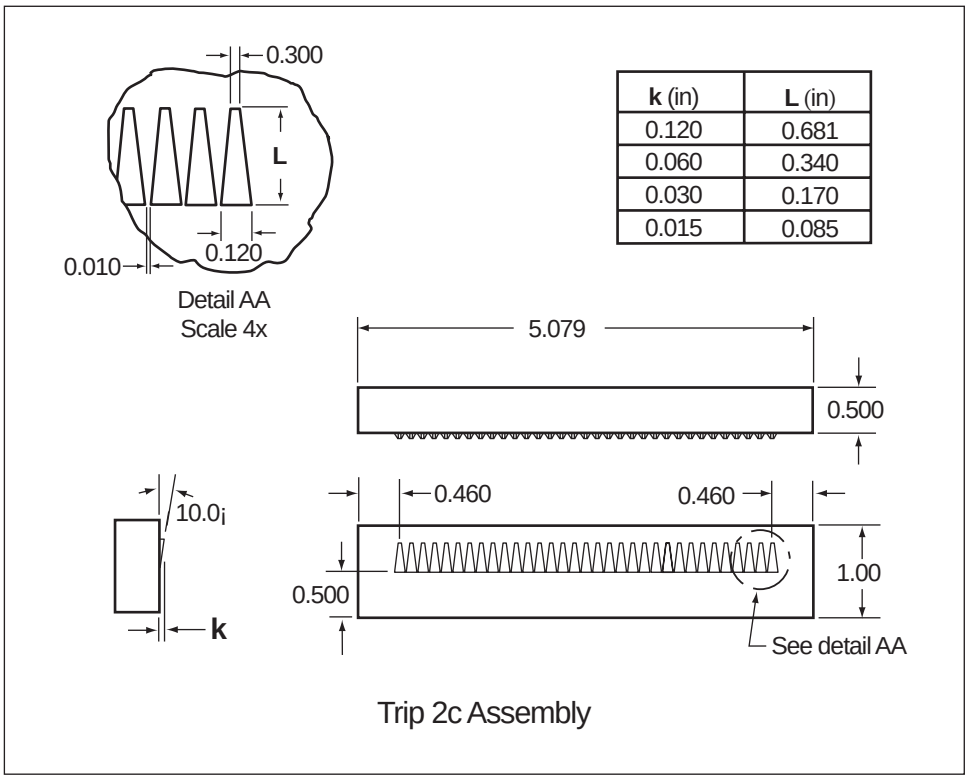

Figure 13a. Detailed sketch of Trip Configuration 2c.

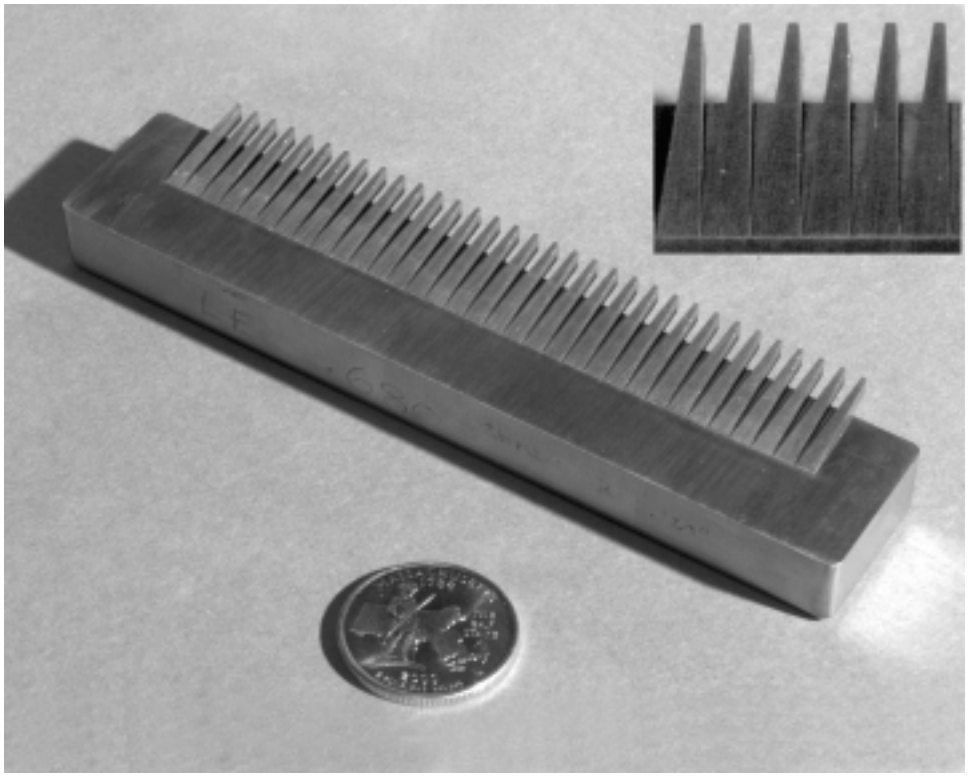

Figure 13b. Photograph of Trip Configuration 2c.

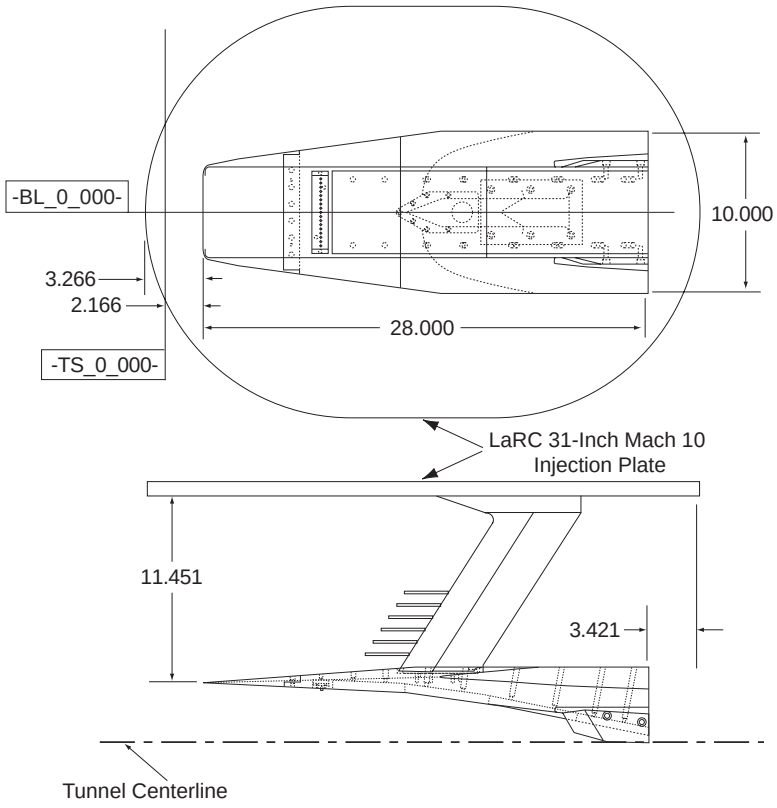

Figure 14. Detailed sketch of model assembly with short strut.

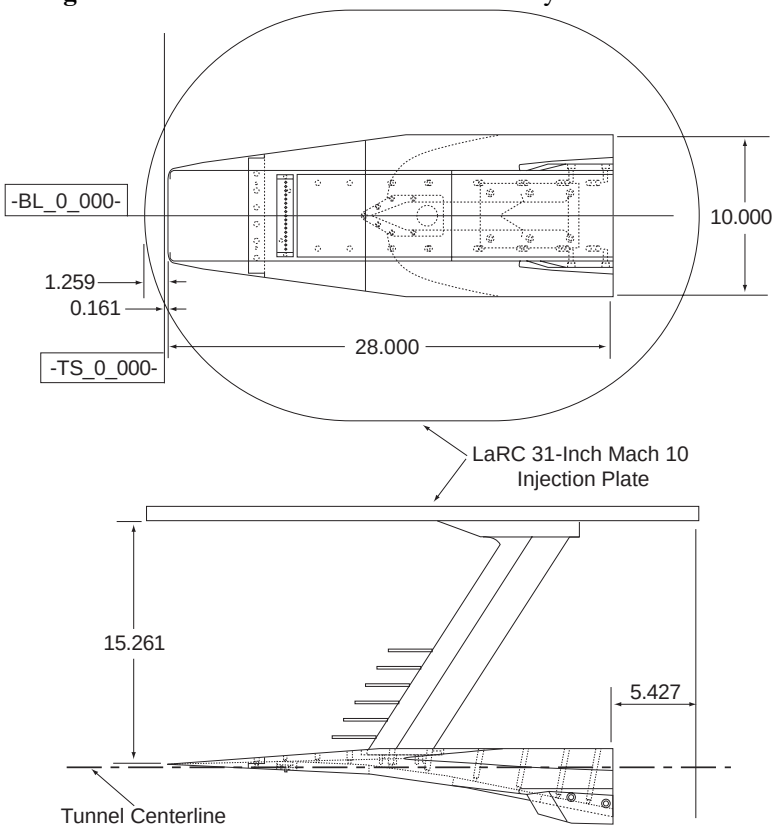

Figure 15. Detailed sketch of model assembly with long strut.

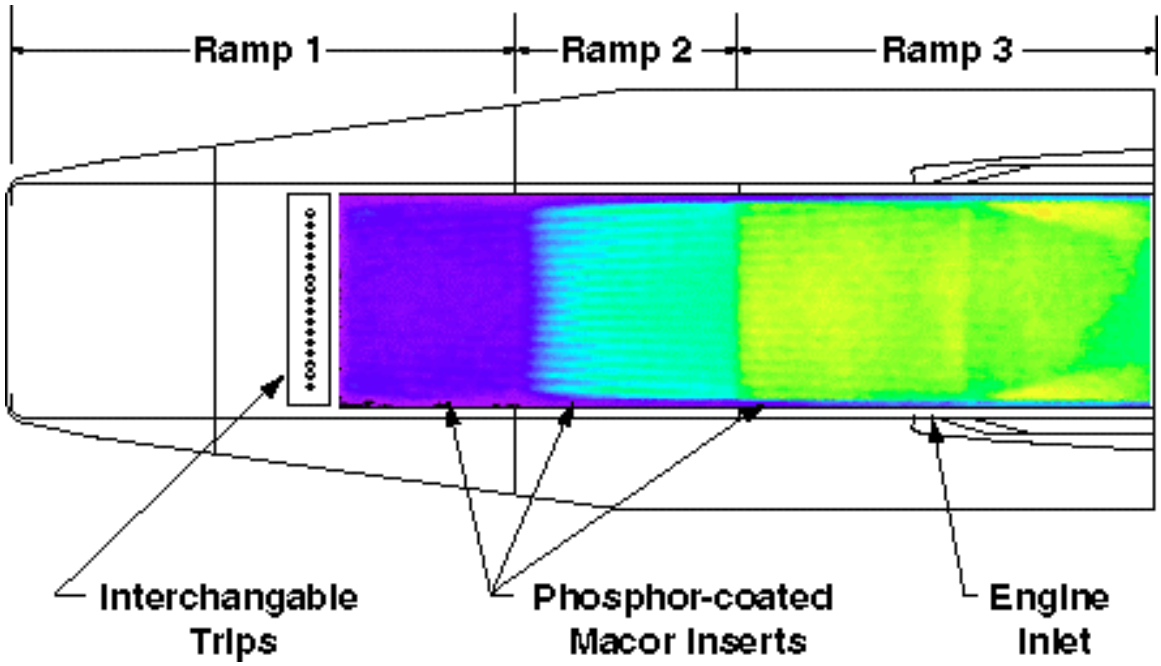

Figure 16. Comparison of phosphor image to model scale.

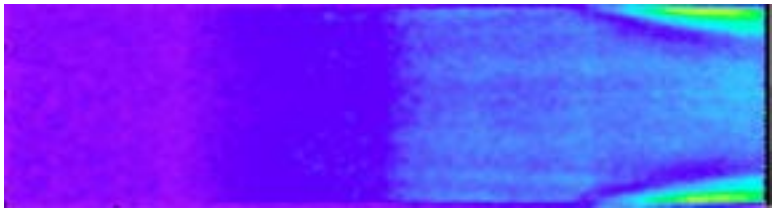

Test 338 Run 1
α = 2-deg
Re = 1.14 x 10^6/ft
Trip # 1
k = 0.000-in.
Open Cowl

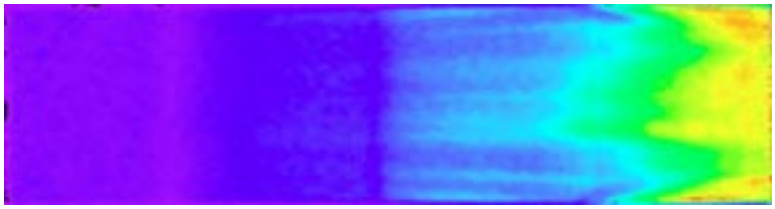

Test 338 Run 2
α = 2-deg
Re = 2.20 x 10^6/ft
Trip # 1
k = 0.000-in.
Open Cowl

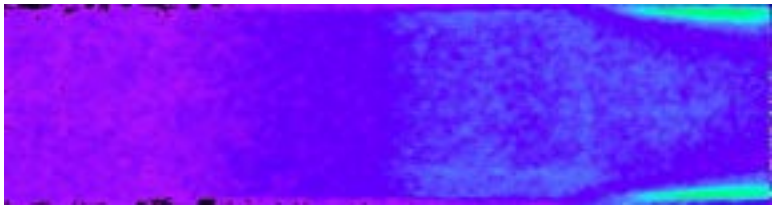

Test 338 Run 3
α = 2-deg
Re = 0.57 x 10^6/ft
Trip # 1
k = 0.000-in.
Open Cowl

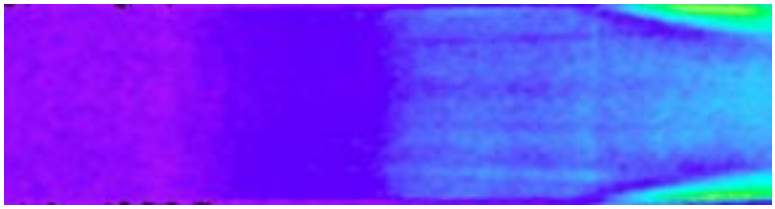

Test 338 Run 4
α = 2-deg
Re = 1.13 x 10^6/ft
Trip # 1
k = 0.000-in.
Open Cowl

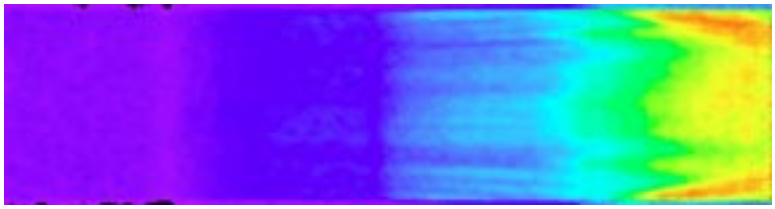

Test 338 Run 5
α = 2-deg
Re = 2.23 x 10^6/ft
Trip # 1
k = 0.000-in.
Open Cowl

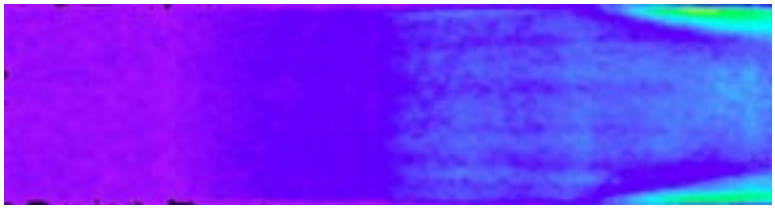

Test 338 Run 6
α = 2-deg
Re = 1.14 x 10^6/ft
Trip # 1
k = 0.015-in.
Open Cowl

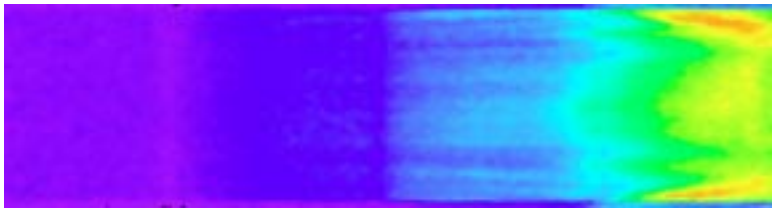

Test 338 Run 7
α = 2-deg
Re = 2.18 x 10^6/ft
Trip # 1
k = 0.015-in.
Open Cowl

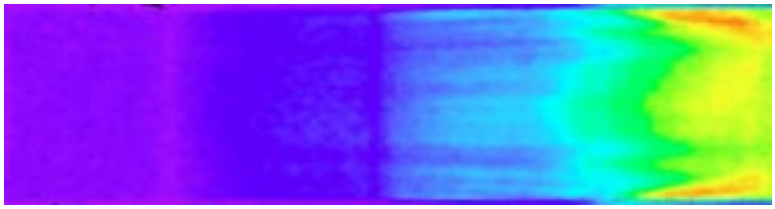

Test 338 Run 8
α = 2-deg
Re = 2.23 x 10^6/ft
Trip # 1
k = 0.015-in.
Open Cowl

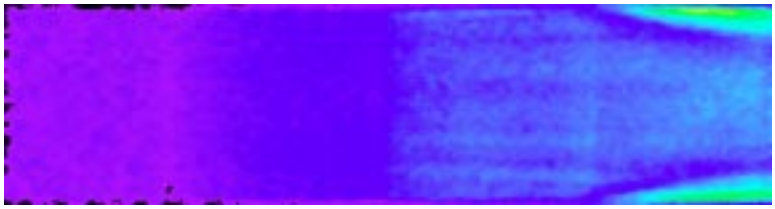

Test 338 Run 9
α = 2-deg
Re = 1.12 x 10^6/ft
Trip # 1
k = 0.030-in.
Open Cowl

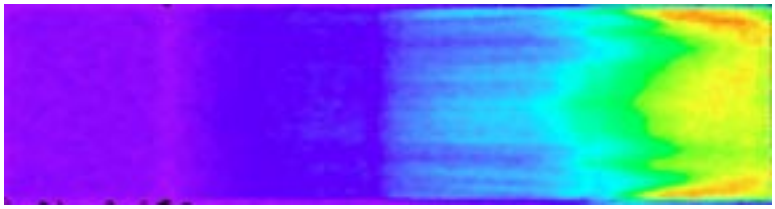

Test 338 Run 10
α = 2-deg
Re = 2.18 x 10^6/ft
Trip # 1
k = 0.030-in.
Open Cowl

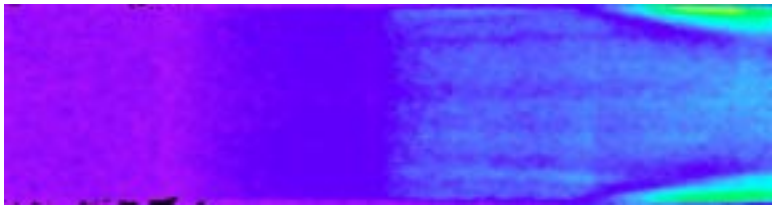

Test 338 Run 11
α = 2-deg
Re = 1.12 x 10^6/ft
Trip # 1
k = 0.045-in.
Open Cowl

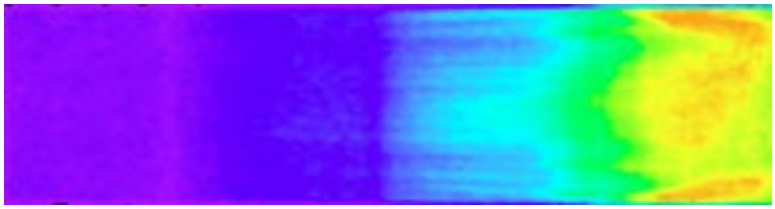

Test 338 Run 12
α = 2-deg
Re = 2.19 x 10^6/ft
Trip # 1
k = 0.045-in.
Open Cowl

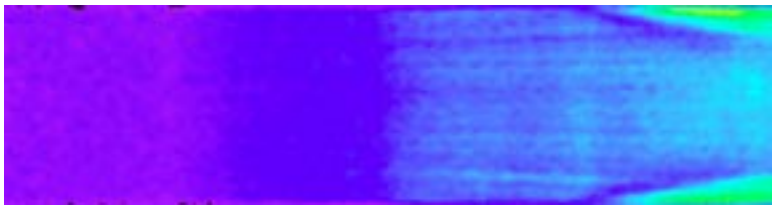

Test 338 Run 13
α = 2-deg
Re = 1.11 x 10^6/ft
Trip # 1
k = 0.060-in.
Open Cowl

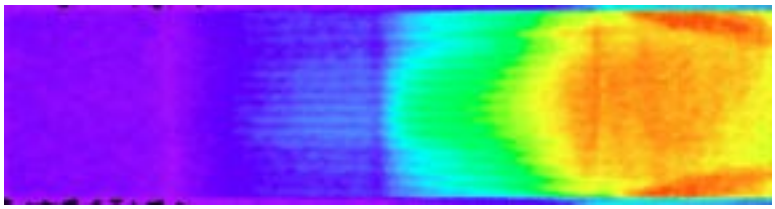

Test 338 Run 14
α = 2-deg
Re = 2.21 x 10^6/ft
Trip # 1
k = 0.060-in.
Open Cowl

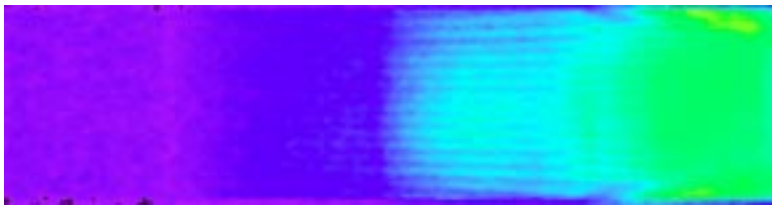

Test 338 Run 15
α = 2-deg
Re = 1.10 x 10^6/ft
Trip # 1
k = 0.090-in.
Open Cowl

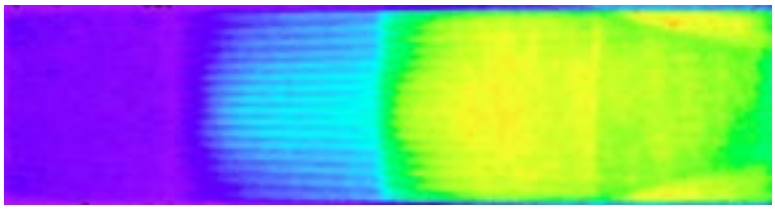

Test 338 Run 16
α = 2-deg
Re = 2.20 x 10^6/ft
Trip # 1
k = 0.090-in.
Open Cowl

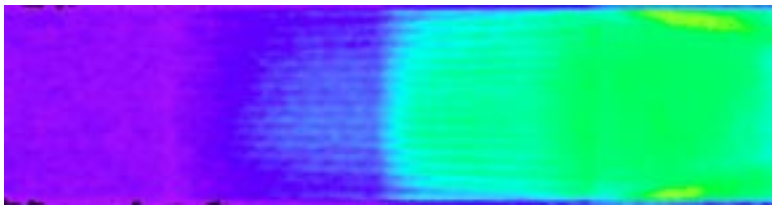

Test 338 Run 17
α = 2-deg
Re = 1.12 x 10^6/ft
Trip # 1
k = 0.120-in.
Open Cowl

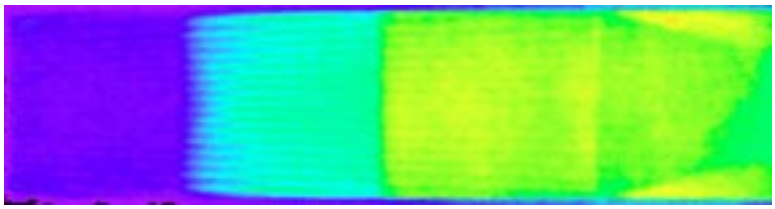

Test 338 Run 18
α = 2-deg
Re = 2.23 x 10^6/ft
Trip # 1
k = 0.120-in.
Open Cowl

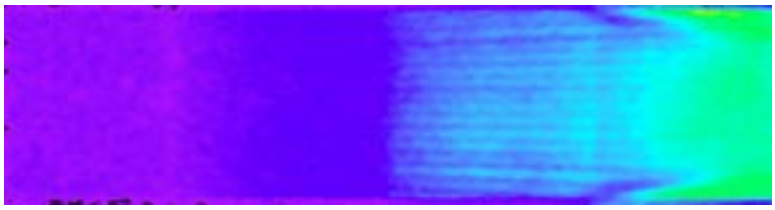

Test 338 Run 19
α = 2-deg
Re = 1.09 x 10^6/ft
Trip # 1
k = 0.075-in.
Open Cowl

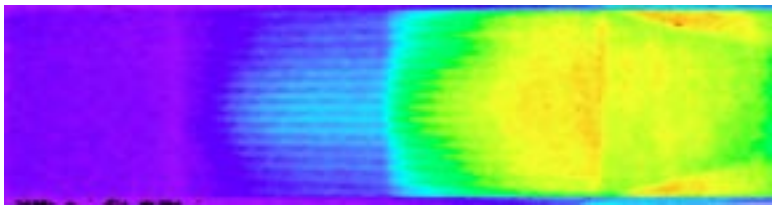

Test 338 Run 20
α = 2-deg
Re = 2.20 x 10^6/ft
Trip # 1
k = 0.075-in.
Open Cowl

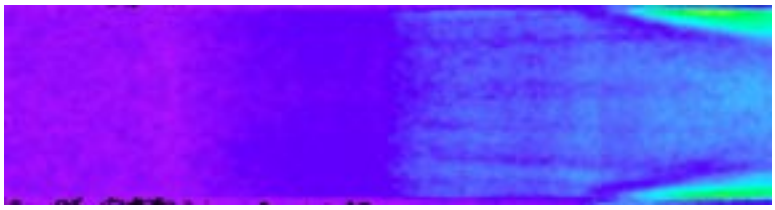

Test 338 Run 21
α = 2-deg
Re = 1.12 x 10^6/ft
No Trip
Model Baseline
Open Cowl

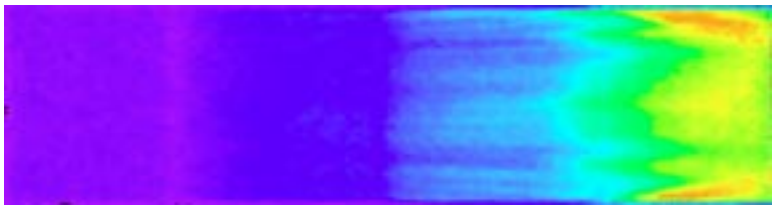

Test 338 Run 22
α = 2-deg
Re = 2.25 x 10^6/ft
No Trip
Model Baseline
Open Cowl

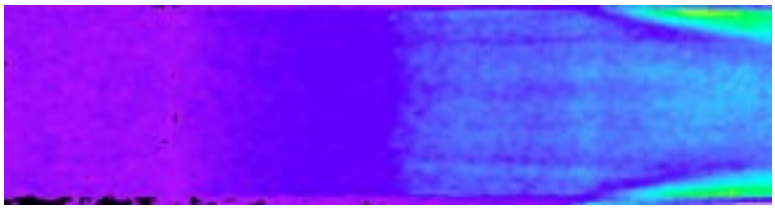

Test 338 Run 23
α = 2-deg
Re = 1.14 x 10^6/ft
Trip # 2b
k = 0.060-in.
Open Cowl

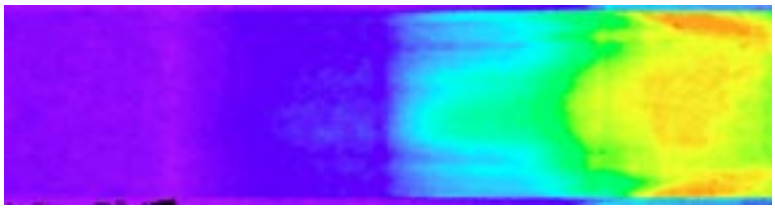

Test 338 Run 24
α = 2-deg
Re = 2.18 x 10^6/ft
Trip # 2b
k = 0.060-in.
Open Cowl

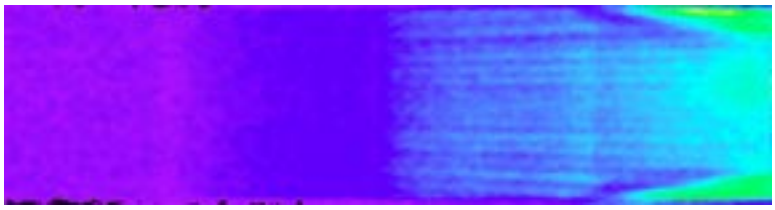

Test 338 Run 25
α = 2-deg
Re = 1.12 x 10^6/ft
Trip # 3
k = 0.060-in.
Open Cowl

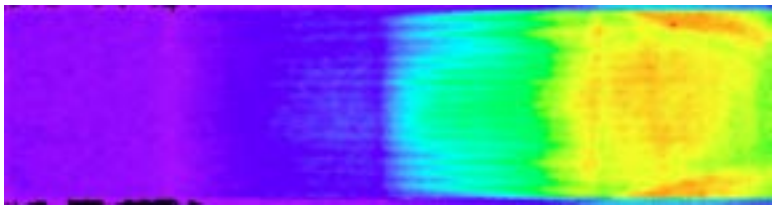

Test 338 Run 26
α = 2-deg
Re = 2.17 x 10^6/ft
Trip # 3
k = 0.060-in.
Open Cowl

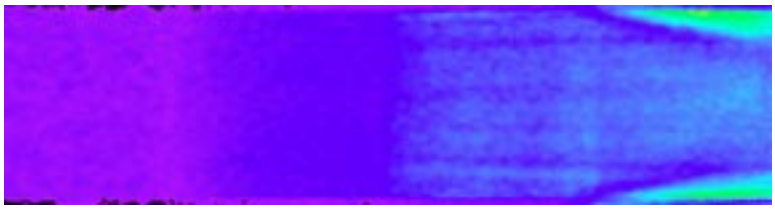

Test 338 Run 27
α = 2-deg
Re = 1.12 x 10^6/ft
Trip # 2a
k = 0.060-in.
Open Cowl

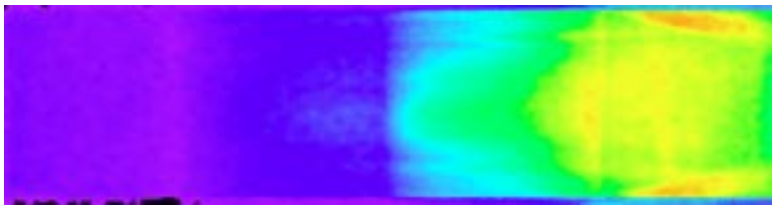

Test 338 Run 28
α = 2-deg
Re = 2.27 x 10^6/ft
Trip # 2a
k = 0.060-in.
Open Cowl

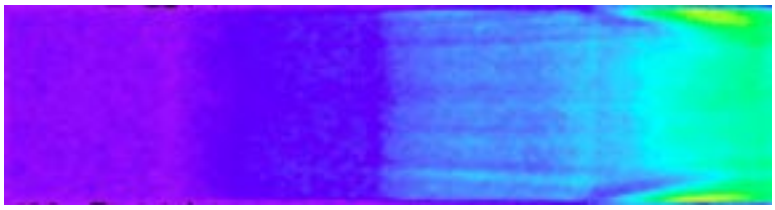

Test 338 Run 29
α = 3-deg
Re = 1.13 x 10^6/ft
No Trip
Model Baseline
Open Cowl

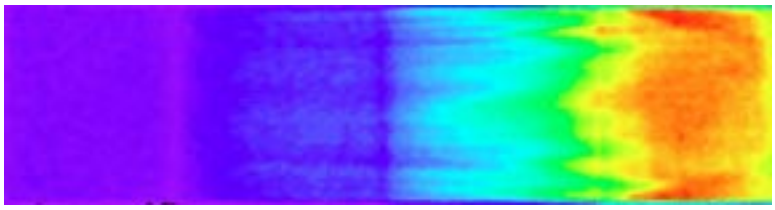

Test 338 Run 30
α = 3-deg
Re = 2.23 x 10^6/ft
No Trip
Model Baseline
Open Cowl

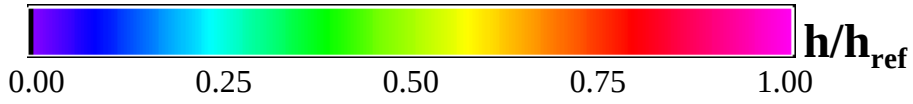

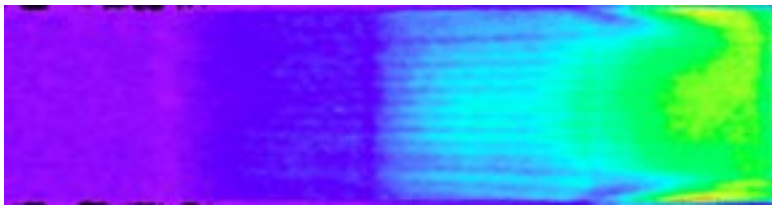

Test 338 Run 31
α = 3-deg
Re = 1.12 x 10^6/ft
Trip # 1
k = 0.060-in.
Open Cowl

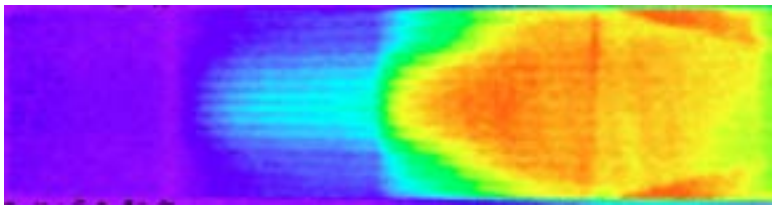

Test 338 Run 32
α = 3-deg
Re = 2.11 x 10^6/ft
Trip # 1
k = 0.060-in.
Open Cowl

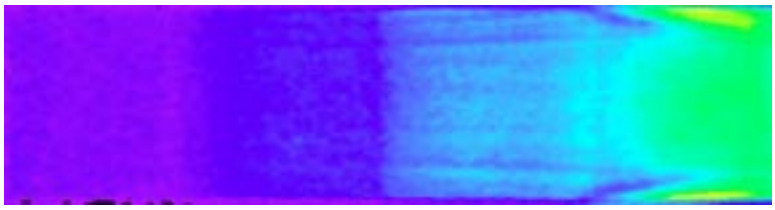

Test 338 Run 33
α = 3-deg
Re = 1.11 x 10^6/ft
Trip # 2a
k = 0.060-in.
Open Cowl

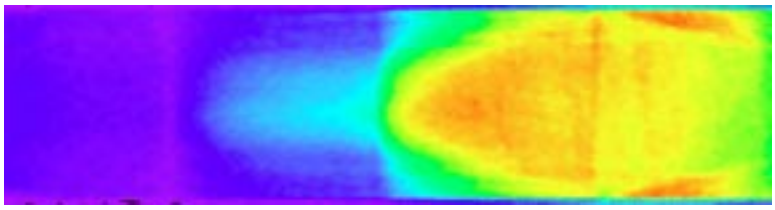

Test 338 Run 34
α = 3-deg
Re = 2.22 x 10^6/ft
Trip # 2a
k = 0.060-in.
Open Cowl

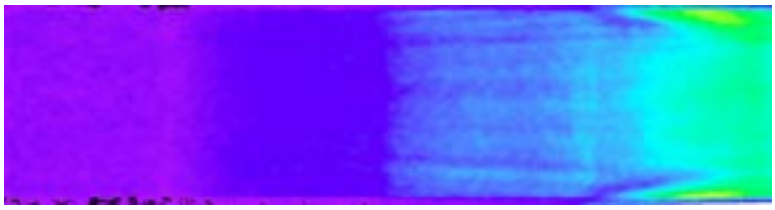

Test 338 Run 35
α = 3-deg
Re = 1.14 x 10^6/ft
Trip # 2b
k = 0.060-in.
Open Cowl

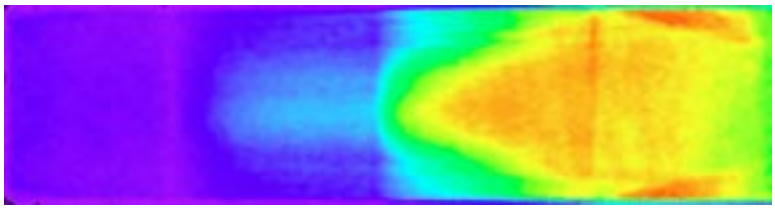

Test 338 Run 36
α = 3-deg
Re = 2.24 x 10^6/ft
Trip # 2b
k = 0.060-in.
Open Cowl

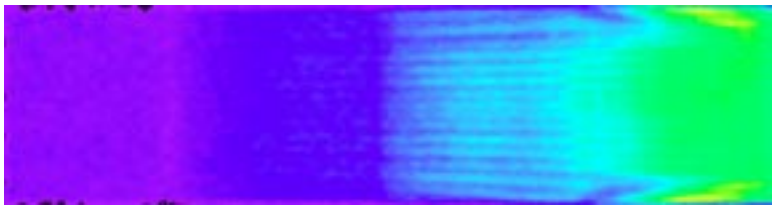

Test 338 Run 37
α = 3-deg
Re = 1.14 x 10^6/ft
Trip # 3
k = 0.060-in.
Open Cowl

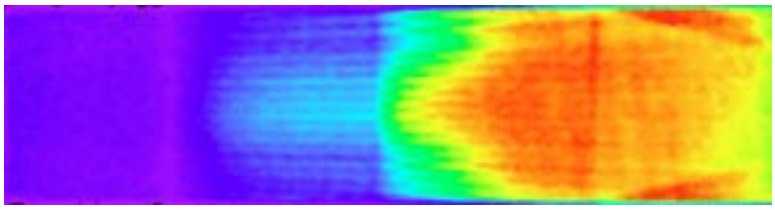

Test 338 Run 38
α = 3-deg
Re = 2.24 x 10^6/ft
Trip # 3
k = 0.060-in.
Open Cowl

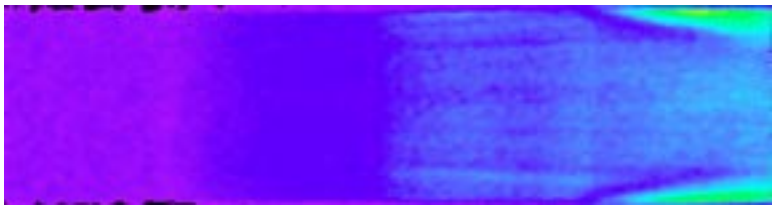

Test 338 Run 39
α = 2-deg
Re = 1.10 x 10^6/ft
Trip # 0
k = 0.060-in.
Open Cowl

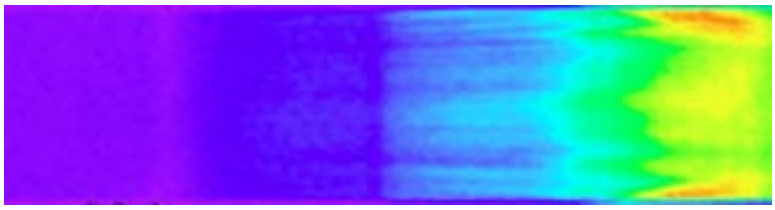

Test 338 Run 40
α = 2-deg
Re = 2.21 x 10^6/ft
Trip # 0
k = 0.060-in.
Open Cowl

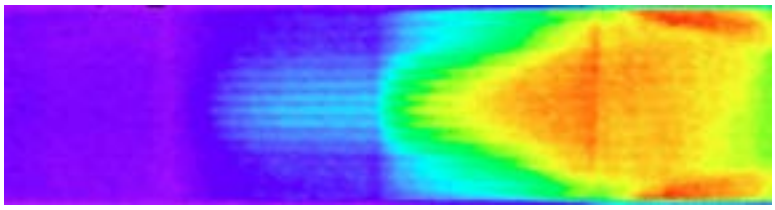

Test 338 Run 42
α = 2-deg
Re = 2.22 x 10^6/ft
Trip # 1
k = 0.060-in.
Open Cowl

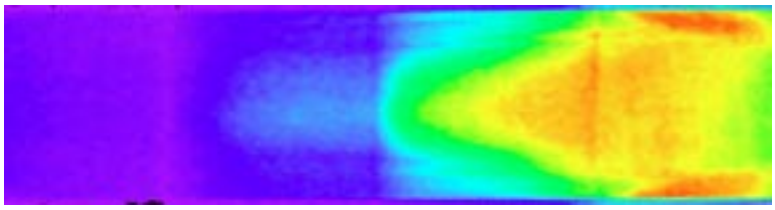

Test 338 Run 43
α = 2-deg
Re = 2.23 x 10^6/ft
Trip # 2a
k = 0.060-in.
Open Cowl

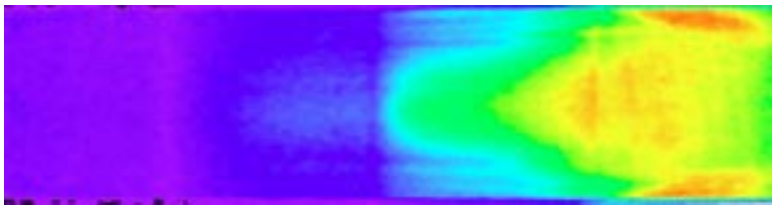

Test 338 Run 44
α = 2-deg
Re = 2.23 x 10^6/ft
Trip # 2b
k = 0.060-in.
Open Cowl

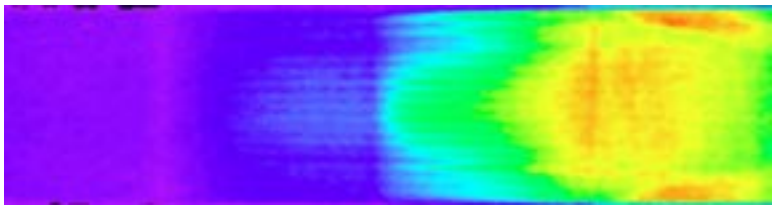

Test 338 Run 45
α = 2-deg
Re = 2.27 x 10^6/ft
Trip # 3
k = 0.060-in.
Open Cowl

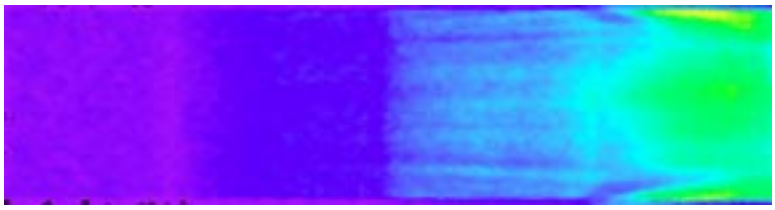

Test 338 Run 46
α = 4-deg
Re = 1.11 x 10^6/ft
No Trip
Model Baseline
Open Cowl

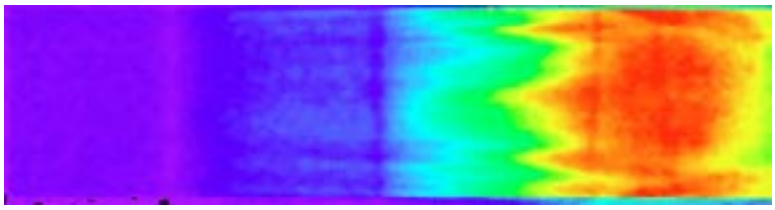

Test 338 Run 47
α = 4-deg
Re = 2.20 x 10^6/ft
No Trip
Model Baseline
Open Cowl

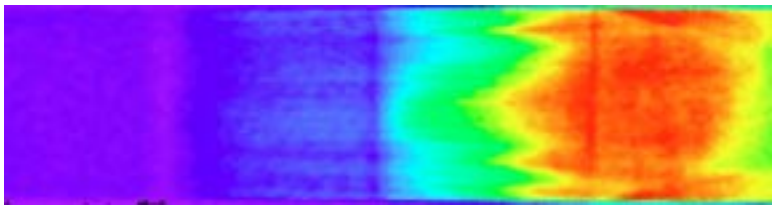

Test 338 Run 48
α = 4-deg
Re = 2.21 x 10^6/ft
Trip # 1
k = 0.030-in.
Open Cowl

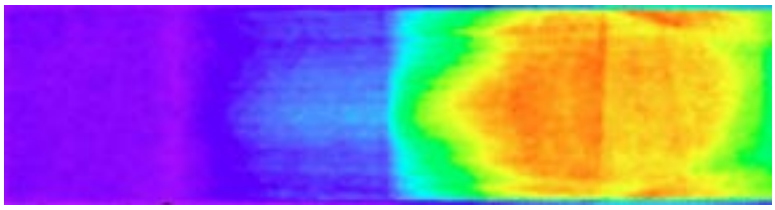

Test 338 Run 49
α = 4-deg
Re = 2.22 x 10^6/ft
Trip # 1
k = 0.045-in.
Open Cowl

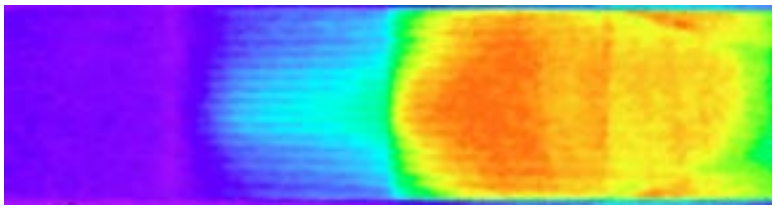

Test 338 Run 50
α = 4-deg
Re = 2.19 x 10^6/ft
Trip # 1
k = 0.060-in.
Open Cowl

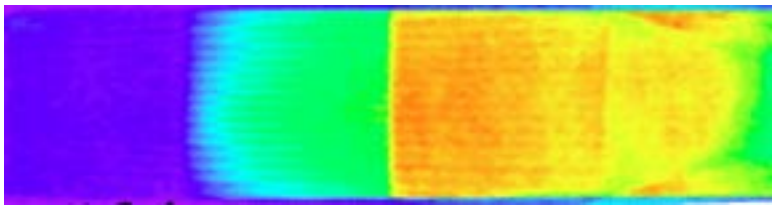

Test 338 Run 51
α = 4-deg
Re = 2.24 x 10^6/ft
Trip # 1
k = 0.075-in.
Open Cowl

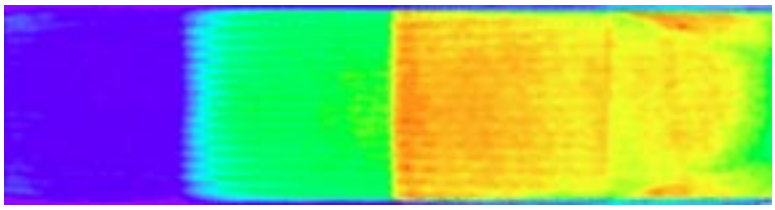

Test 338 Run 52
α = 4-deg
Re = 2.20 x 10^6/ft
Trip # 1
k = 0.090-in.
Open Cowl

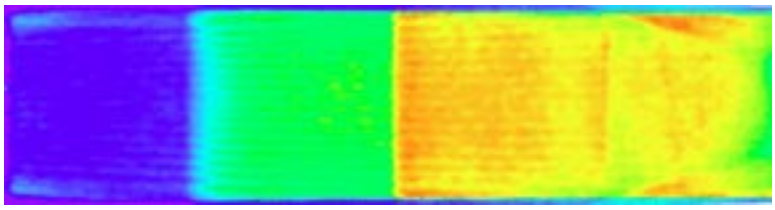

Test 338 Run 53
α = 4-deg
Re = 2.20 x 10^6/ft
Trip # 1
k = 0.120-in.
Open Cowl

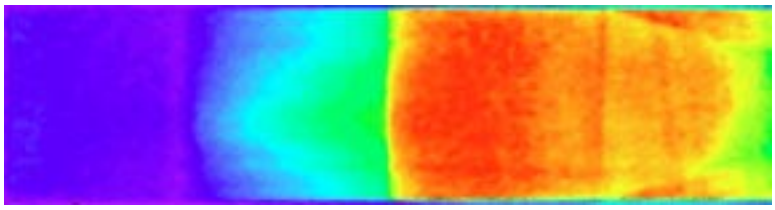

Test 338 Run 54
α = 4-deg
Re = 2.27 x 10^6/ft
Trip # 2a
k = 0.060-in.
Open Cowl

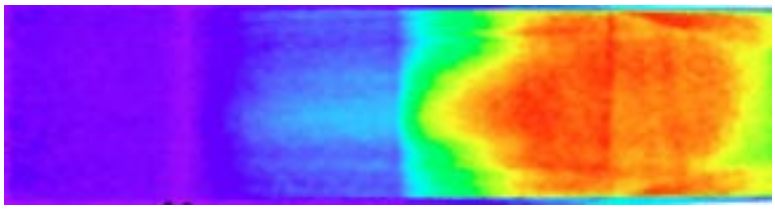

Test 338 Run 55
α = 4-deg
Re = 2.14 x 10^6/ft
Trip # 2a
k = 0.045-in.
Open Cowl

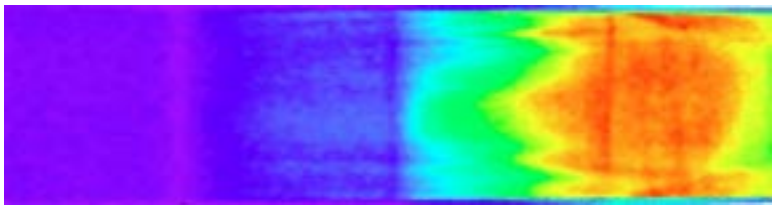

Test 338 Run 56
α = 4-deg
Re = 2.19 x 10^6/ft
Trip # 2a
k = 0.030-in.
Open Cowl

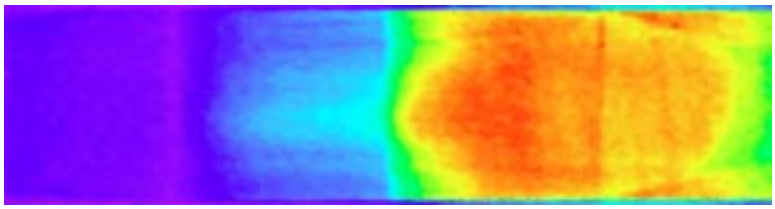

Test 338 Run 57
α = 4-deg
Re = 2.24 x 10^6/ft
Trip # 2b
k = 0.060-in.
Open Cowl

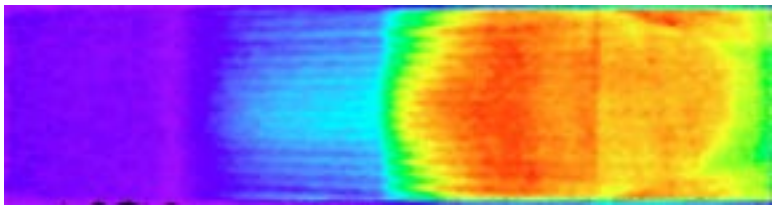

Test 338 Run 58
α = 4-deg
Re = 2.23 x 10^6/ft
Trip # 3
k = 0.060-in.
Open Cowl

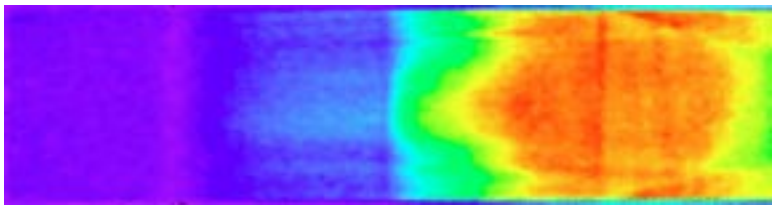

Test 338 Run 59
α = 4-deg
Re = 2.30 x 10^6/ft
Trip # 2b
k = 0.045-in.
Open Cowl

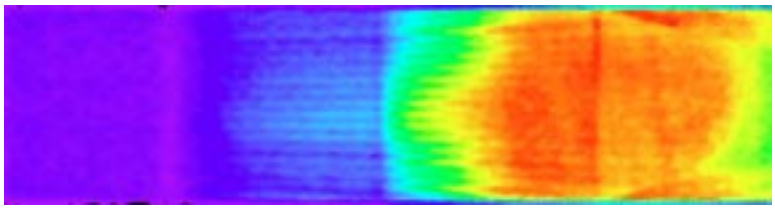

Test 338 Run 60
α = 4-deg
Re = 2.22 x 10^6/ft
Trip # 3
k = 0.045-in.
Open Cowl

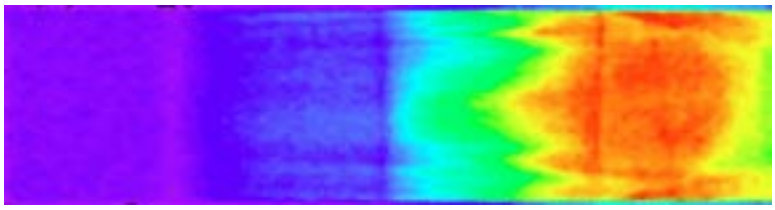

Test 338 Run 61
α = 4-deg
Re = 2.22 x 10^6/ft
Trip # 2b
k = 0.030-in.
Open Cowl

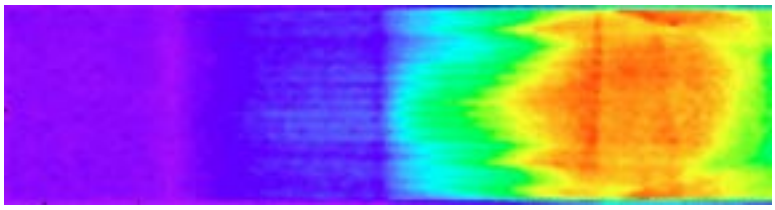

Test 338 Run 62
α = 4-deg
Re = 2.22 x 10^6/ft
Trip # 3
k = 0.030-in.
Open Cowl

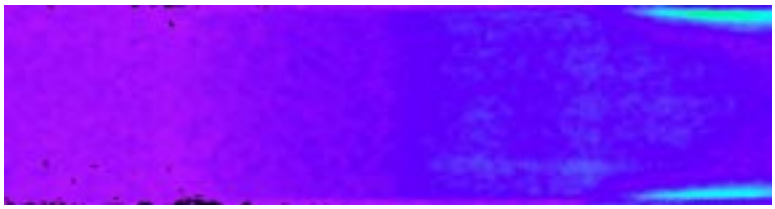

Test 338 Run 63
α = 0-deg
Re = 1.11 x 10^6/ft
No Trip
Model Baseline
Open Cowl

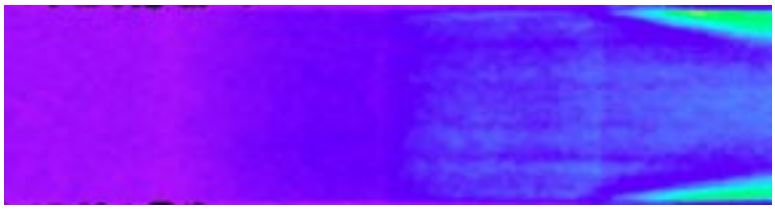

Test 338 Run 64
α = 0-deg
Re = 2.19 x 10^6/ft
No Trip
Model Baseline
Open Cowl

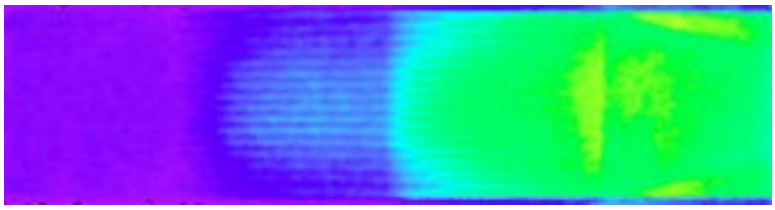

Test 338 Run 65
α = 0-deg
Re = 2.21 x 10^6/ft
Trip # 1
k = 0.120-in.
Open Cowl

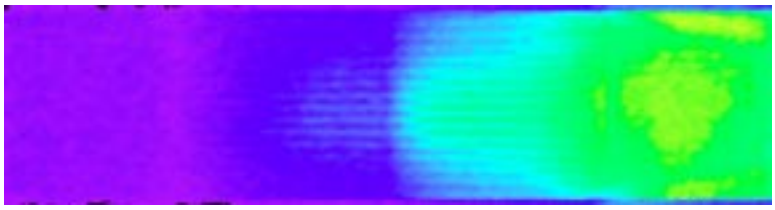

Test 338 Run 66
α = 0-deg
Re = 2.21 x 10^6/ft
Trip # 1
k = 0.090-in.
Open Cowl

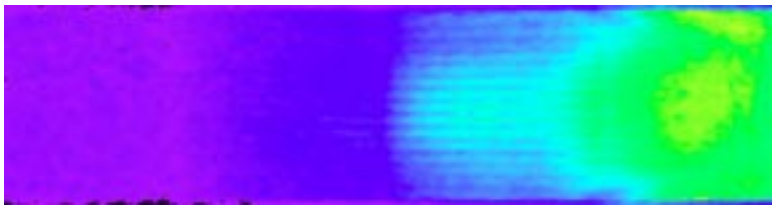

Test 338 Run 67
α = 0-deg
Re = 2.24 x 10^6/ft
Trip # 1
k = 0.075-in.
Open Cowl

Test 338 Run 68
α = 0-deg
Re = 2.27 x 10^6/ft
Trip # 1
k = 0.060-in.
Open Cowl

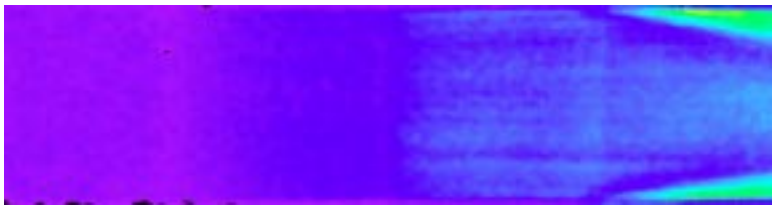

Test 338 Run 69
α = 0-deg
Re = 2.17 x 10^6/ft
Trip # 1
k = 0.030-in.
Open Cowl

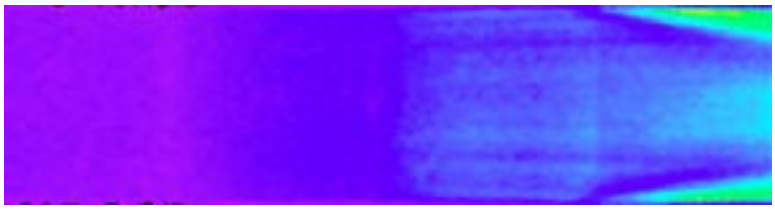

Test 338 Run 70
α = 0-deg
Re = 2.18 x 10^6/ft
Trip # 2a
k = 0.060-in.
Open Cowl

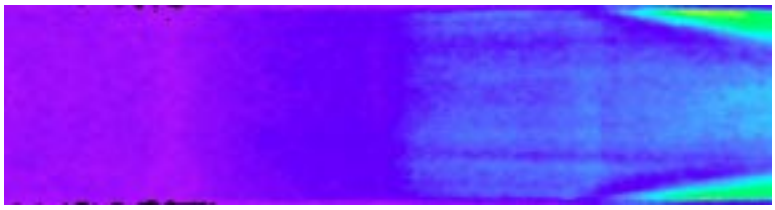

Test 338 Run 71
α = 0-deg
Re = 2.21 x 10^6/ft
Trip # 2b
k = 0.060-in.
Open Cowl

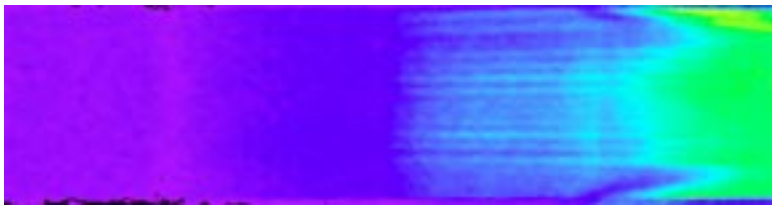

Test 338 Run 72
α = 0-deg
Re = 2.24 x 10^6/ft
Trip # 3
k = 0.060-in.
Open Cowl

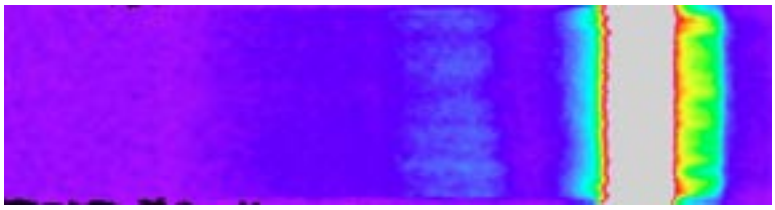

Test 338 Run 73
α = 2-deg
Re = 1.10 x 10^6/ft
No Trip
Model Baseline
Closed Cowl

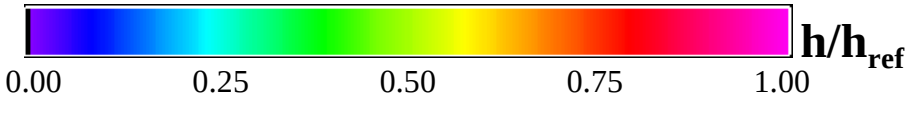

Test 338 Run 74
α = 2-deg
Re = 0.56 x 10^6/ft
No Trip
Model Baseline
Closed Cowl

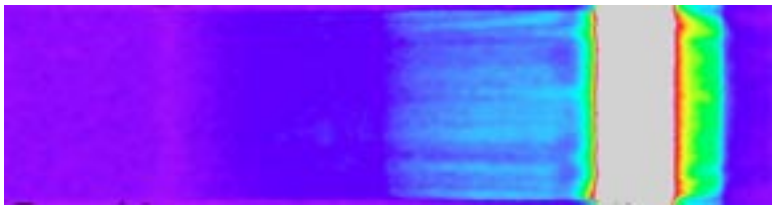

Test 338 Run 75
α = 2-deg
Re = 2.23 x 10^6/ft
No Trip
Model Baseline
Closed Cowl

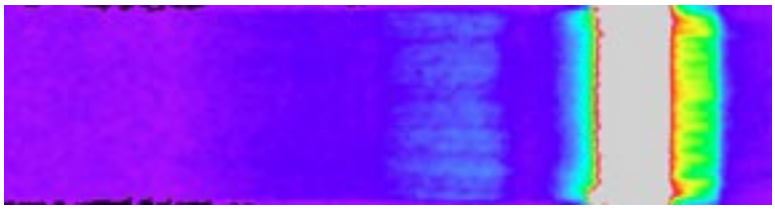

Test 338 Run 76
α = 2-deg
Re = 1.11 x 10^6/ft
Trip # 1
k = 0.060-in.
Closed Cowl

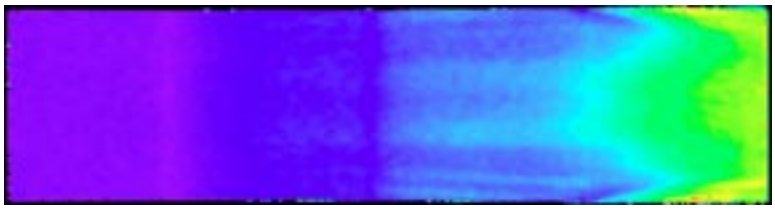

Test 338 Run 77
α = 2-deg
Re = 2.21 x 10^6/ft
No Trip
Model Baseline
Open Cowl

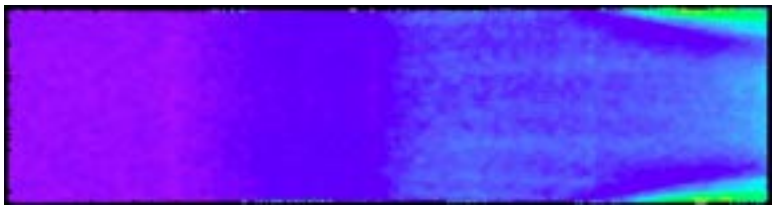

Test 338 Run 78
α = 2-deg
Re = 1.11 x 10^6/ft
No Trip
Model Baseline
Open Cowl

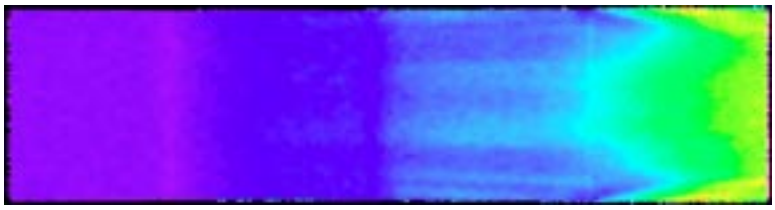

Test 338 Run 79
α = 2-deg
Re = 2.22 x 10^6/ft
No Trip
Model Baseline
Open Cowl

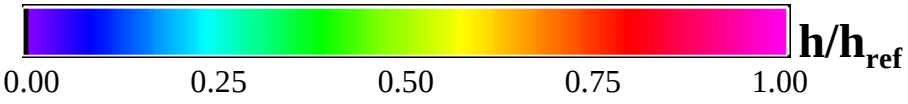

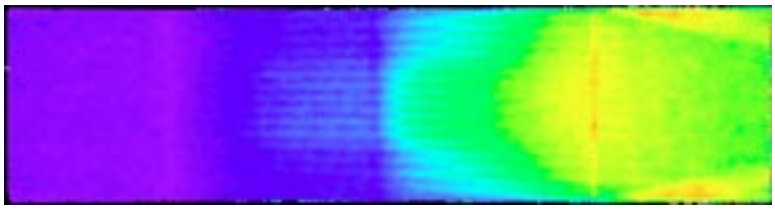

Test 338 Run 80
α = 2-deg
Re = 2.15 x 10^6/ft
Trip # 1
k = 0.060-in.
Open Cowl

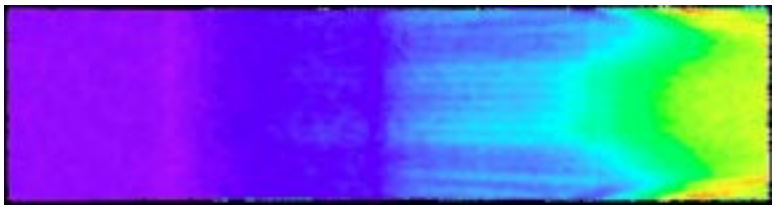

Test 338 Run 81
α = 2-deg
Re = 2.22 x 10^6/ft
Trip # 1
k = 0.030-in.
Open Cowl

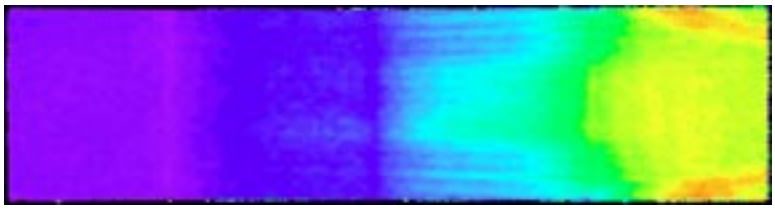

Test 338 Run 82
α = 2-deg
Re = 2.24 x 10^6/ft
Trip # 1
k = 0.045-in.
Open Cowl

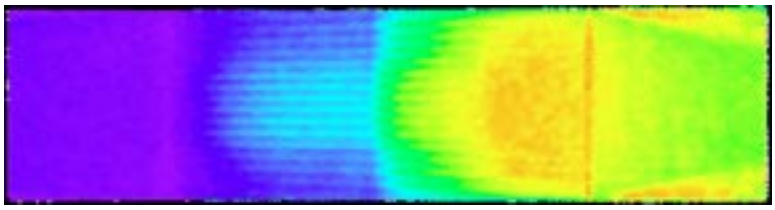

Test 338 Run 83
α = 2-deg
Re = 2.22 x 10^6/ft
Trip # 1
k = 0.075-in.
Open Cowl

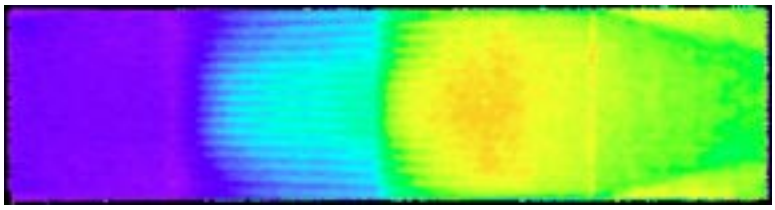

Test 338 Run 84
α = 2-deg
Re = 2.21 x 10^6/ft
Trip # 1
k = 0.090-in.
Open Cowl

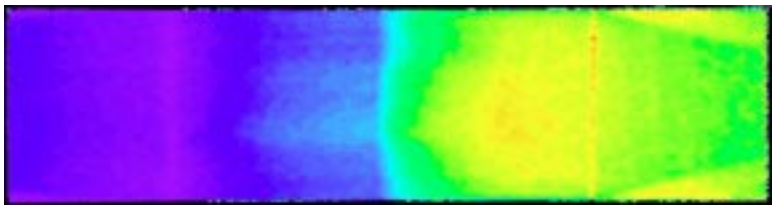

Test 338 Run 87
α = 2-deg
Re = 2.22 x 10^6/ft
Trip # 2a
k = 0.090-in.
Open Cowl

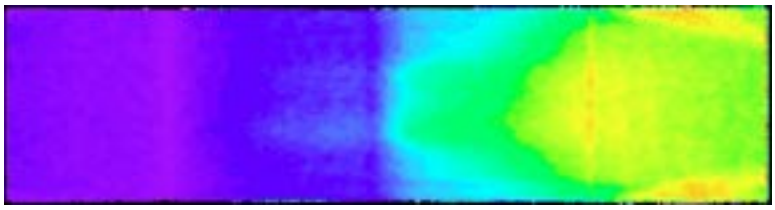

Test 338 Run 89
α = 2-deg
Re = 2.20 x 10^6/ft
Trip # 2a
k = 0.060-in.
Open Cowl

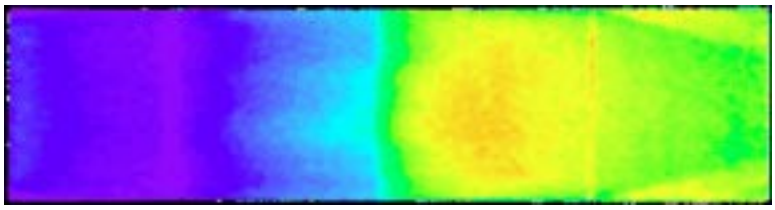

Test 338 Run 90
α = 2-deg
Re = 2.22 x 10^6/ft
Trip # 2a
k = 0.120-in.
Open Cowl

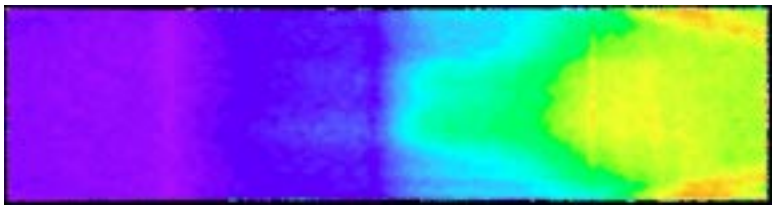

Test 338 Run 91
α = 2-deg
Re = 2.22 x 10^6/ft
Trip # 2b
k = 0.060-in.
Open Cowl

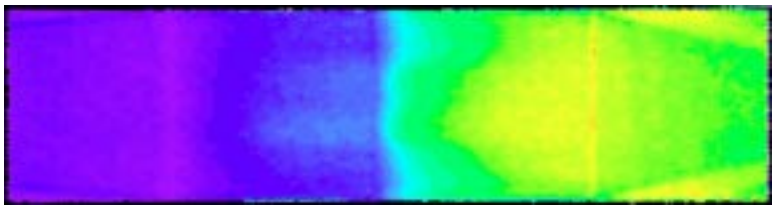

Test 338 Run 93
α = 2-deg
Re = 2.25 x 10^6/ft
Trip # 2b
k = 0.090-in.
Open Cowl

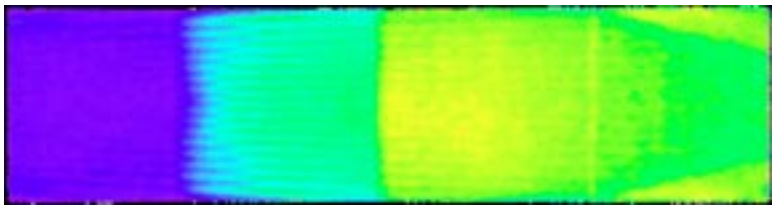

Test 338 Run 94
α = 2-deg
Re = 2.25 x 10^6/ft
Trip # 1
k = 0.120-in.
Open Cowl

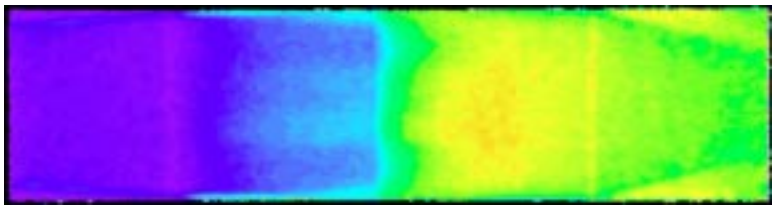

Test 338 Run 95
α = 2-deg
Re = 2.25 x 10^6/ft
Trip # 2b
k = 0.120-in.
Open Cowl

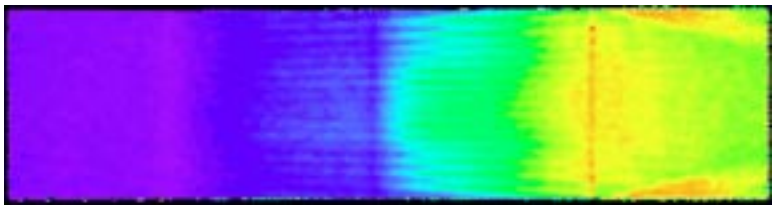

Test 338 Run 96
α = 2-deg
Re = 2.21 x 10^6/ft
Trip # 3
k = 0.060-in.
Open Cowl

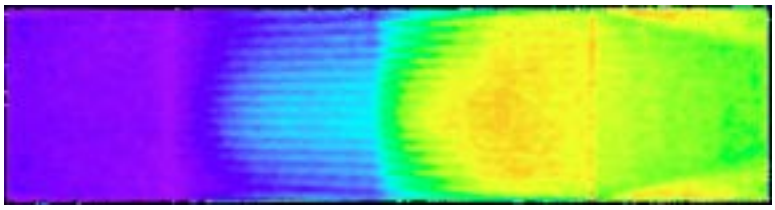

Test 338 Run 97
α = 2-deg
Re = 2.22 x 10^6/ft
Trip # 3
k = 0.090-in.
Open Cowl

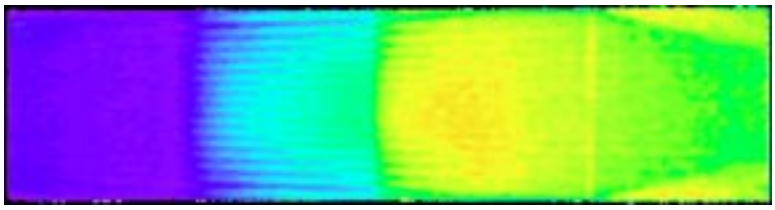

Test 338 Run 98
α = 2-deg
Re = 2.26 x 10^6/ft
Trip # 3
k = 0.120-in.
Open Cowl

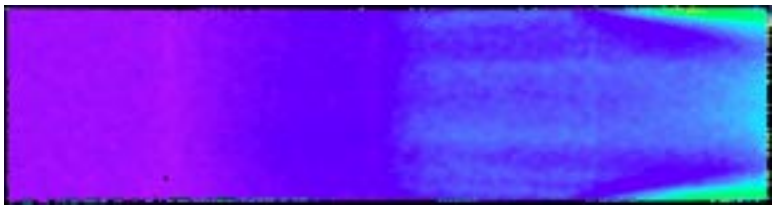

Test 338 Run 99
α = 0-deg
Re = 2.26 x 10^6/ft
No Trip
Model Baseline
Open Cowl

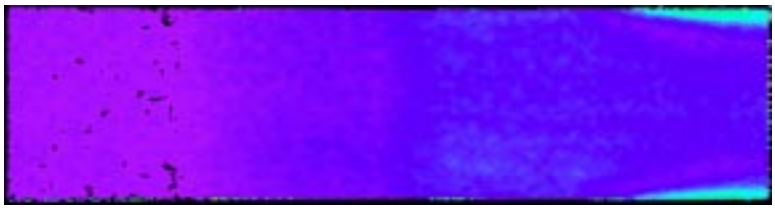

Test 338 Run 100
α = 0-deg
Re = 1.13 x 10^6/ft
No Trip
Model Baseline
Open Cowl

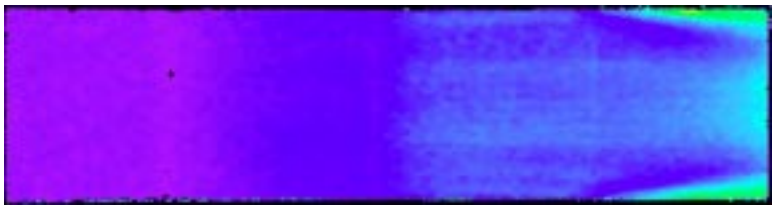

Test 338 Run 101
α = 0-deg
Re = 2.22 x 10^6/ft
Trip # 1
k = 0.030-in.
Open Cowl

h/h_{ref}

0.00 0.25 0.50 0.75 1.00

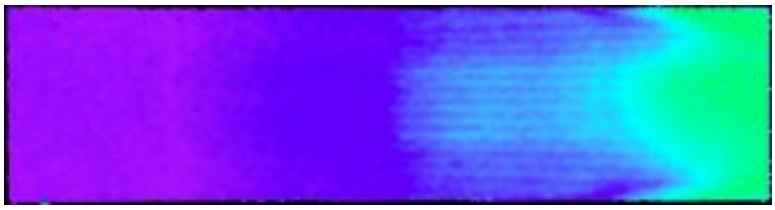

Test 338 Run 102
α = 0-deg
Re = 2.22 x 10^6/ft
Trip # 1
k = 0.060-in.
Open Cowl

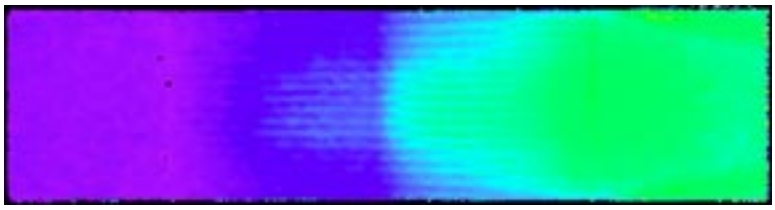

Test 338 Run 103
α = 0-deg
Re = 2.21 x 10^6/ft
Trip # 1
k = 0.090-in.
Open Cowl

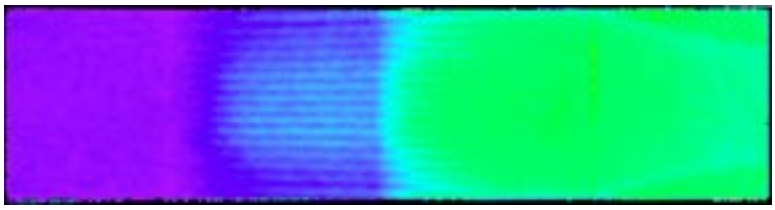

Test 338 Run 104
α = 0-deg
Re = 2.19 x 10^6/ft
Trip # 1
k = 0.120-in.
Open Cowl

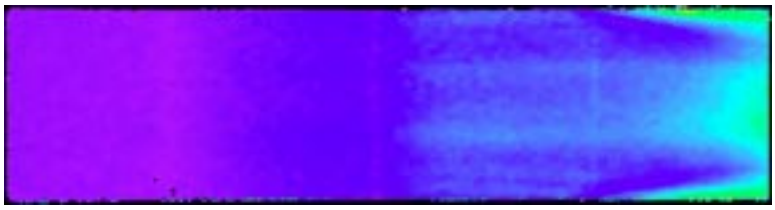

Test 338 Run 105
α = 0-deg
Re = 2.28 x 10^6/ft
Trip # 2a
k = 0.060-in.
Open Cowl

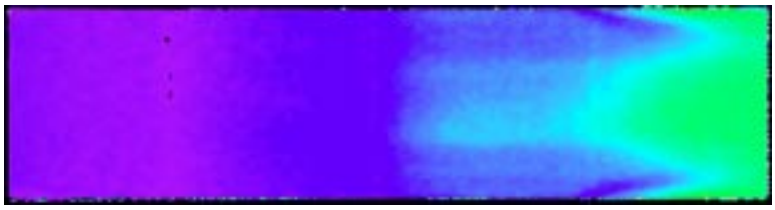

Test 338 Run 106
α = 0-deg
Re = 2.25 x 10^6/ft
Trip # 2a
k = 0.090-in.
Open Cowl

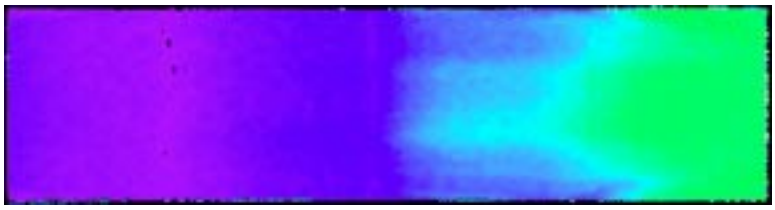

Test 338 Run 107
α = 0-deg
Re = 2.23 x 10^6/ft
Trip # 2a
k = 0.120-in.
Open Cowl

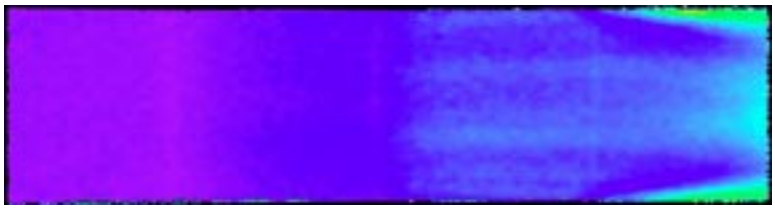

Test 338 Run 108
α = 0-deg
Re = 2.24 x 10^6/ft
Trip # 2b
k = 0.060-in.
Open Cowl

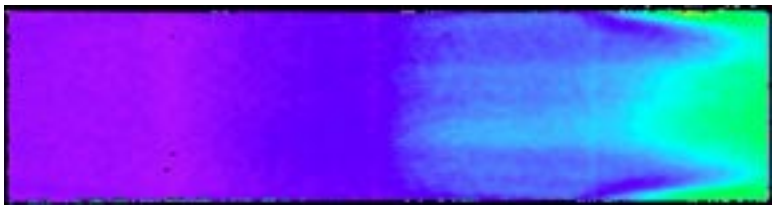

Test 338 Run 109
α = 0-deg
Re = 2.23 x 10^6/ft
Trip # 2b
k = 0.090-in.
Open Cowl

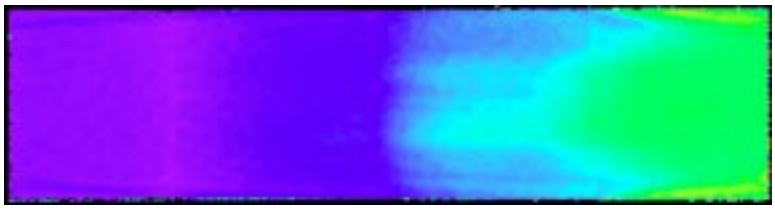

Test 338 Run 110
α = 0-deg
Re = 2.23 x 10^6/ft
Trip # 2b
k = 0.120-in.
Open Cowl

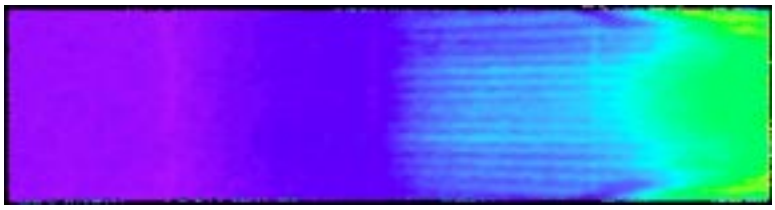

Test 338 Run 111
α = 0-deg
Re = 2.21 x 10^6/ft
Trip # 3
k = 0.060-in.
Open Cowl

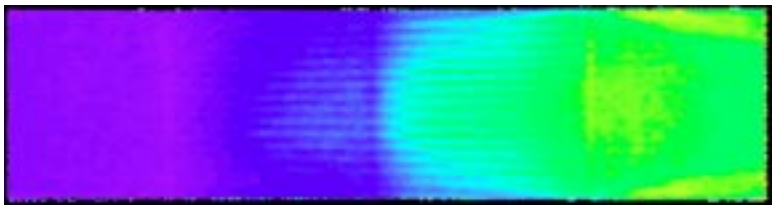

Test 338 Run 112
α = 0-deg
Re = 2.23 x 10^6/ft
Trip # 3
k = 0.090-in.
Open Cowl

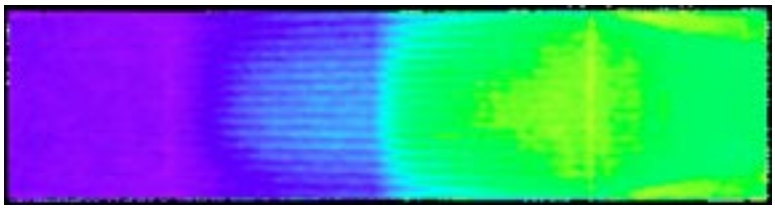

Test 338 Run 113
α = 0-deg
Re = 2.19 x 10^6/ft
Trip # 3
k = 0.120-in.
Open Cowl

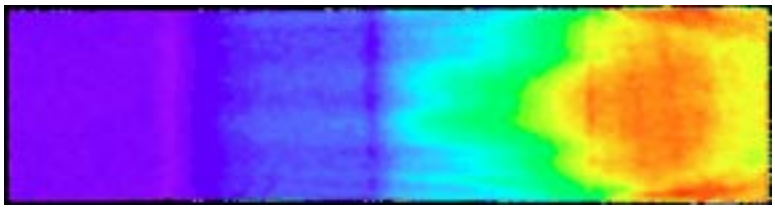

Test 338 Run 114
α = 4-deg
Re = 2.24 x 10^6/ft
No Trip
Model Baseline
Open Cowl

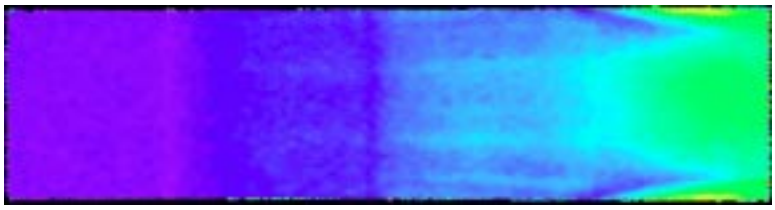

Test 338 Run 115
α = 4-deg
Re = 1.12 x 10^6/ft
No Trip
Model Baseline
Open Cowl

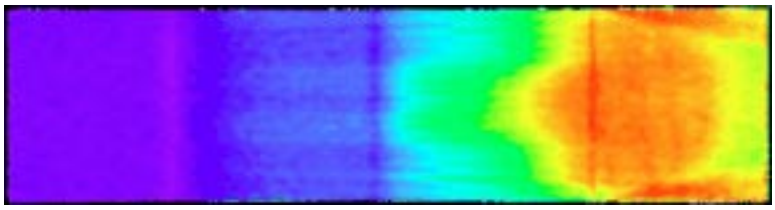

Test 338 Run 116
α = 4-deg
Re = 2.23 x 10^6/ft
Trip # 1
k = 0.030-in.
Open Cowl

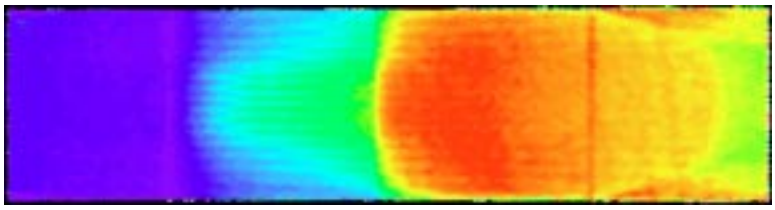

Test 338 Run 117
α = 4-deg
Re = 2.23 x 10^6/ft
Trip # 1
k = 0.060-in.
Open Cowl

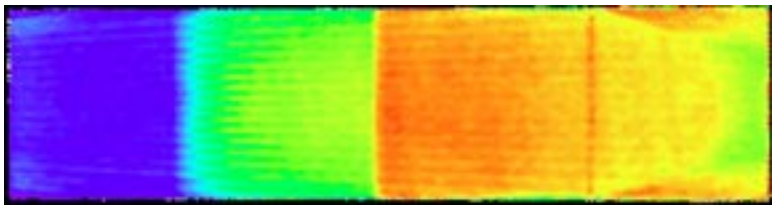

Test 338 Run 118
α = 4-deg
Re = 2.21 x 10^6/ft
Trip # 1
k = 0.090-in.
Open Cowl

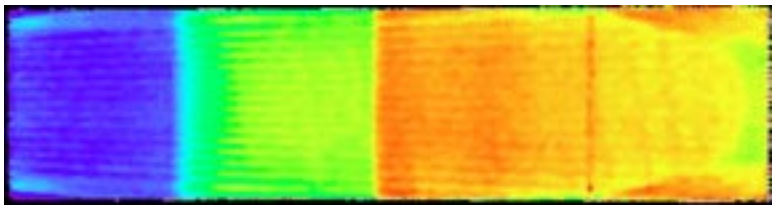

Test 338 Run 119
α = 4-deg
Re = 2.22 x 10^6/ft
Trip # 1
k = 0.120-in.
Open Cowl

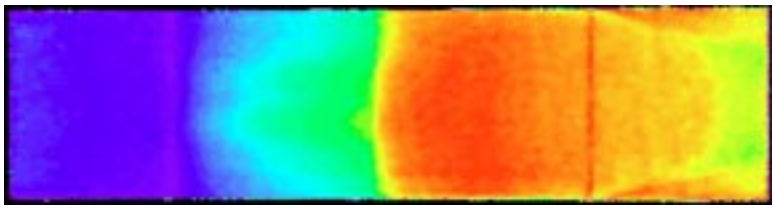

Test 338 Run 120
α = 4-deg
Re = 2.22 x 10^6/ft
Trip # 2a
k = 0.060-in.
Open Cowl

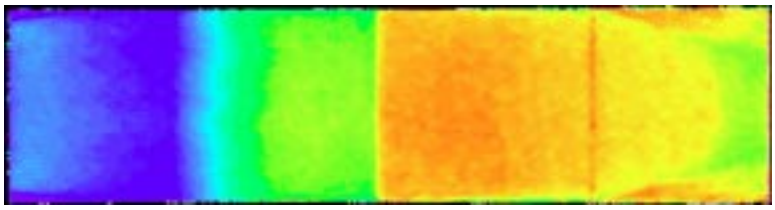

Test 338 Run 121
α = 4-deg
Re = 2.18 x 10^6/ft
Trip # 2a
k = 0.090-in.
Open Cowl

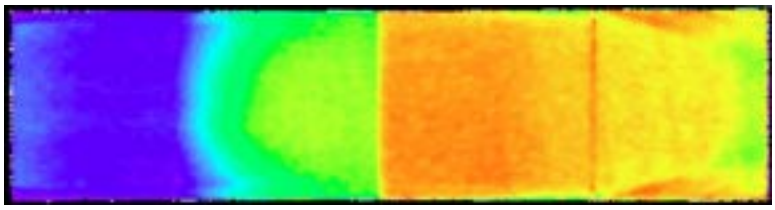

Test 338 Run 122
α = 4-deg
Re = 2.22 x 10^6/ft
Trip # 2a
k = 0.090-in.
Open Cowl

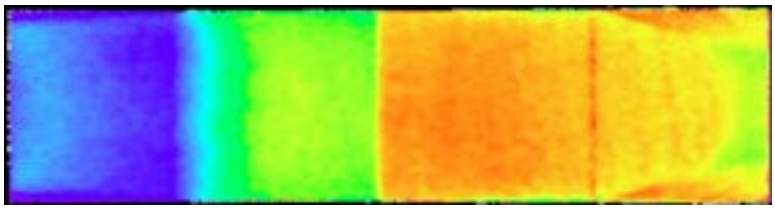

Test 338 Run 123
α = 4-deg
Re = 2.26 x 10^6/ft
Trip # 2a
k = 0.120-in.
Open Cowl

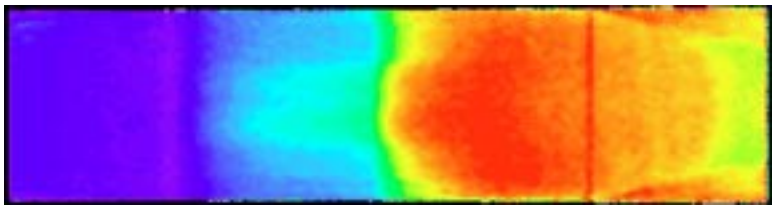

Test 338 Run 124
α = 4-deg
Re = 2.24 x 10^6/ft
Trip # 2b
k = 0.060-in.
Open Cowl

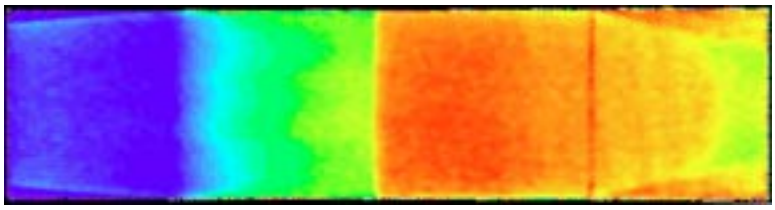

Test 338 Run 125
α = 4-deg
Re = 2.18 x 10^6/ft
Trip # 2b
k = 0.090-in.
Open Cowl

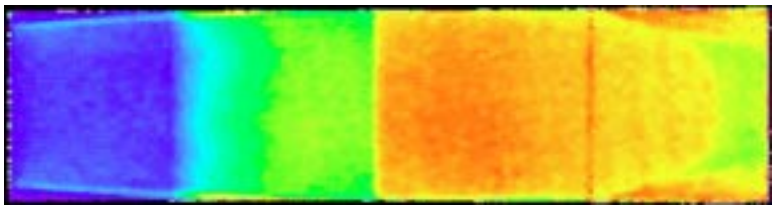

Test 338 Run 126
α = 4-deg
Re = 2.21 x 10^6/ft
Trip # 2b
k = 0.120-in.
Open Cowl

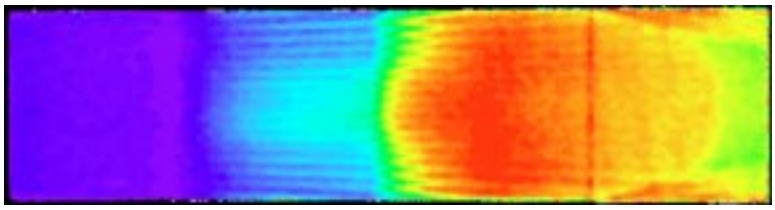

Test 338 Run 127
α = 4-deg
Re = 2.24 x 10^6/ft
Trip # 3
k = 0.060-in.
Open Cowl

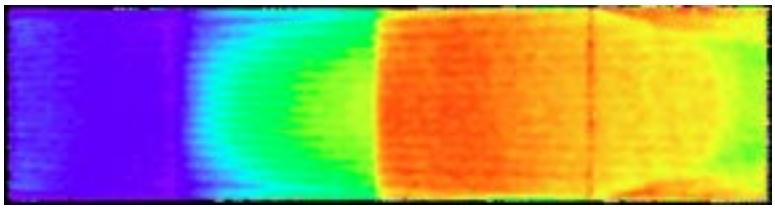

Test 338 Run 128
α = 4-deg
Re = 2.21 x 10^6/ft
Trip # 3
k = 0.090-in.
Open Cowl

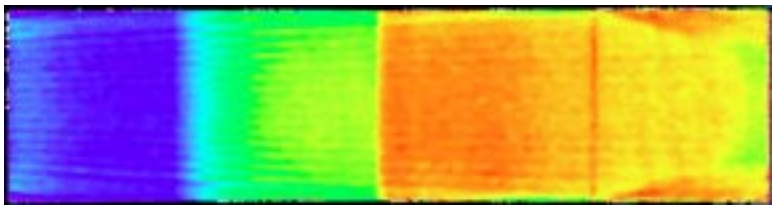

Test 338 Run 129
α = 4-deg
Re = 2.24 x 10^6/ft
Trip # 3
k = 0.120-in.
Open Cowl

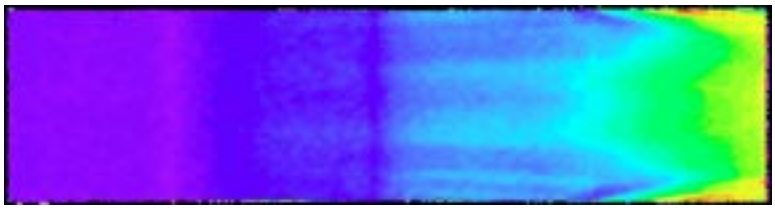

Test 338 Run 130
α = 2-deg
Re = 2.23 x 10^6/ft
Trip # 2a
k = 0.015-in.
Open Cowl

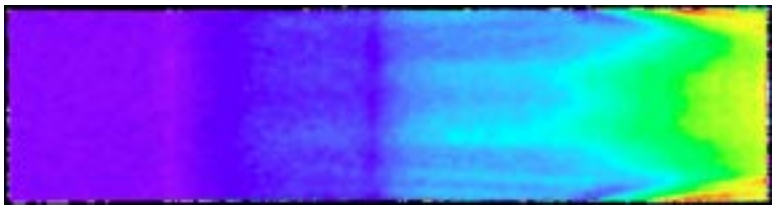

Test 338 Run 131
α = 2-deg
Re = 2.21 x 10^6/ft
Trip # 2a
k = 0.030-in.
Open Cowl

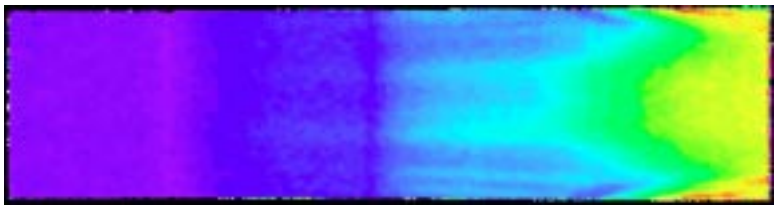

Test 338 Run 132
α = 2-deg
Re = 2.25 x 10^6/ft
Trip # 2b
k = 0.045-in.
Open Cowl

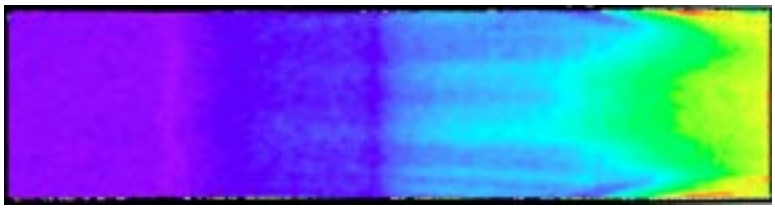

Test 338 Run 133
α = 2-deg
Re = 2.24 x 10^6/ft
Trip # 2a
k = 0.030-in.
Open Cowl

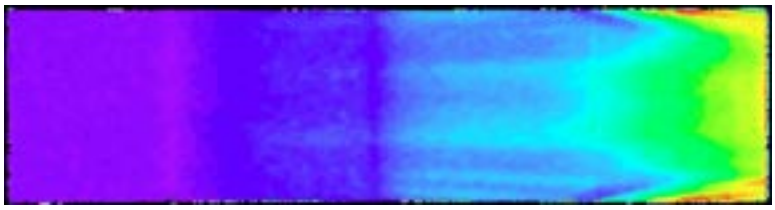

Test 338 Run 134
α = 2-deg
Re = 2.18 x 10^6/ft
Trip # 2b
k = 0.015-in.
Open Cowl

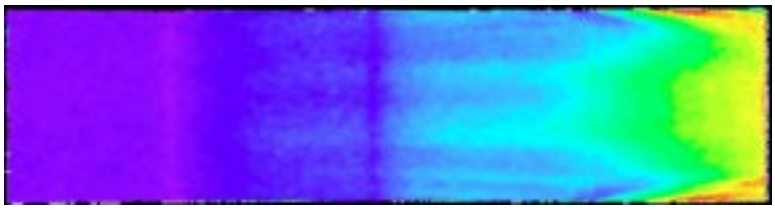

Test 338 Run 135
α = 2-deg
Re = 2.23 x 10^6/ft
Trip # 2b
k = 0.030-in.
Open Cowl

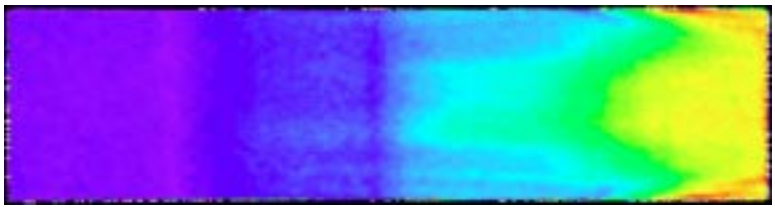

Test 338 Run 136
α = 2-deg
Re = 2.19 x 10^6/ft
Trip # 2a
k = 0.045-in.
Open Cowl

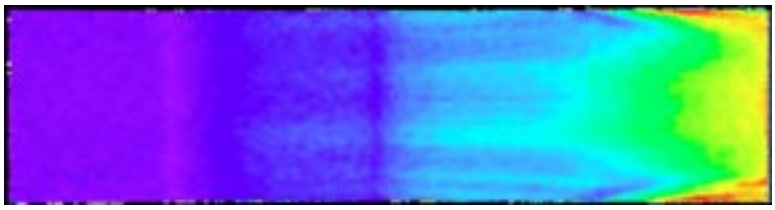

Test 338 Run 137
α = 2-deg
Re = 2.21 x 10^6/ft
Trip # 3
k = 0.015-in.
Open Cowl

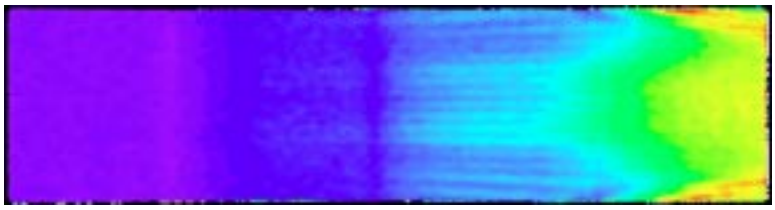

Test 338 Run 138
α = 2-deg
Re = 2.24 x 10^6/ft
Trip # 3
k = 0.030-in.
Open Cowl

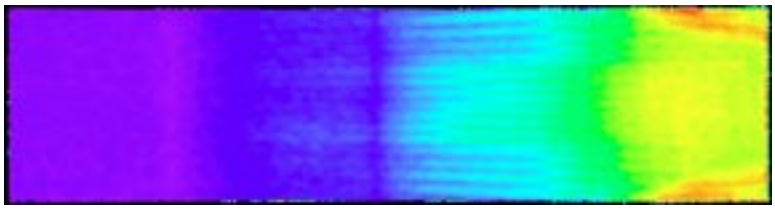

Test 338 Run 139
α = 2-deg
Re = 2.20 x 10^6/ft
Trip # 3
k = 0.045-in.
Open Cowl

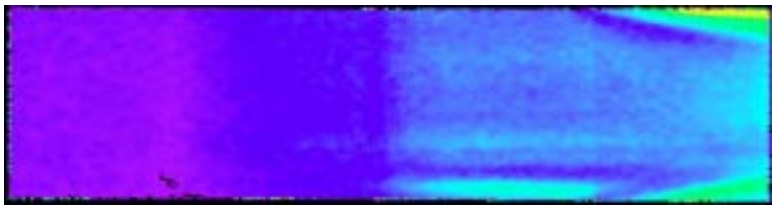

Test 338 Run 140
α = 2-deg
β = 2-deg
Re = 1.15 x 10^6/ft
No Trip
Model Baseline
Open Cowl

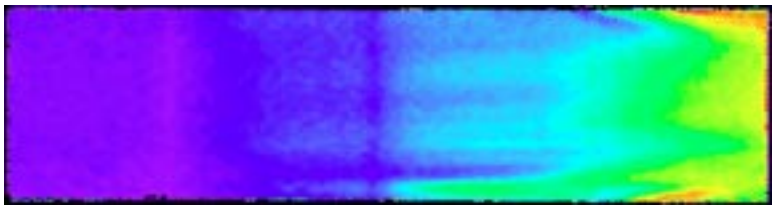

Test 338 Run 141
α = 2-deg
β = 2-deg
Re = 2.19 x 10^6/ft
No Trip
Model Baseline
Open Cowl

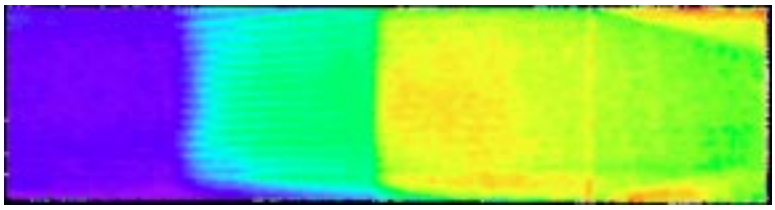

Test 338 Run 142
α = 2-deg
β = 2-deg
Re = 2.25 x 10^6/ft
Trip # 1
k = 0.120-in.
Open Cowl

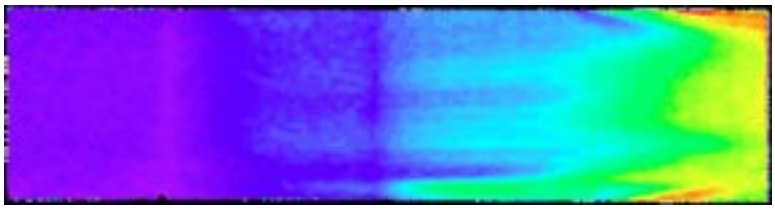

Test 338 Run 143
α = 2-deg
β = 2-deg
Re = 2.22 x 10^6/ft
Trip # 1
k = 0.015-in.
Open Cowl

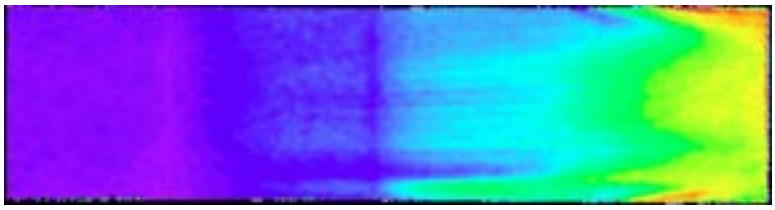

Test 338 Run 144
α = 2-deg
β = 2-deg
Re = 2.22 x 10^6/ft
Trip # 1
k = 0.030-in.
Open Cowl

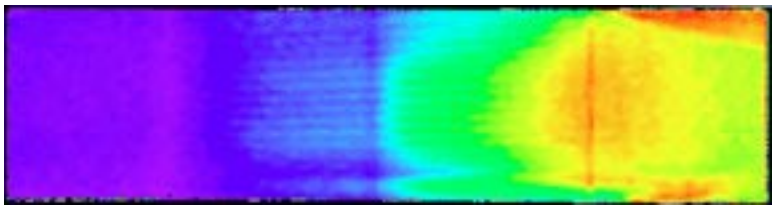

Test 338 Run 146
α = 2-deg
β = 2-deg
Re = 2.25 x 10^6/ft
Trip # 1
k = 0.060-in.
Open Cowl

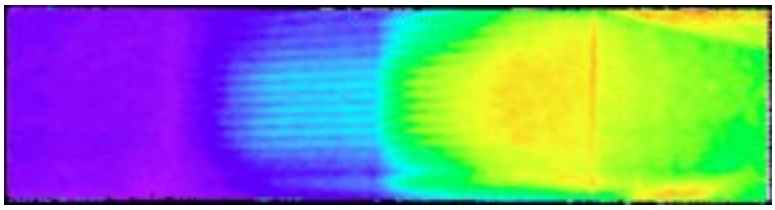

Test 338 Run 147
α = 2-deg
β = 2-deg
Re = 2.21 x 10^6/ft
Trip # 1
k = 0.075-in.
Open Cowl

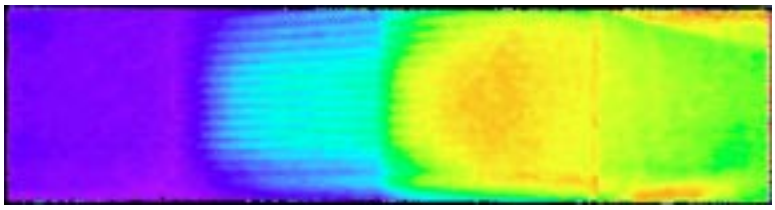

Test 338 Run 148
α = 2-deg
β = 2-deg
Re = 2.21 x 10^6/ft
Trip # 1
k = 0.090-in.
Open Cowl

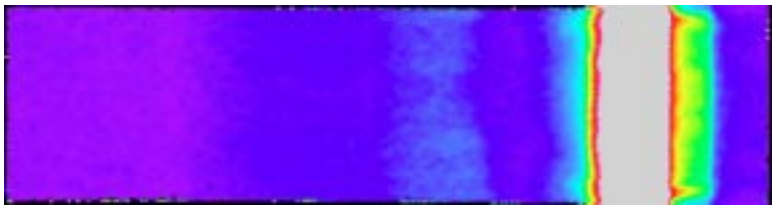

Test 338 Run 149
α = 2-deg
Re = 1.13 x 10^6/ft
No Trip
Model Baseline
Closed Cowl

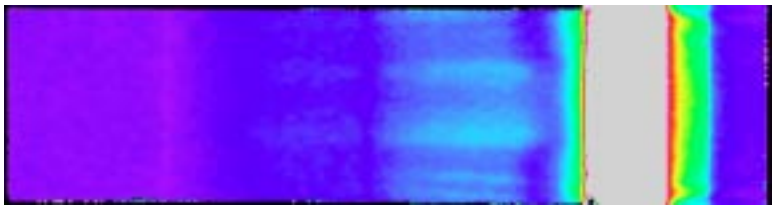

Test 338 Run 150
α = 2-deg
Re = 2.19 x 10^6/ft
No Trip
Model Baseline
Closed Cowl

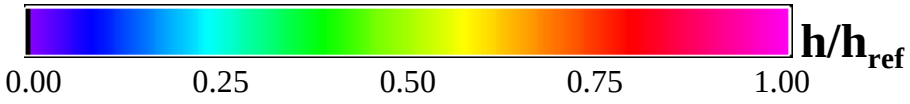

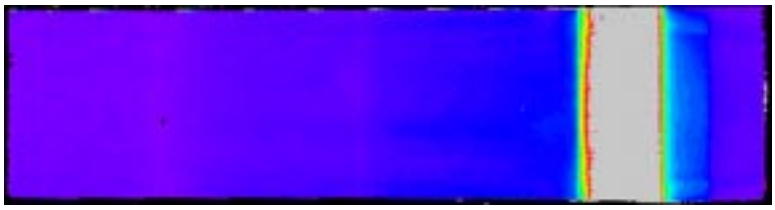

Test 349 Run 1
α = 2-deg
Re_∞/ft = 2.21 x 10^6
No Trip
Model Baseline
Closed cowl

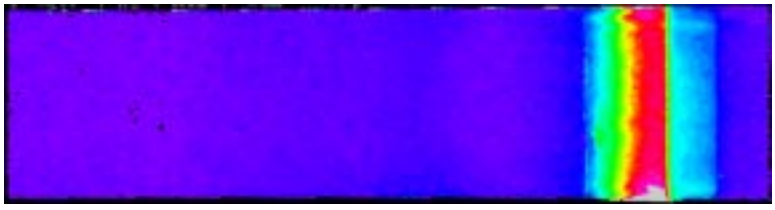

Test 349 Run 2
α = 2-deg
Re_∞/ft = 0.59 x 10^6
No Trip
Model Baseline
Closed cowl

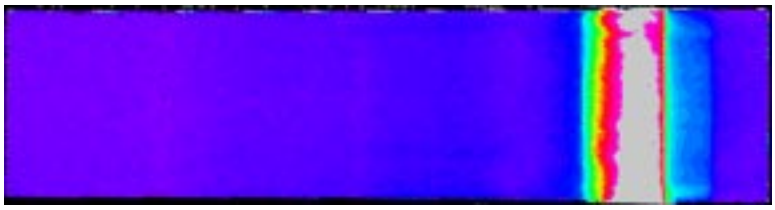

Test 349 Run 3
α = 2-deg
Re_∞/ft = 1.10 x 10^6
No Trip
Model Baseline
Closed cowl

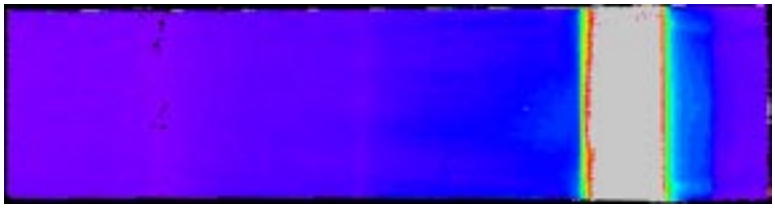

Test 349 Run 4
α = 2-deg
Re_∞/ft = 2.21 x 10^6
Trip # 1
k = 0.030-in.
Closed cowl

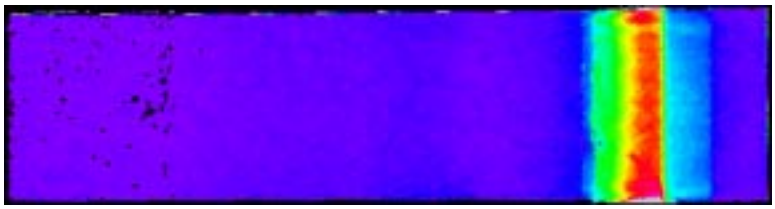

Test 349 Run 5
α = 2-deg
Re_∞/ft = 0.57 x 10^6
Trip # 1
k = 0.030-in.
Closed cowl

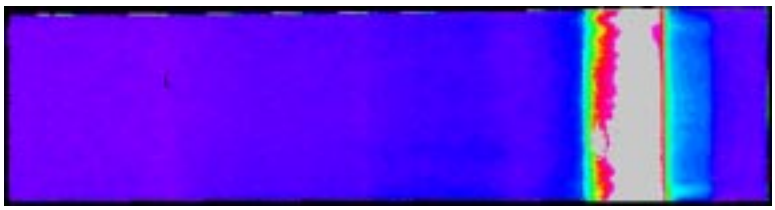

Test 349 Run 6
α = 2-deg
Re_∞/ft = 1.13 x 10^6
Trip # 1
k = 0.030-in.
Closed cowl

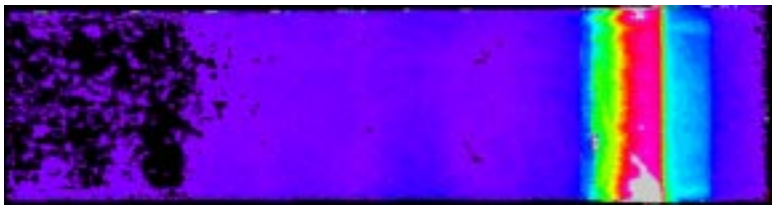

Test 349 Run 7
α = 2-deg
Re_∞/ft = 0.62 x 10^6
Trip # 1
k = 0.045-in.
Closed cowl

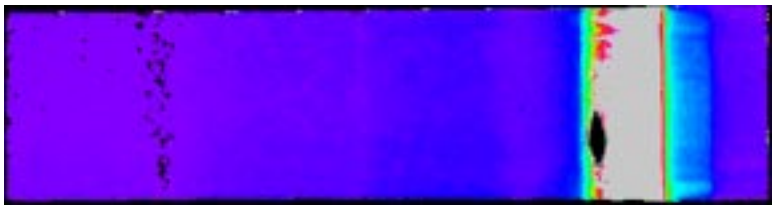

Test 349 Run 8
α = 2-deg
Re_∞/ft = 1.13 x 10^6
Trip # 1
k = 0.045-in.
Closed cowl

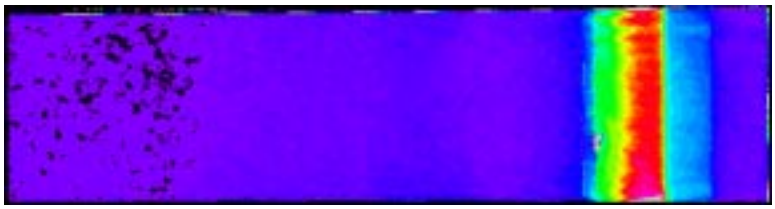

Test 349 Run 9
α = 2-deg
Re_∞/ft = 0.60 x 10^6
Trip # 1
k = 0.060-in.
Closed cowl

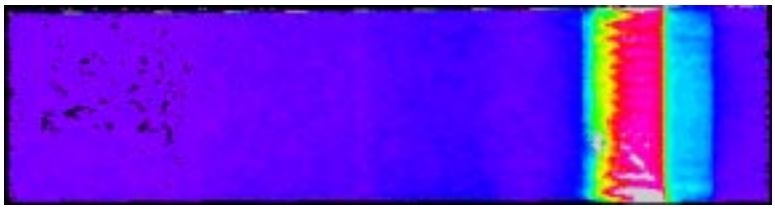

Test 349 Run 10
α = 2-deg
Re_∞/ft = 0.60 x 10^6
Trip # 1
k = 0.090-in.
Closed cowl

Note the scale change after Run 10

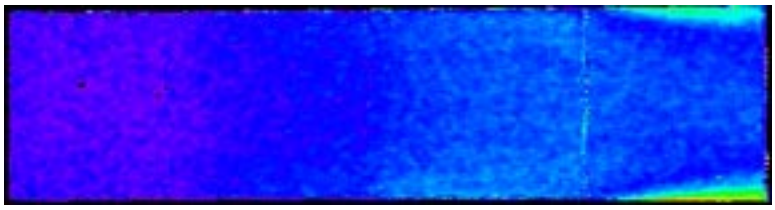

Test 349 Run 11
α = 2-deg
Re_∞/ft = 0.54 x 10^6
No Trip
Model Baseline
Open cowl

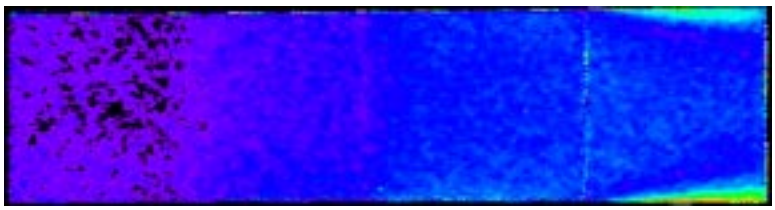

Test 349 Run 12
α = 2-deg
Re_∞/ft = 0.54 x 10^6
No Trip
Model Baseline
Open cowl

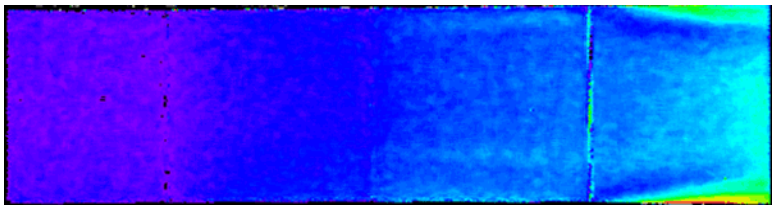

Test 349 Run 13
α = 2-deg
Re_∞/ft = 1.12 x 10^6
No Trip
Model Baseline
Open cowl

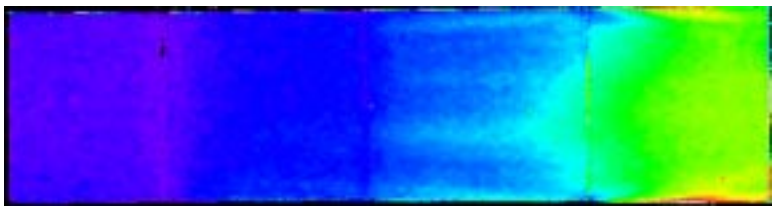

Test 349 Run 14
α = 2-deg
Re_∞/ft = 2.22 x 10^6
No Trip
Model Baseline
Open cowl

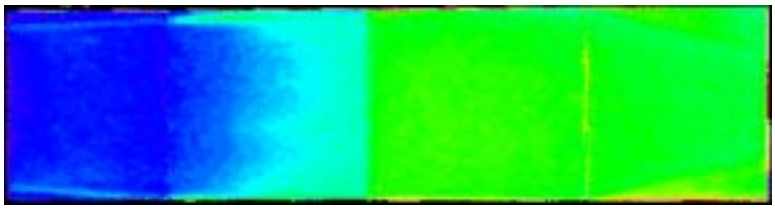

Test 349 Run 15
α = 2-deg
Re_∞/ft = 2.25 x 10^6
Trip # 2c
k = 0.120-in.
Open cowl

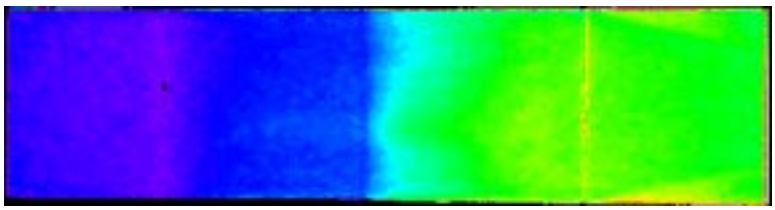

Test 349 Run 16
α = 2-deg
Re_∞/ft = 2.22 x 10^6
Trip # 2c
k = 0.060-in.
Open cowl

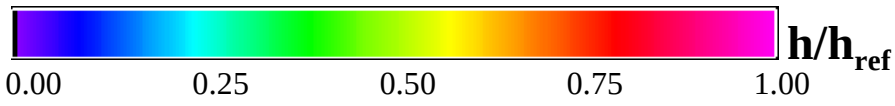

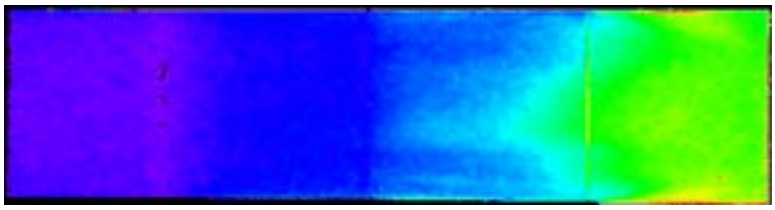

Test 349 Run 17
α = 2-deg
Re_∞/ft = 2.25 x 10^6
Trip # 2c
k = 0.030-in.
Open cowl

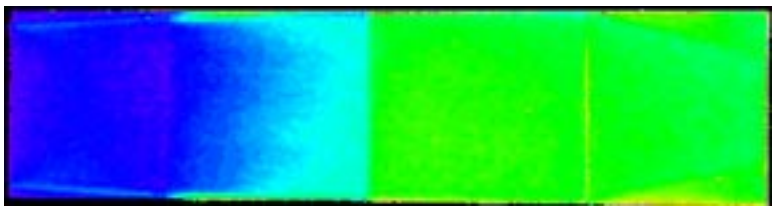

Test 349 Run 18
α = 2-deg
Re_∞/ft = 2.22 x 10^6
Trip # 2c
k = 0.120-in.
Open cowl

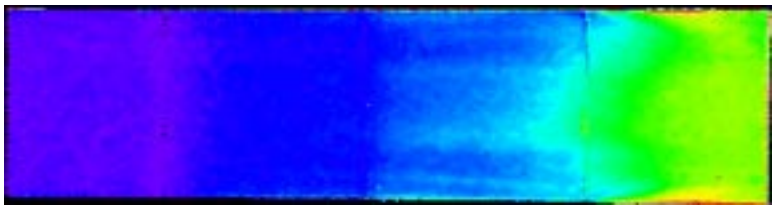

Test 349 Run 19
α = 2-deg
Re_∞/ft = 2.25 x 10^6
Trip # New Cav
k = 0.060-in.
Open cowl

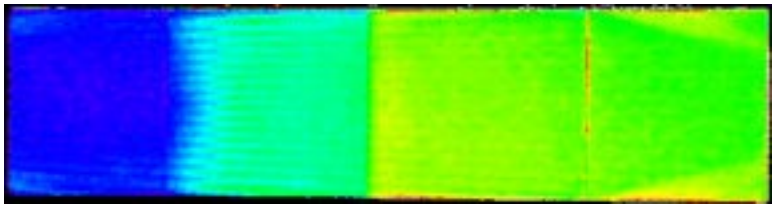

Test 349 Run 20
α = 2-deg
Re_∞/ft = 2.22 x 10^6
Trip # 1
k = 0.120-in.
Open cowl

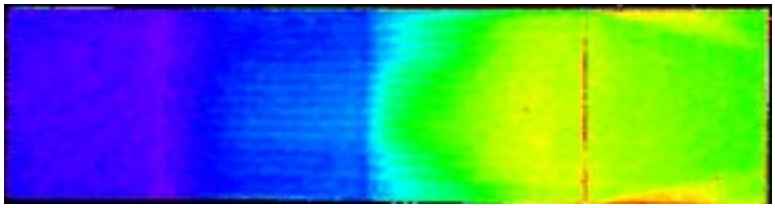

Test 349 Run 21
α = 2-deg
Re_∞/ft = 2.18 x 10^6
Trip # 1
k = 0.060-in.
Open cowl

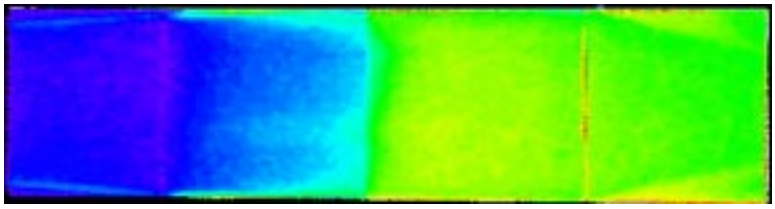

Test 349 Run 22
α = 2-deg
Re_∞/ft = 2.25 x 10^6
Trip # 2b
k = 0.120-in.
Open cowl

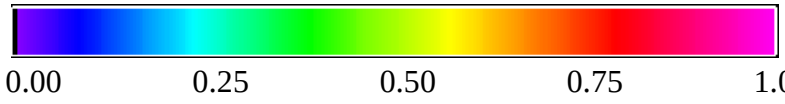

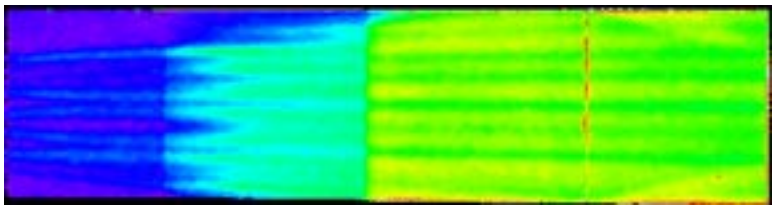

Test 349 Run 23
α = 2-deg
Re_∞/ft = 2.21 x 10^6
Trip Blowing
Max Shop Air (~100 psi)
Open cowl

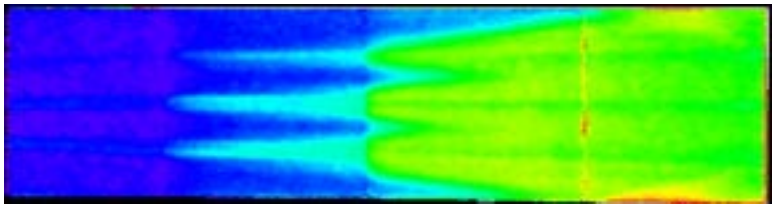

Test 349 Run 24
α = 2-deg
Re_∞/ft = 2.24 x 10^6
Trip Blowing
Less Than Max Shop Air
Open cowl

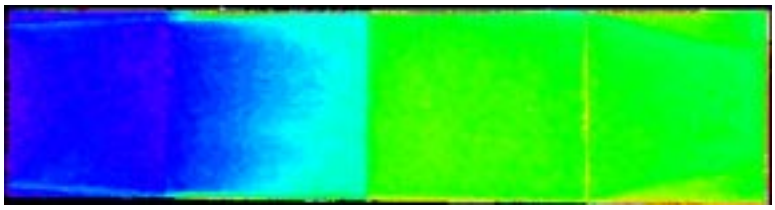

Test 349 Run 25
α = 2-deg
Re_∞/ft = 2.21 x 10^6
Trip # 2c
k = 0.120-in.
Open cowl

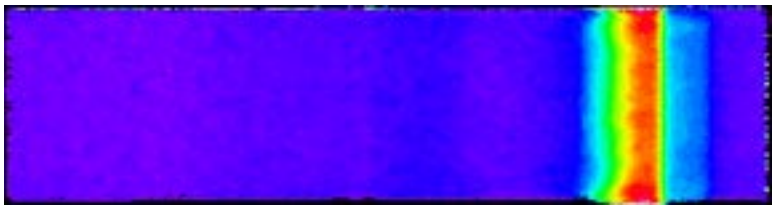

Test 351 Run 1
α = 2-deg
Re_∞/ft = 0.56 x 10^6
No Trip
Model Baseline
Closed cowl

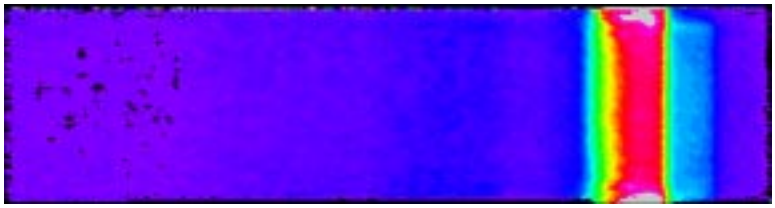

Test 351 Run 2
α = 2-deg
Re_∞/ft = 0.60 x 10^6
Trip # 1
k = 0.120-in.
Closed cowl

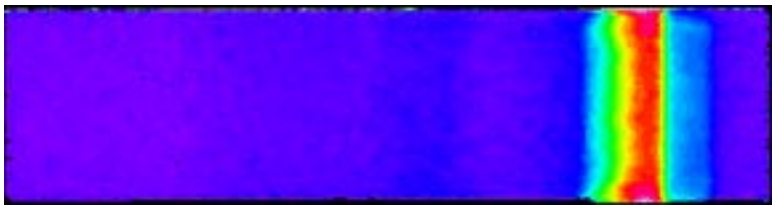

Test 351 Run 3
α = 2-deg
Re_∞/ft = 0.57 x 10^6
Trip # 1
k = 0.060-in.
Closed cowl

Test 351 Run 4
α = 2-deg
Re_∞/ft = 0.58 x 10^6
Trip # 2b
k = 0.120-in.
Closed cowl

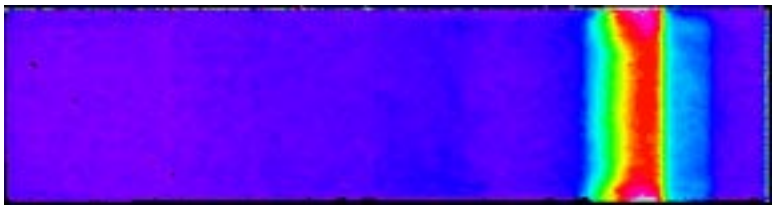

Test 351 Run 5
α = 2-deg
Re_∞/ft = 0.57 x 10^6
Trip # 2c
k = 0.120-in.
Closed cowl

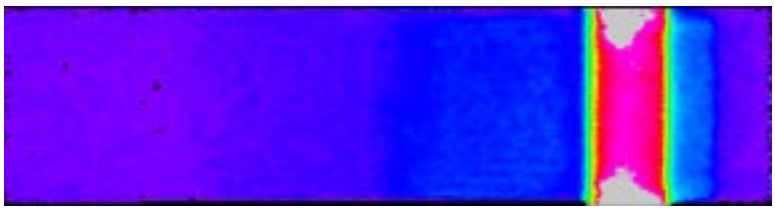

Test 351 Run 7
α = 4-deg
Re_∞/ft = 0.57 x 10^6
Trip # 1
k = 0.120-in.
Closed cowl

h/h_{ref}

0.00 0.50 1.00 1.50 2.00 2.50

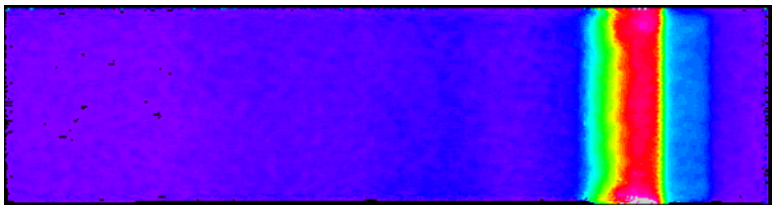

Test 351 Run 8
α = 4-deg
Re_∞/ft = 0.56 x 10^6
No Trip
Model Baseline
Closed cowl

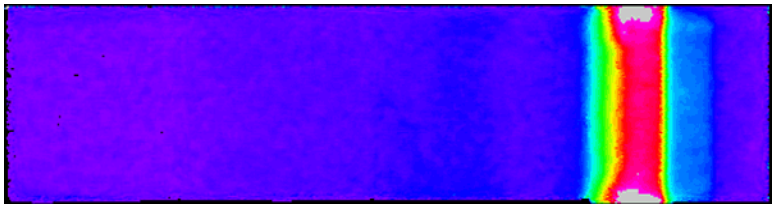

Test 351 Run 9
α = 4-deg
Re_∞/ft = 0.57 x 10^6
Trip # 2c
k = 0.120-in.
Closed cowl

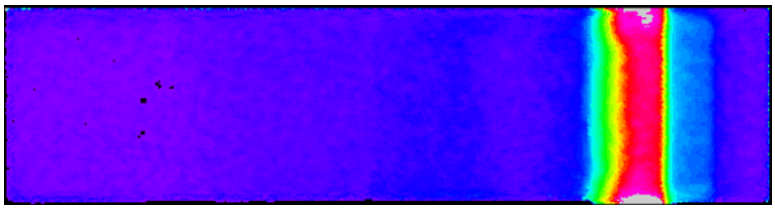

Test 351 Run 10
α = 4-deg
Re_∞/ft = 0.56 x 10^6
Trip # 2b
k = 0.120-in.
Closed cowl

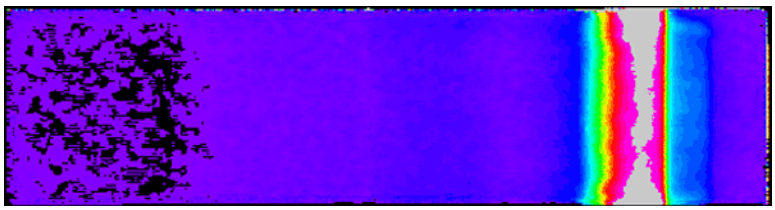

Test 351 Run 11
α = 2-deg
Re_∞/ft = 1.14 x 10^6
No Trip
Model Baseline
Closed cowl

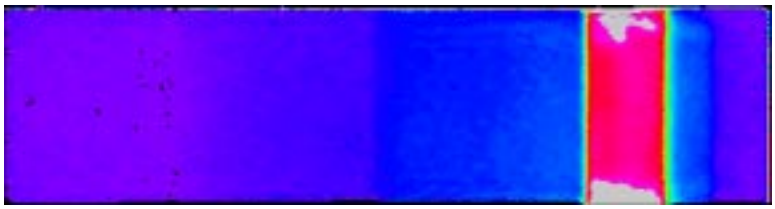

Test 351 Run 12
α = 2-deg
Re_∞/ft = 1.16 x 10^6
Trip # 1
k = 0.120-in.
Closed cowl

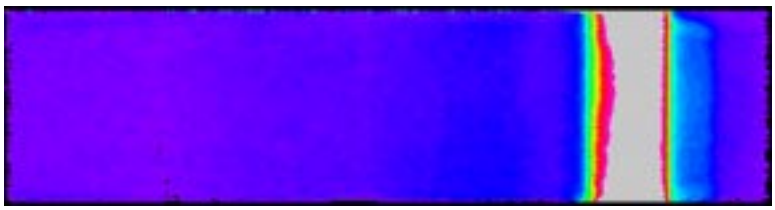

Test 351 Run 13
α = 2-deg
Re_∞/ft = 1.14 x 10^6
Trip # 2b
k = 0.120-in.
Closed cowl

Test 351 Run 14
α = 2-deg
Re_∞/ft = 1.07 x 10^6
Trip # 2c
k = 0.120-in.
Closed cowl

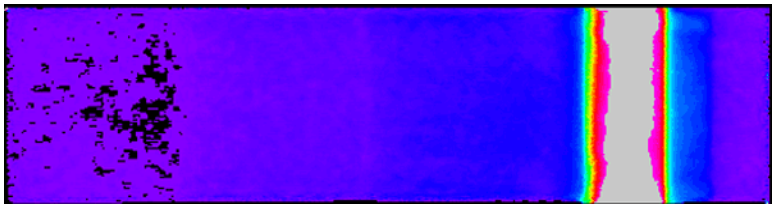

Test 351 Run 15
α = 4-deg
Re_∞/ft = 1.18 x 10^6
No Trip
Model Baseline
Closed cowl

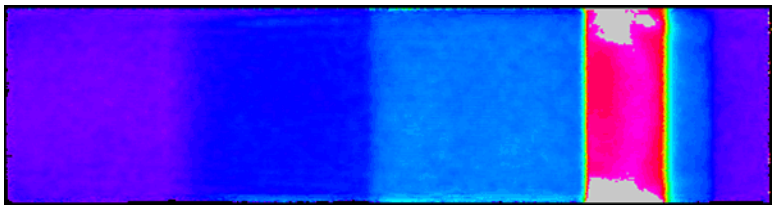

Test 351 Run 16
α = 4-deg
Re_∞/ft = 1.22 x 10^6
Trip # 1
k = 0.120-in.
Closed cowl

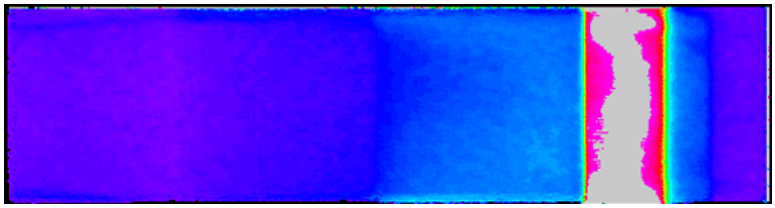

Test 351 Run 17
α = 4-deg
Re_∞/ft = 1.18 x 10^6
Trip # 2c
k = 0.120-in.
Closed cowl

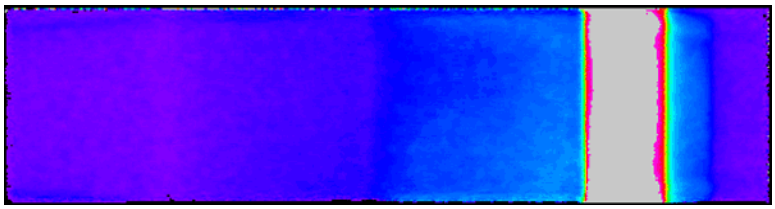

Test 351 Run 18
α = 4-deg
Re_∞/ft = 1.09 x 10^6
Trip # 2b
k = 0.120-in.
Closed cowl

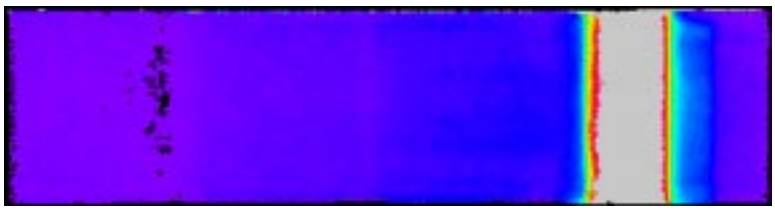

Test 351 Run 19
α = 2-deg
Re_∞/ft = 2.27 x 10^6
No Trip
Model Baseline
Closed cowl

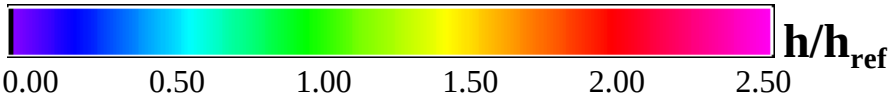

Test 338 Run 153 α = 2-deg Re = 2.2x10^6/ft No Trip Baseline Open Cowl

Test 338 Run 154 α = 2-deg Re = 2.2x10^6/ft No Trip Baseline Open Cowl

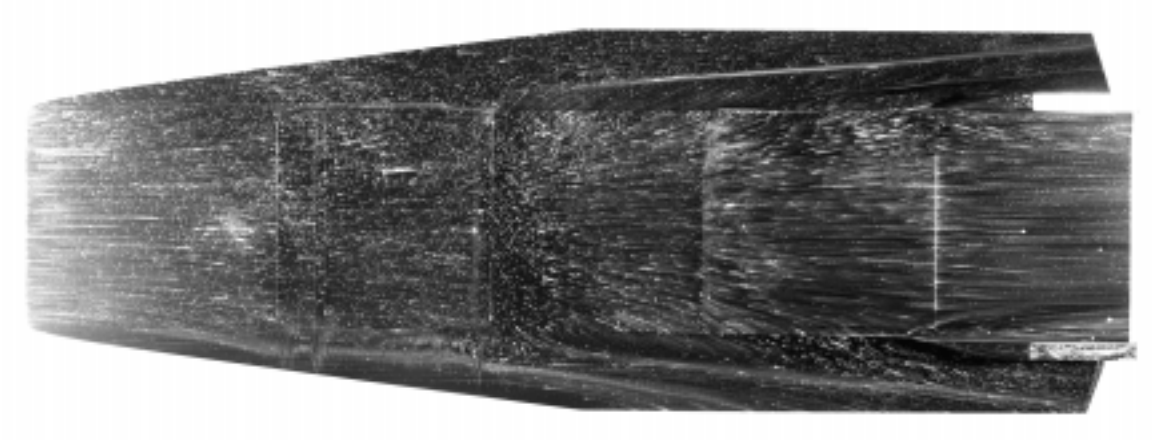

Test 338 Run 155 α = 2-deg Re = 2.2x10^6/ft No Trip Baseline Open Cowl

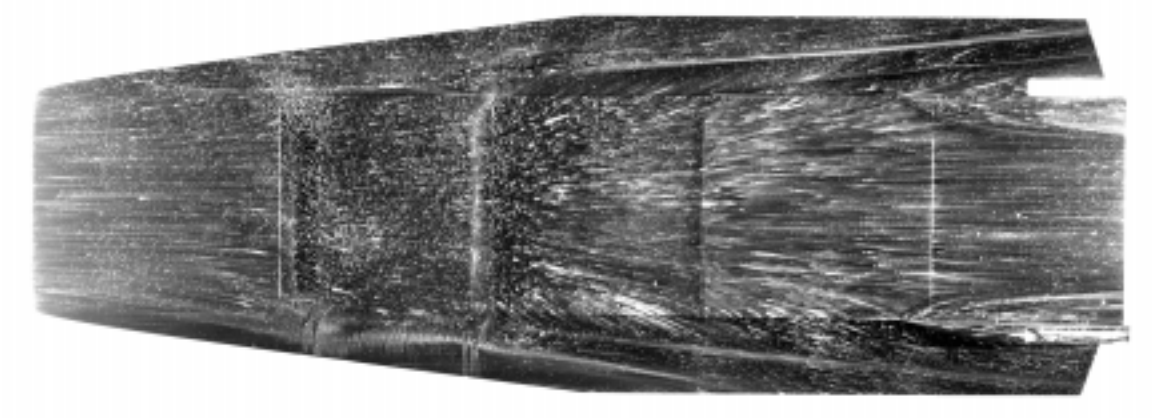

Test 338 Run 156 α = 2-deg Re = 2.2x10^6/ft Trip 1 k = 0.045-in Open Cowl

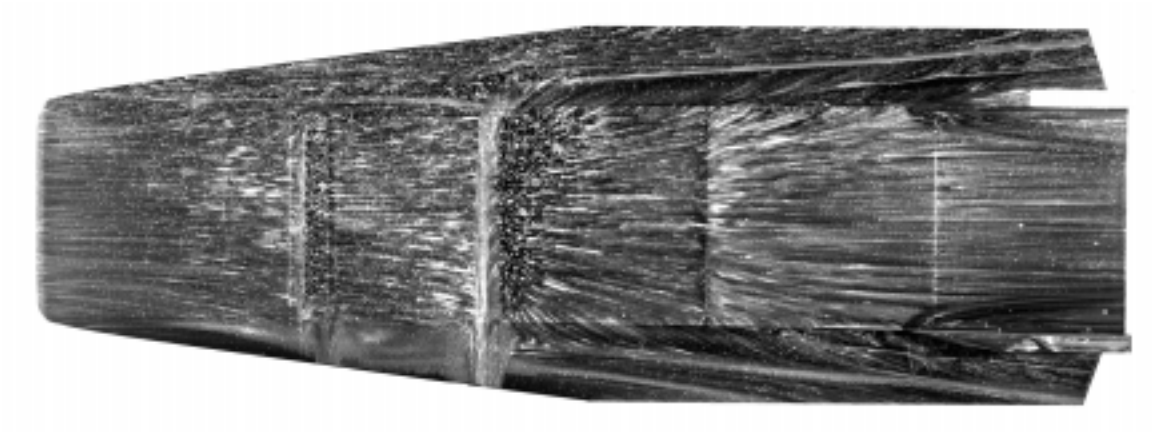

Test 338 Run 157 α = 2-deg Re = 2.2x10^6/ft Trip 1 k = 0.045-in Open Cowl

Test 338 Run 158 α = 2-deg Re = 2.2x10^6/ft Trip 1 k = 0.060-in Open Cowl

Test 338 Run 159 α = 2-deg Re = 2.2x10^6/ft Trip 1 k = 0.060-in Open Cowl

Test 338 Run 160 α = 2-deg Re = 2.2x10^6/ft Trip 2a k = 0.060-in Open Cowl

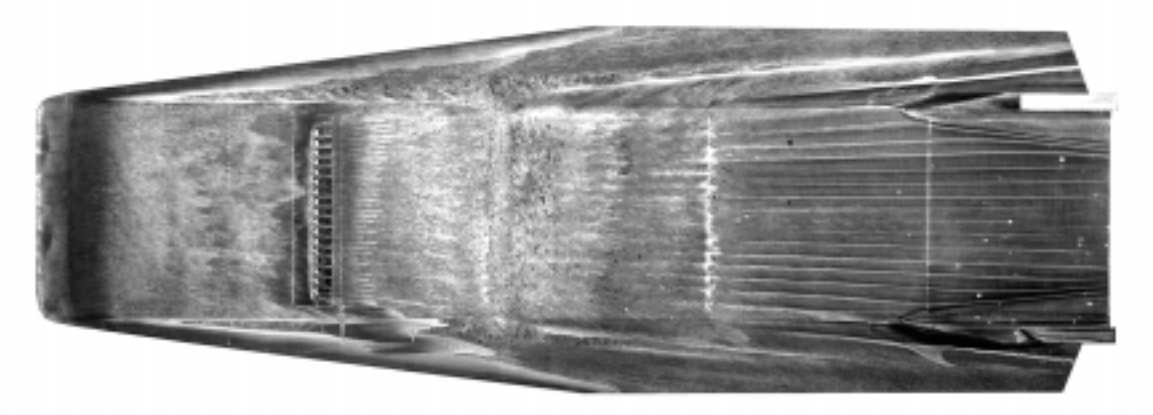

Test 338 Run 161 α = 2-deg Re = 2.2x10^6/ft Trip 3 k = 0.060-in Open Cowl

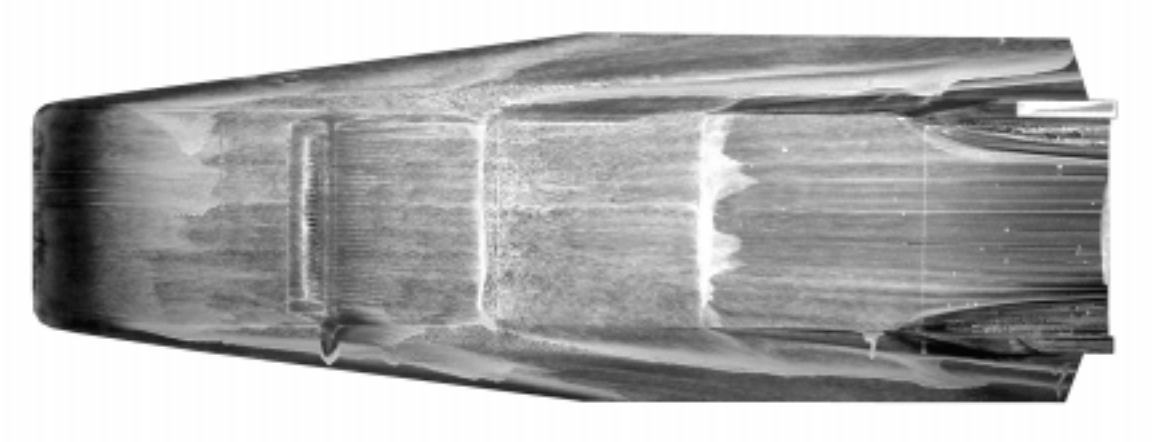

Test 338 Run 162 α = 2-deg Re = 2.2x10^6/ft Trip 2b k = 0.060-in Open Cowl

Test 338 Run 163 α = 2-deg Re = 2.2x10^6/ft No Trip Baseline Open Cowl

Test 338 Run 165 α = 2-deg Re = 2.2x10^6/ft No Trip Baseline Closed Cowl

Test 338 Run 166 α = 2-deg Re = 2.2x10^6/ft Trip 1 k = 0.060-in Closed Cowl

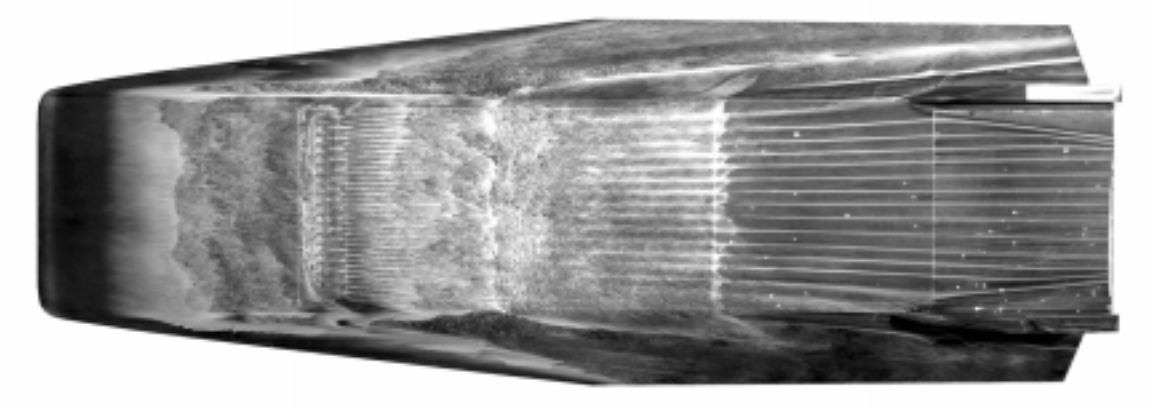

Test 338 Run 167 α = 2-deg Re = 2.2x10^6/ft Trip 1 k = 0.060-in Open Cowl

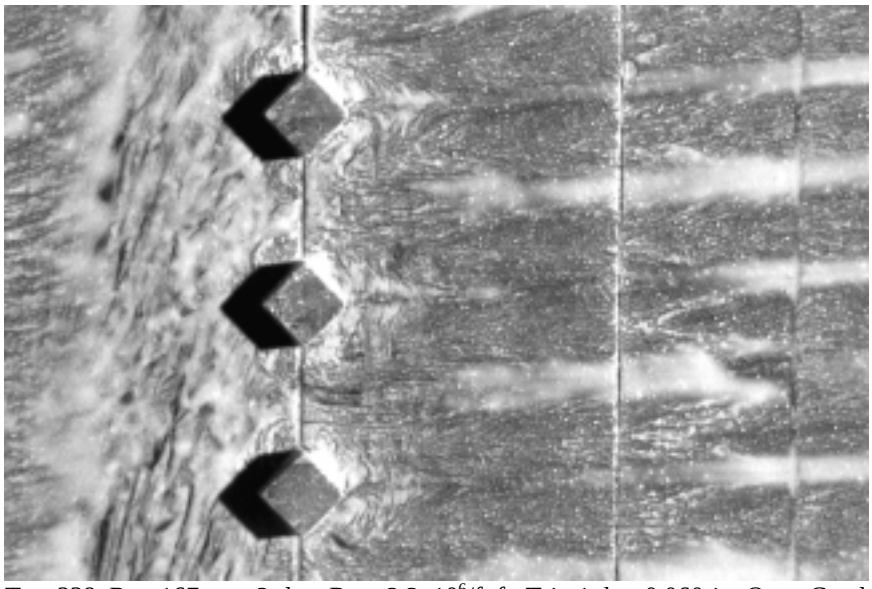

Test 338 Run 167 α = 2-deg Re = 2.2x10^6/ft ft Trip 1 k = 0.060-in Open Cowl

Test 338 Run 168 α = 0-deg Re = 2.2x10^6/ft No Trip Baseline Open Cowl

Test 338 Run 169 α = 4-deg Re = 2.2x10^6/ft No Trip Baseline Open Cowl

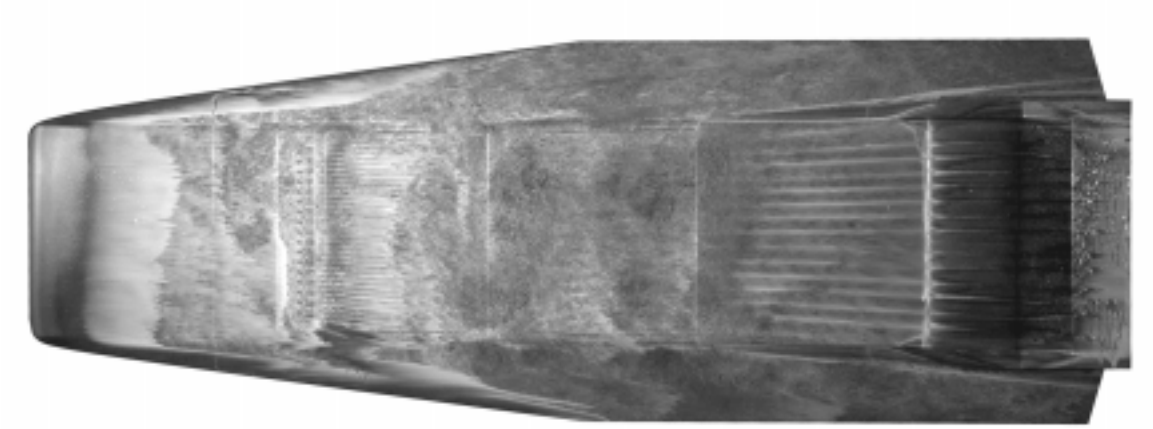

Test 346 Run 1 α = 2-deg Re = 2.2x10^6/ft Trip 1 k = 0.060-in Closed Cowl

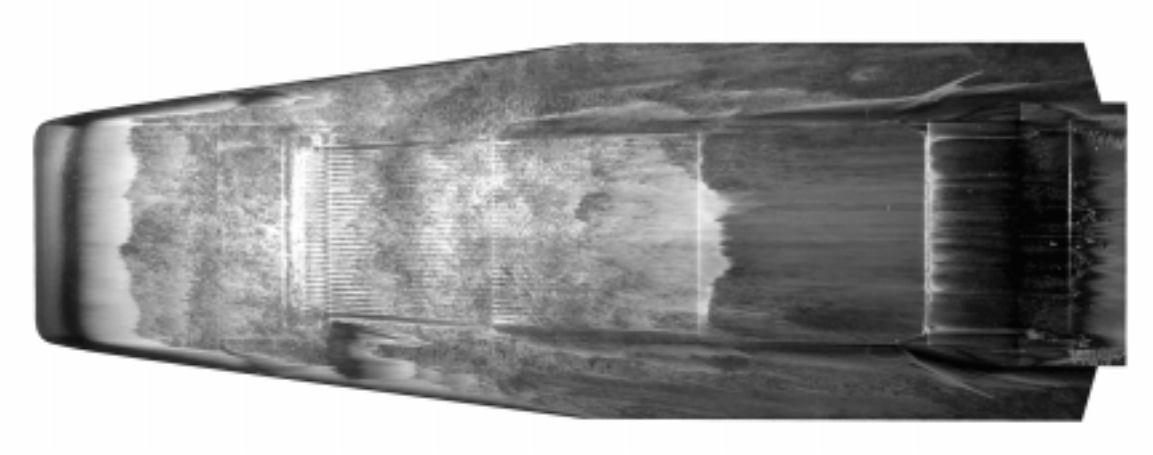

Test 346 Run 2 α = 2-deg Re = 2.2x10^6/ft Trip 2b k = 0.120-in Closed Cowl

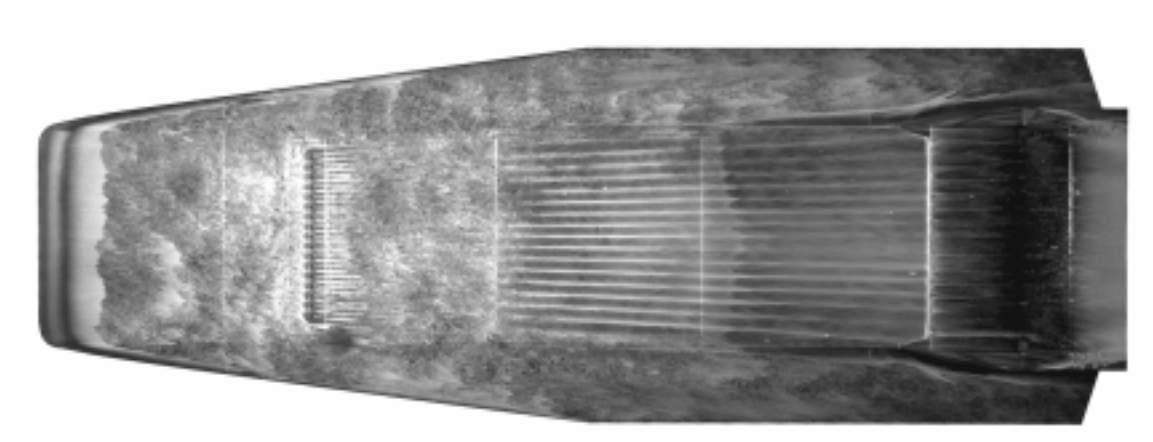

Test 346 Run 3 α = 2-deg Re = 2.2x10^6/ft Trip 1 k = 0.120-in Closed Cowl

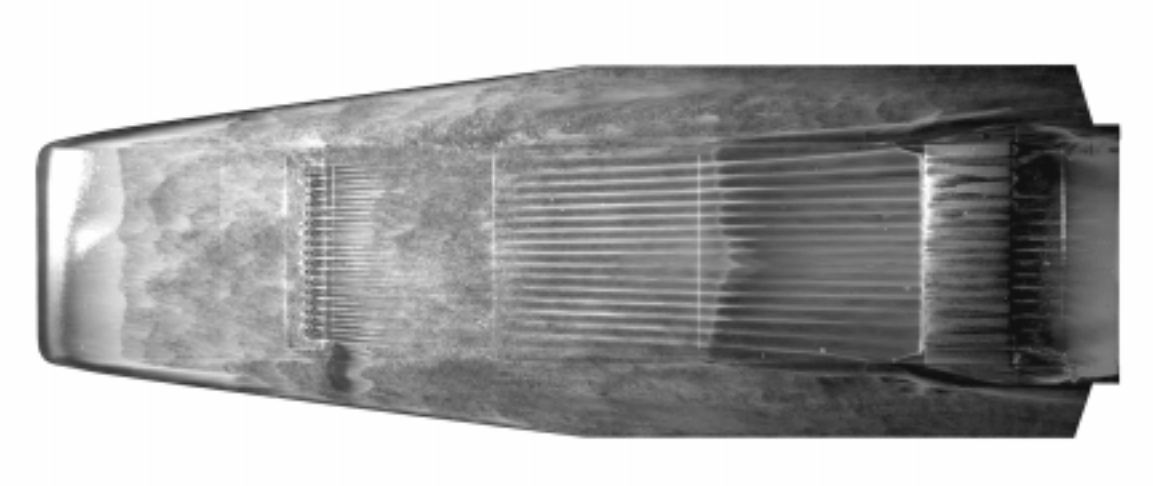

Test 346 Run 4 α = 2-deg Re = 2.2x10^6/ft Trip 3 k = 0.120-in Closed Cowl

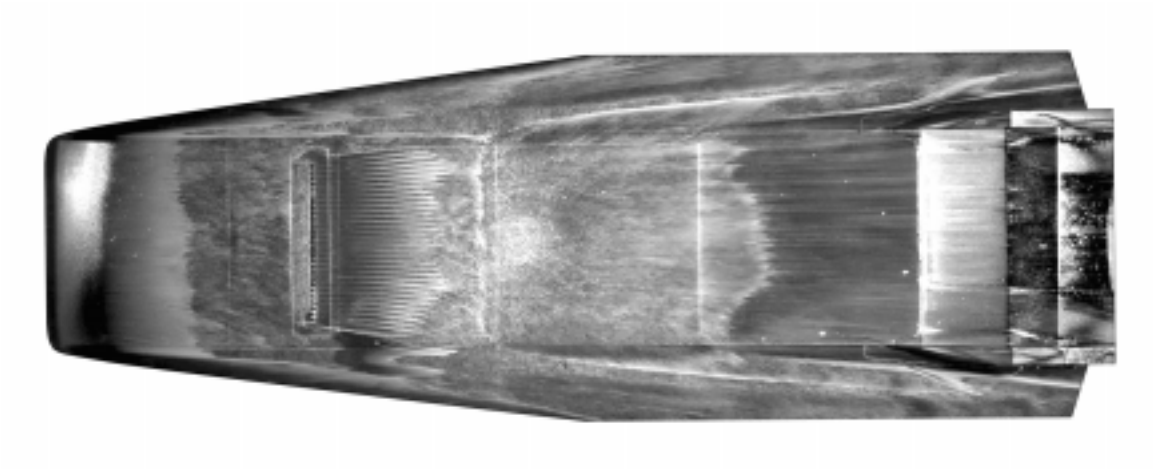

Test 346 Run 5 α = 2-deg Re = 2.2x10^6/ft Trip 2a k = 0.120-in Closed Cowl

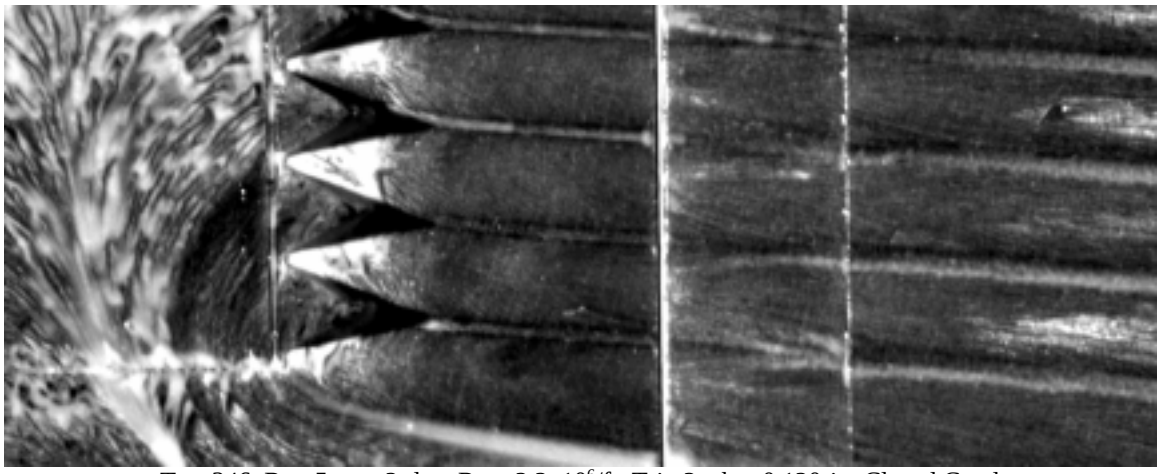

Test 346 Run 5 α = 2-deg Re = 2.2x10^6/ft Trip 2a k = 0.120-in Closed Cowl

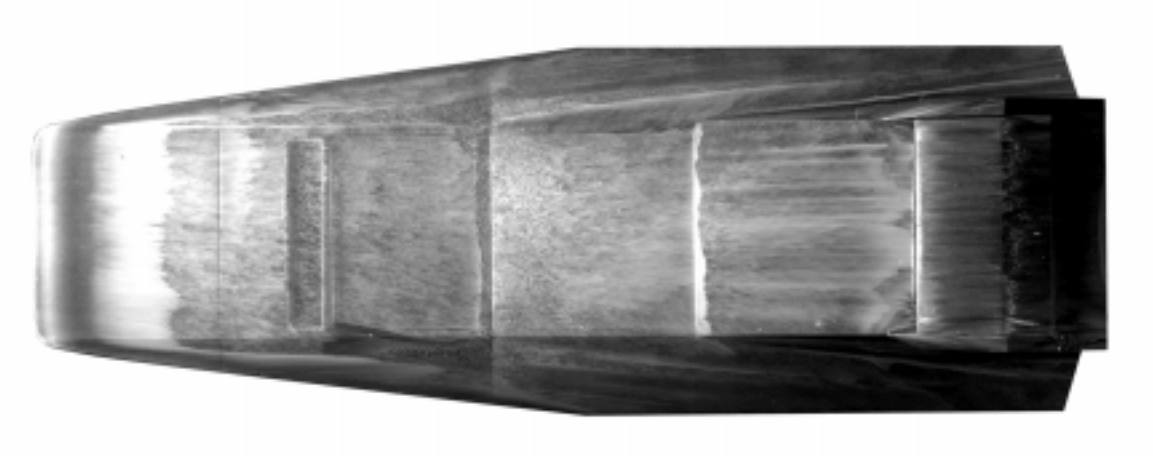

Test 346 Run 6 α = 2-deg Re = 2.2x10^6/ft No Trip Baseline Closed Cowl

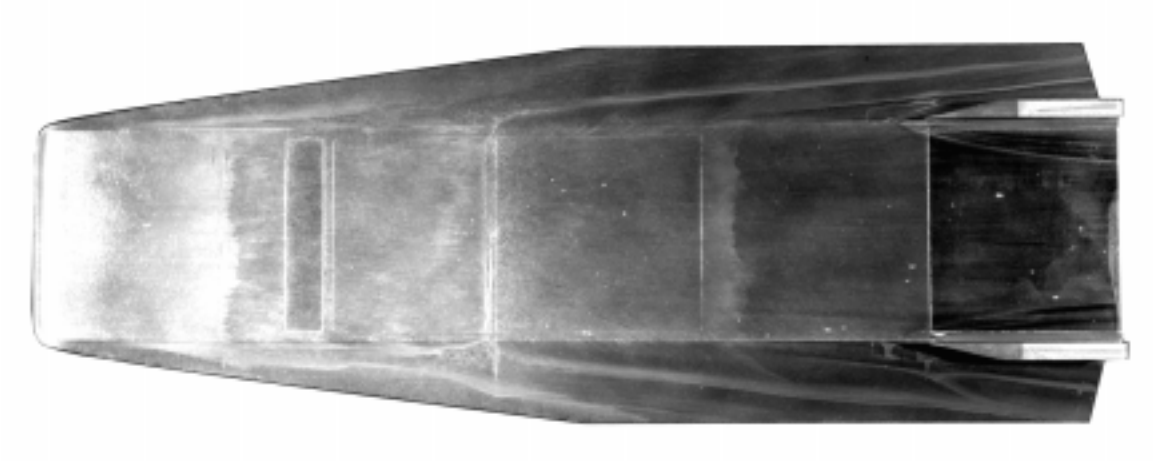

Test 346 Run 7 α = 2-deg Re = 2.2x10^6/ft No Trip Baseline Open Cowl

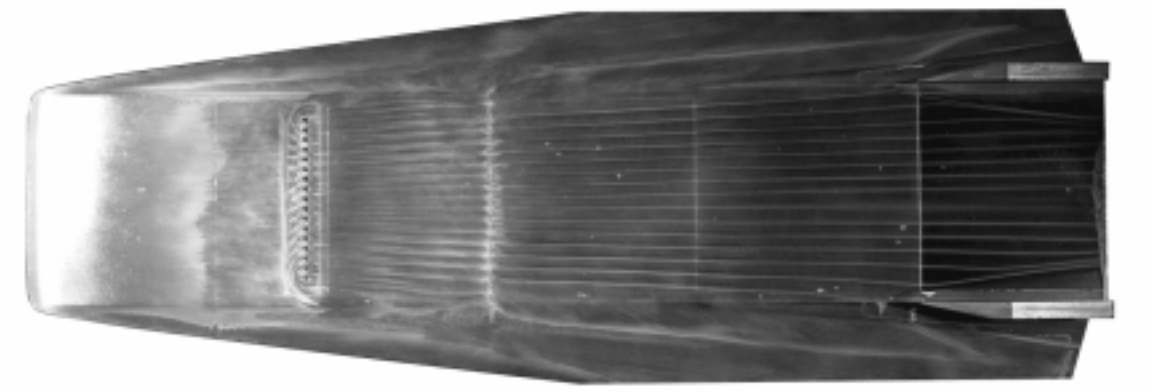

Test 346 Run 8 α = 2-deg Re = 2.2x10^6/ft Trip 3 k = 0.120-in Open Cowl

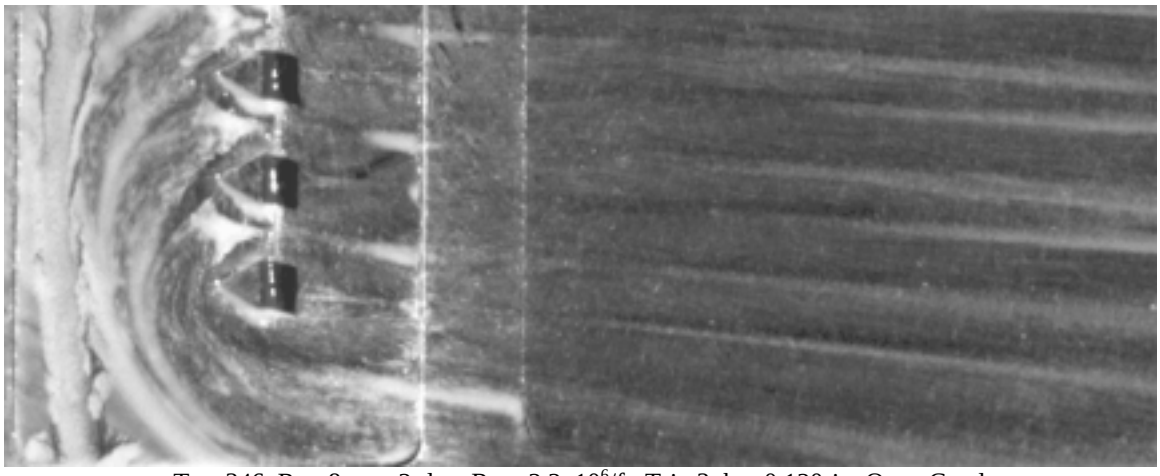

Test 346 Run 8 α = 2-deg Re = 2.2x10^6/ft Trip 3 k = 0.120-in Open Cowl

Test 346 Run 10 α = 2-deg Re = 2.2x10^6/ft Trip 2b k = 0.120-in Open Cowl

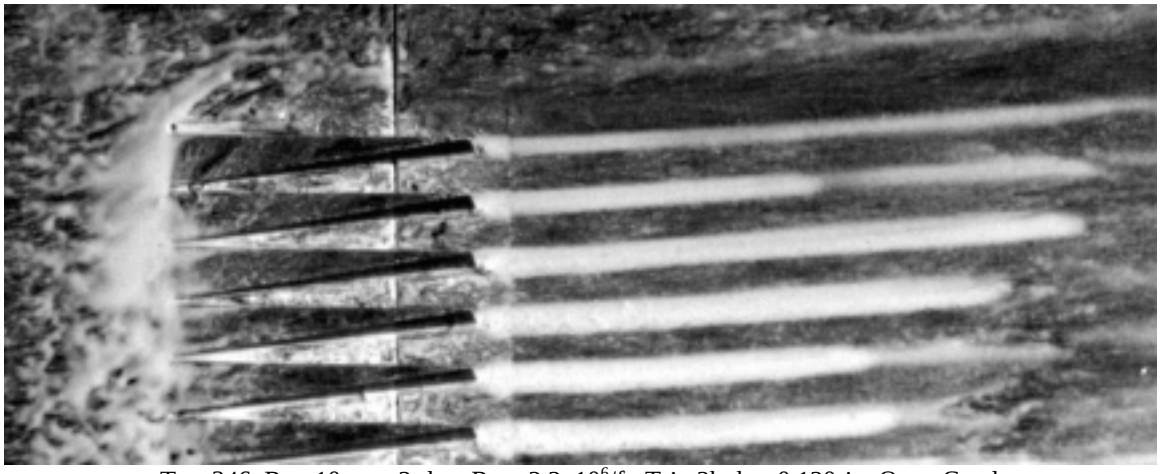

Test 346 Run 10 α = 2-deg Re = 2.2x10^6/ft Trip 2b k = 0.120-in Open Cowl

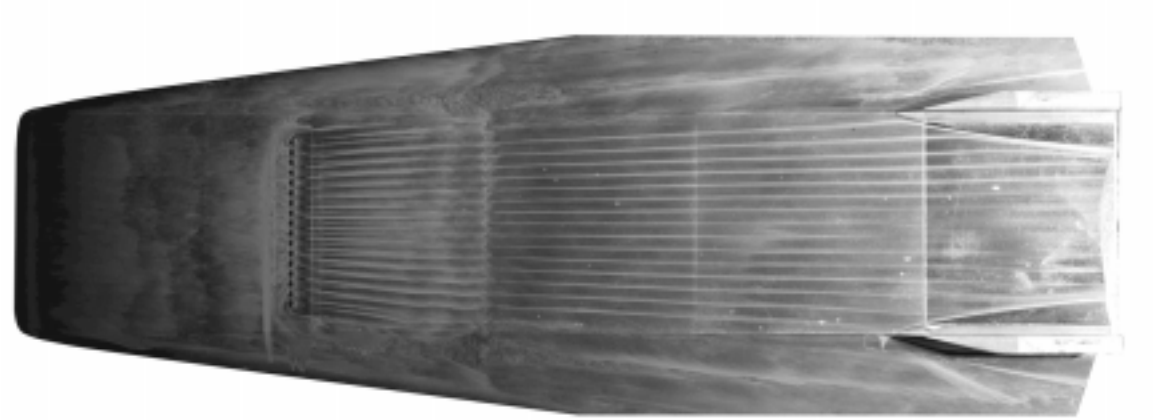

Test 346 Run 11 α = 2-deg Re = 2.2x10^6/ft Trip 1 k = 0.120-in Open Cowl

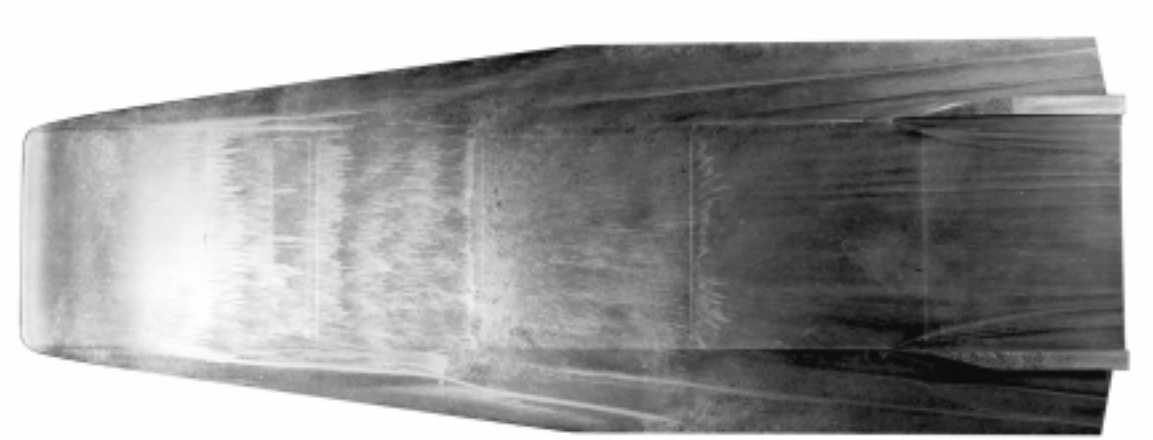

Test 346 Run 14 α = 2-deg Re = 2.2x10^6/ft No Trip Baseline Open Cowl

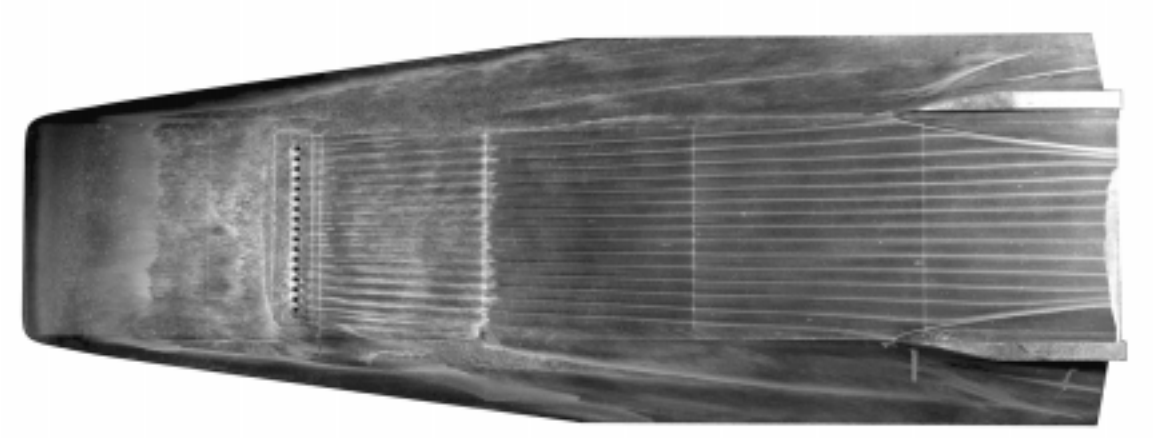

Test 346 Run 15 α = 2-deg Re = 2.2x10^6/ft Trip 1 k = 0.120-in Open Cowl

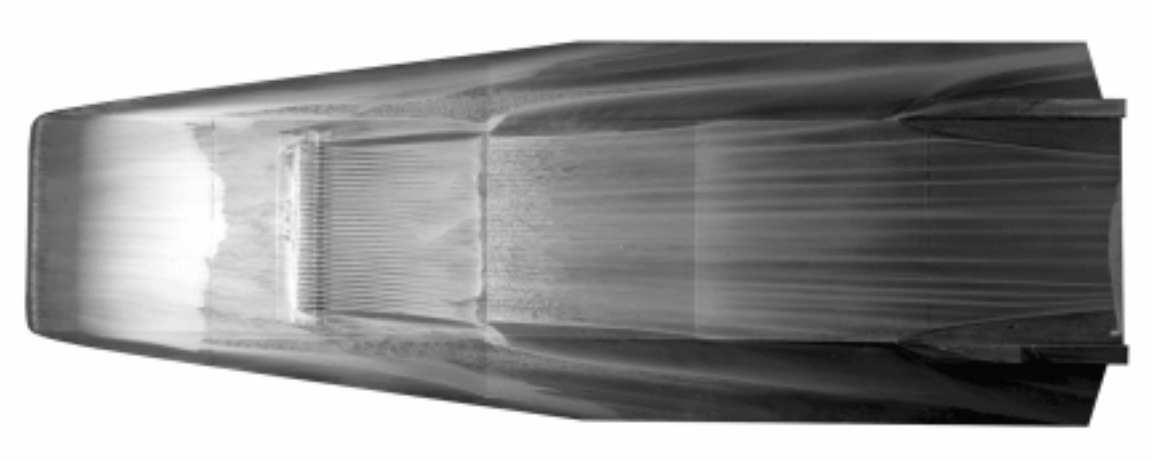

Test 346 Run 18 α = 2-deg Re = 2.2x10^6/ft Trip 2b k = 0.120-in Open Cowl

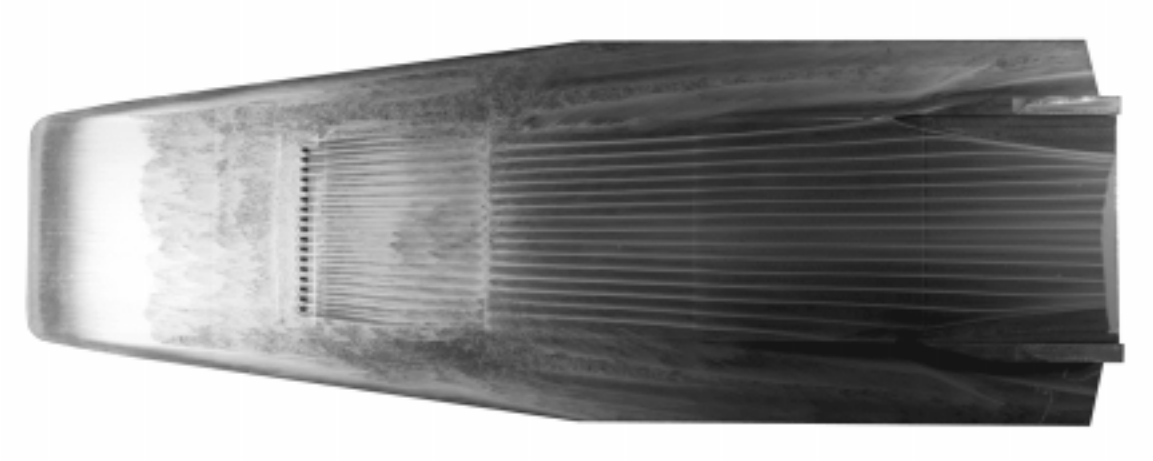

Test 346 Run 19 α = 2-deg Re = 2.2x10^6/ft Trip 3 k = 0.120-in Open Cowl

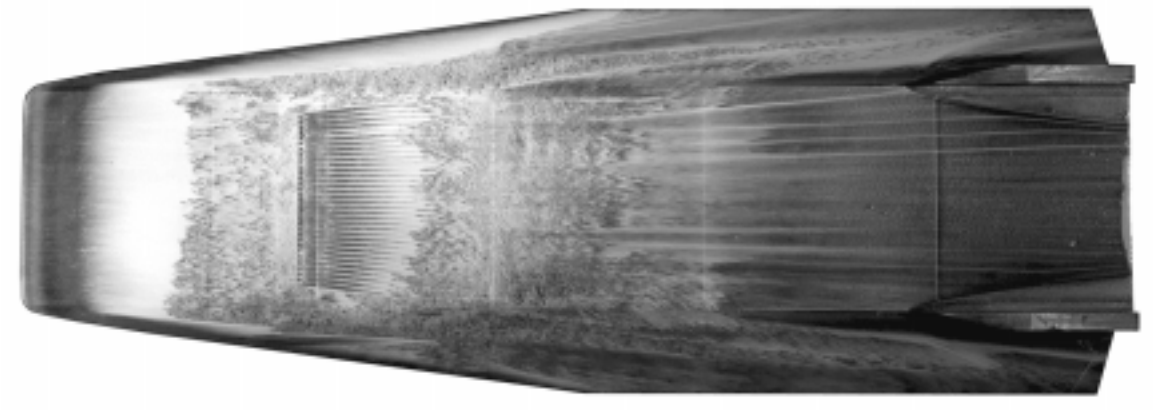

Test 346 Run 20 α = 2-deg Re = 2.2x10^6/ft Trip 2a k = 0.120-in Open Cowl

REPORT DOCUMENTATION PAGE

Form Approved
OMB No. 0704-0188

1. AGENCY USE ONLY (Leave blank)	2. REPORT DATE	3. REPORT TYPE AND DATES COVERED
	August 2000	Technical Memorandum

4. TITLE AND SUBTITLE
Forced Boundary-Layer Transition on X-43 (Hyper-X) in NASA LaRC 31-Inch Mach 10 Air Tunnel

5. FUNDING NUMBERS
WU 242-80-01-01

6. AUTHOR(S)
Scott A. Berry, Michael DiFulvio, and Matthew K. Kowalkowski

7. PERFORMING ORGANIZATION NAME(S) AND ADDRESS(ES)
NASA Langley Research Center
Hampton, VA 23681-2199

8. PERFORMING ORGANIZATION REPORT NUMBER
L-18017

9. SPONSORING/MONITORING AGENCY NAME(S) AND ADDRESS(ES)
National Aeronautics and Space Administration
Washington, DC 20546-0001

10. SPONSORING/MONITORING AGENCY REPORT NUMBER
NASA/TM-2000-210315

11. SUPPLEMENTARY NOTES

12a. DISTRIBUTION/AVAILABILITY STATEMENT
Unclassified-Unlimited
Subject Category 34 Distribution: Nonstandard
Availability: NASA CASI (301) 621-0390

12b. DISTRIBUTION CODE

13. ABSTRACT (Maximum 200 words)
Aeroheating and boundary layer transition characteristics for the X-43 (Hyper-X) configuration have been experimentally examined in the Langley 31-Inch Mach 10 Air Tunnel. Global surface heat transfer distributions, and surface streamline patterns were measured on a 0.333-scale model of the Hyper-X forebody. Parametric variations include angles-of-attack of 0-deg, 2-deg, 3-deg, and 4-deg; Reynolds numbers based on model length of 1.2 to 5.1 million; and inlet cowl door both open and closed. The effects of discrete roughness elements on the forebody boundary layer, which included variations in trip configuration and height, were investigated. This document is intended to serve as a release of preliminary data to the Hyper-X program; analysis is limited to observations of the experimental trends in order to expedite dissemination.

14. SUBJECT TERMS
Boundary-layer transition, hypersonic, roughness

15. NUMBER OF PAGES
78

16. PRICE CODE
A05

17. SECURITY CLASSIFICATION OF REPORT	18. SECURITY CLASSIFICATION OF THIS PAGE	19. SECURITY CLASSIFICATION OF ABSTRACT	20. LIMITATION OF ABSTRACT
Unclassified	Unclassified	Unclassified	UL